UNIVERSITY OF CALIFORNIA
RIVERSIDE

In situ Seismic Velocities of Granitic Rocks, Mojave Desert, California

A Thesis submitted in partial satisfaction
of the requirements for the degree of

Master of Science

in

Geological Sciences

by

Steven Orvil Zappe

December, 1979

Thesis Committee:

Professor Donald Stierman, Chairman

Professor Tien-Chang Lee

Professor Shawn Biehler

APPROVAL PAGE

The thesis of Steven Orvil Zappe is approved:

Committee Chairman

University of California, Riverside
December, 1979

ACKNOWLEDGEMENTS

I want to acknowledge and express my appreciation for the efforts of Don Stierman and Doug Cavit in collecting the data, and the critical review of this manuscript by Don Stierman, Tien-Chang Lee, Shawn Biehler, and Marlene Ngit Sim Kam. A special thanks goes to my fiancee (and now my wife) Linda, who encouraged and supported me from beginning to end. Assistance was provided by the Agricultural Experiment Station, an intramural grant from the Academic Senate, and the Institute of Geophysics and Planetary Physics, all at UCR. This manuscript was composed and printed on the PRIME 400 interactive computer with funds allocated by the Department of Earth Sciences at UCR.

ABSTRACT OF THE THESIS

In situ Seismic Velocities of Granitic Rocks,
Mojave Desert, California

by

Steven Orvil Zappe

Master of Science, Graduate Program in Geological Sciences
University of California, Riverside, December 1979
Assistant Professor Donald J. Stierman, Chairman

Downhole velocity surveys were conducted in 9 wells, ranging in depth from 80 to 160 meters, situated in the granitic rocks of the Mojave Desert. Weight drop and horizontal traction techniques were utilized for the generation of compressional and shear waves, respectively.

The P-wave data for all wells were interpreted by

interval velocity calculations. The mean bottom of hole (BOH) velocity is 4.41 ± 0.89 km/sec. S-wave data from three wells were analyzed by determining the ratio of P to S-wave velocity (Vp/Vs) from arrival times of the two phases. Inferred S-wave velocities from this method are between 1.7 and 2.7 km/sec, with Poisson's ratios from 0.27 to 0.36.

P-wave BOH velocities in the five wells in the western Mojave average 4.43 ± 1.22 km/sec, while velocities in the four eastern Mojave wells average 4.40 ± 0.37 km/sec. The large variation from the mean in the western Mojave is attributable to progressively lower velocities near the Garlock fault, where the velocity decays exponentially as a function of distance from the fault. Aside from the influence of the Garlock fault, these velocities closely match the western regional velocity of 5.5 km/sec determined from published crustal studies. The small variation and relatively lower regional velocity in the eastern Mojave are tentatively attributed to the homogenization effect on the physical properties of rocks by widespread regional fracturing arising from the complex tectonic setting.

Several mathematical functions were tested with respect to the time-depth data to look for evidence of a velocity gradient, but the data were not sufficiently precise to confirm this gradient. The most favorable function is an exponential decay of the form

$$T = A + BZ + C\exp(GZ) \tag{5}$$

fitted to the time-depth data. The value of G is limited by physical constraints and is determined subjectively, with the remaining coefficients computed by least-squares minimization.

TABLE OF CONTENTS

LIST OF TABLES

LIST OF FIGURES

INTRODUCTION

The dependence of seismic velocity upon confining pressure has been well established in laboratory experiments. Studies performed by Birch (1960) and others have shown that both P and S-wave velocities in dry rock samples increase with increasing pressure. However, the discrepancy between these laboratory studies and in situ characteristics of crystalline and sedimentary rocks has been noted for many years (i.e., Leet and Ewing, 1932; Nicholls, 1961; Swain, 1962). It was established that fluid saturation plays an important role in the physical properties of porous rocks, although in low porosity (<1%) rock this effect was thought to be minimal. In 1968, Simmons and Nur reported that in situ P-wave velocities (Vp) in granite measured in two 3 kilometer boreholes exhibited very little variation with depth, rather than the variation with pressure predicted from laboratory measurement on dry samples. Studies in Russia by Gogonenkov and Shlychkin (1969) found that in situ measurements in granite in a 4 kilometer borehole compared favorably to laboratory measurements made upon saturated samples at atmospheric pressure and room temperature. The acoustic log showed that the overall velocity gradient was, as in the case of Simmons and Nur (1968), not distinguishable against the background of local inhomogeneities.

In 1969, Nur and Simmons conducted lab experiments to resolve this paradoxical behavior between laboratory and in situ velocities, and confirmed the important influence of fluid saturation on the seismic properties of low porosity rocks. They found that the rate of increase in velocity with pressure for compressional waves is less for saturated rocks than for dry rocks, and that Vp for saturated rocks at atmospheric pressure is greater than for dry rocks, with the dry and saturated Vp curves converging at pressures above 1 kbar. On the other hand, shear wave velocities (Vs) are virtually unaffected by the presence of water. The mechanism proposed to explain these results is that the porosity of the rocks is due to the presence of microcracks, which, when air in the cracks is replaced by water, results in an increase of up to 50% in Vp while Vs remains unchanged. As the effective pressure (defined as external pressure - pore pressure) increases the microcracks are thought to close, and in doing so force the water out of the pores. Above 2 kbar, most cracks are apparently closed, and the dry and saturated curves coincide.

Most published work dealing with in situ velocities entails measurements performed in deep boreholes (on the order of 1 to 3 km deep) in which there seems to be satisfactory agreement with laboratory velocities. Little work has been published of _in situ_ measurements in holes less than 1 km deep, where the expected pressure dependency of velocity should be more apparent. Studies by Gibbs _et al_ (1975, 1976) in holes between 25 - 30 meters deep found that P-wave velocities in granitic rocks in central California were lower than would be expected from lab measurements on such rocks. Stierman _et al_ (1979) found from studies near the San Andreas fault in central California that Vp did not increase with depth as quickly as predicted from lab measurements. This was explained, primarily by the presence of large fractures (macrocracks) in addition to microcracks. It was shown that fracture porosities on the order of 5% can lower P-wave velocities down to 70% of lab sample values (Stierman and Kovach, 1979).

Short surface refraction surveys are more difficult to apply accurately to velocity-depth functions for granitic rocks than borehole measurements. Simmons and Nur (1968) pointed out that the "scatter in arrival times at larger distances is usually too large to distinguish between velocity - depth relations that reach 6 km/sec at a few kilometers and those that reach 6 km/sec at depth of only tens of meters." Refraction data gathered in large scale crustal studies are generally interpreted as layered models for the upper 20 - 30 km (Mojave Desert, Kanamori and Hadley, 1975) rather than velocity gradients, although plutonic rocks normally are not characterized by sharp horizontal interfaces. A satisfactory mechanism for the velocity increase modeled in the upper 4 to 5 km consistent with the regional geology of the Mojave Desert remains an important unanswered question.

This study is intended to bridge the gap between surface refraction studies and crustal models by dealing with shallow downhole measurements, as well as to provide additional data for comparison between <u>in situ</u> and laboratory measurements of the physical properties of rocks. The objectives are therefore:

1) To characterize the seismic velocities of near surface granitic rocks in the Mojave Desert, and
2) to measure seismic velocities at shallow depths (<1km) with sufficient resolution to investigate the possibility for a gradational increase in seismic velocities.

TECTONIC AND GEOLOGIC SETTING

This study was conducted in the Mojave Desert physiographic province of California, referred to as the Mojave block (Hewett, 1954a). Bound on the southwest by the right lateral San Andreas fault and on the northwest by the left lateral Garlock fault, the Mojave is subjected to the stress field related to these faults. There is no well-defined eastern boundary separating the Mojave block from the Basin and Range province (Figure 1).

Faulting within the western Mojave is characterized by families of NW trending dip-slip faults with displacements on the order of several hundred meters and limited lateral motion (Hewett, 1954b). There is evidence of Recent activity on these faults, such as on the Blackwater, but none of them are known to intersect the Garlock fault.

In the eastern Mojave the general trend of faulting is less obvious. Great thrust faults of Mesozoic age dominate east of Baker. Several of these faults have no topographic expression and are considered inactive (Dibblee and Hewett, 1970).

The intrusive rocks investigated in this report are described in general terms by Hewett (1954a) as coarse grained granitic rocks of Mesozoic age. In the eastern Mojave the composition is primarily quartz monzonite to granite. A wider variety of rocks, ranging from gabbro and diorite to quartz monzonite and granite, occurs in the western Mojave. In general, the acidic rocks are younger than the gabbros and diorites.

PREVIOUS WORK

Probably the earliest work done concerning _in situ_ seismic velocities in crystalline rock was an experiment conducted by Leet and Ewing (1932) to determine elastic wave velocities of granites at quarries in Quincy and Rockport, Massachusetts, and Westerly, Rhode Island. Dynamite explosions generated the seismic waves which were recorded on portable seismographs located between 15 and 1400 meters from the shot. P-wave velocities varied between 4.96 km/sec at Quincy to 5.08 km/sec at Rockport, and an S-wave velocity of 2.48 km/sec was measured at Quincy. With a measured density at Quincy of 2.65 gm/cc various elastic moduli were determined, among them the bulk modulus and Poisson's ratio calculated at 44 x 10**10 dyne/sq cm and 0.33, respectively. Since this surface refraction study yielded linear time distance relationships intersecting the origin, it was surmised that the depth of penetration was on the order of 20 meters, and that the velocities reflected the effect of pressures of only a few atmospheres. One important conclusion drawn from the close agreement of P-wave velocity for the widely separated and mineralogically distinct granites was that minor differences in composition do not strongly influence seismic velocity.

Nicholls (1961) determined the <u>in situ</u> compressional and shear wave velocities and calculated elastic constants in a granite gneiss located at Lithonia, Georgia. Shock waves were generated by small charges of high explosives (25 to 180 grams) in 20 cm deep holes. The shallow holes cratered upon detonation, resulting in the production of shear waves. Accelerometers and velocity gauges affixed to steel mounts grouted into gauge holes measured vertical and transverse motion between 10 and 100 meters from the shots. Velocities in the granite gneiss were 5.56 km/sec and 3.15 km/sec for Vp and Vs respectively, and for a measured density of 2.63 gm/cc, the bulk modulus and Poisson's ratio were computed at 46.5 x 10**10 dyne/sq cm and 0.26, respectively. These values differed significantly with results from standardized laboratory tests in which velocities were calculated from the length and fundamental frequencies of longitudinal and torsional vibrations of a specimen. In particular, Poisson's ratio measured by standardized procedures yielded a negative quantity.

Carroll <u>et al</u> (1966) measured compressional and shear wave velocities in tunnels through granites of different composition located in Colorado and the Nevada Test Site (NTS) in an attempt to determine their elastic properties. The waves were generated by electric blasting caps occasionally boosted with a few decigrams of powder. At the Colorado site, measurements were made using a linear array of 3 single component accelerometers located between 9 to 30 meters from the source along the surface of the tunnel wall, while in the NTS tunnel the accelerometers were spaced 0.6 meters apart on a probe inserted into a shallow (9 meter) borehole at various depths. Values for Vp and Vs varied between 5.18 to 6.10 km/sec and 2.44 to 3.75 km/sec respectively, with Poisson's ratio ranging from 0.20 to 0.37.

Gibbs et al (1975, 1976) are continuing to work on a program to measure seismic velocities in over 100 boreholes in a wide variety of rock types (primarily in sediments) in the San Francisco Bay region. They report on 4 studies conducted in quartz diorite. After reviewing a comparison of various techniques of shear wave generation by Warrick (1974) such as "hammer impacts on side walls of shallow pits, Primacord on the free side of a plate fixed to a pit wall, explosions in shallow holes, and horizontal impacts on timbers staked to the Earth", the horizontal traction technique was considered the most reliable method. A sledge hammer and plate are used to generate compressional waves. Travel times are measured at 2.5 meter intervals in 30 meter deep drill holes. Velocity measurements in fresh quartz diorite yield Vp between 3.85 to 3.90 km/sec and Vs between

1.64 to 1.94 km/sec, with Poisson's ratio values of 0.39 and 0.34. Values for deeply weathered quartz diorite grus range from 1.08 to 1.26 km/sec and 0.56 to 0.64 km/sec for Vp and Vs respectively, with a Poisson's ratio of 0.32. The quartz diorite studied by Gibbs <u>et al</u> range from 4 to 7 km of the San Andreas fault.

A summary of the <u>in situ</u> velocities and elastic moduli determined from previous studies are tabulated in Table 1.

DATA AQUISITION

Wells

The boreholes used in this study were drilled by the U. S. Geological Survey (USGS) between December 1976 and March 1977 as a part of a regional heat flow reconnaissance program in the Mojave Desert (Sass et al, 1978). Upon completion of their study, these wells were made available to Dr. Tien-Chang Lee of the University of California at Riverside (UCR) for additional heat flow measurements and other borehole investigations.

The holes, ranging in depth from 80 to 160 meters, were drilled with an air compressor and downhole hammer. and range in depth from 80 to 160 meters. Casing consists of 5 cm i.d. PVC pipe through which a cement-bentonite grout was pumped to seal off the lower 30 to 50 meters of the annulus around the pipe. An additional 3 meters of cement was emplaced at the top after the remainder of the annulus was backfilled with drill cuttings. The wells were secured by covering the heads with utility meter boxes.

Nine wells were studied. Five are in the western Mojave near Red Mountain, while the remaining wells are in the eastern Mojave in the vicinity of Baker (Figure 1). Principle access from Riverside is via US 395 to Red

Mountain or Interstate 15 to Baker, with the wells situated near local paved or dirt roads.

Figures 2 and 3 are general location maps for the wells in the west and east, and include the local geologic settings. Figures A1 through A8 in the Appendix are detailed location maps for each of the wells. Table 2 lists the characteristics of each well and includes the analyzed rock type. Also listed are distances to the western Mojave wells from the Garlock and Blackwater faults. These distances and their influence on the seismic velocities in adjacent rocks will be investigated in the Discussion chapter.

Equipment

I designed a weight drop system to generate compressional waves. Three steel pipes, measuring 4.5 cm in diameter by 2.75 meters long, formed a tripod when joined by a frame composed of three short sleeves and an eye bolt in the center. The legs fit into the sleeves, secured by bolts. Steel disks measuring 30 cm in diameter by 4 cm with a 4 cm hole in the center provided the weight source, each weighing approximately 20 kg. A pipe tee constructed from standard plumbing connectors and pipe held a total of five disks (100 kg). A 10 mm diameter polyethylene rope with a rated safe limit of 180 kg was attached to the pipe tee and passed through a snatch block pulley suspended from the eye bolt. The weights were raised to a maximum height of 1.8 meters by a hand-cranked trailer winch mounted on one of the legs and were dropped by removing the handle and releasing the ratchet. As the tension in the rope slackened, the winch immediately began to feed out the rope before the weights fell, resulting in a free fall. Modifications such as additional weights or longer legs could increase the potential energy beyond the current maximum of 180 joules.

Shear waves were generated by the horizontal traction method of Kobayashi (1959). The soil would be leveled out with a shovel to provide maximum contact with the beam, a railroad tie measuring 16.5 cm x 20 cm x 250 cm. The rear wheels of the recording truck (gross weight = 3 met. ton) held the beam in place. Steel plates faced the ends of the beam to minimize damage from the blows of the 3.6 kg sledge hammer used to produce the impulse.

A 3-component borehole geophone package measuring 4 cm in diameter by 16.5 cm detected the onset of seismic waves. Each geophone is 2.2 cm in diameter by 2.5 cm and has a natural frequency of 8 hz. The original geophones had an impedence of 32 ohms, but later in the project they were replaced with 680 ohm versions. High vacuum silicon grease filled all of the spaces in the package as waterproofing.

Two major shortcomings of this geophone system were the inability to orient the package in the hole and the absence of a means to clamp the geophone against the casing.

The cable consisted of 6 conductors and a shield encased in 8 mm PVC tubing. A 300 meter length of cable was wound onto a hydraulic winch mounted on a small flatbed trailer. A boom and pulley system was rigged to the frame, allowing the trailer to be parked near the edge of a well so that the cable could be lowered into or winched vertically out of the hole. The end to end resistance of the cable is 8 ohms, with 5 meter intervals marked on the covering. At first the geophone package was coupled to the cable with Amphenol connectors, but this proved to be an unreliable setup since there were 18 solder joints which could fail, so eventually the geophones were soldered directly to the cable. An 8 meter length of cable connected the free end of the geophone cable to the amplifier inside the truck.

The recording system used was designed for surface refraction applications. The amplifier was a Dresser SIE P-19 12 channel unit with an amplification range of from 0.01% to 100%. I constructed an adapter box which allowed 3 of the channels to be used for the borehole geophone and 2 to be used by the timing system described below. Input to the box was with banana plugs, and the output to the amplifier was by the standard 26 pin connector. A Dresser

SIE model R-6 24 channel recording oscillograph recorded the amplifier output on light developing paper at a speed of 40 cm/sec. Timing lines were recorded at 10 msec intervals, permitting arrivals to be measured to within ± 1 msec.

Figure 4 depicts an idealized layout of the equipment at a typical well location. The general procedure for logging a well would be to first locate the borehole from directions supplied by the USGS, and then set up the tripod, position the cable trailer, and park the truck on top of the horizontal traction beam. The person managing the weights and hammer used either visual or voice contact to alert the recording equipment operator of a forthcoming event. A set of recordings at each depth consisted of between 2 to 4 weight drops and 2 to 3 hammer swings on either side of the beam. The wells were logged at either 5 or 10 meter intervals, with gains for the borehole geophones increased with depth.

The timing system for recording the initiation of the impulses consisted of two time break geophones, a vertical detector position roughly 50 cm from the edge of the weights and a horizontal detector buried in the dirt near the center of the beam. A noise problem was encountered with the weight drop system, associated with vibration of the legs as the sprockets of the winch rotated during a drop. This noise was much more pronounced at drops from greater heights, but these vertical impacts were consistently recorded on the horizontal time break as a regular sinusoidal wave packet, regardless of height. The time difference between the first break at the vertical time break and the first peak (or trough) at the horizontal time break could be determined for short drops when the noise was low, and then used at greater heights when noise made the first break on the vertical time break ambiguous.

I made several modifications of procedure following preliminary attempts to log the wells. At first the trailer remained hitched to the recording truck, but was later disconnected when I determined that the truck and trailer transmitted extraneous vibrations to the borehole geophone package, such as when the traction beam was hit. An additional precaution taken to reduce noise in the borehole system was to lightly clamp a pair of visegrip pliers to the cable at the wellhead, allowing the package to hang free in the well. This also permitted some degree of choice as to which wall the package would rest against by shifting the position of the visegrips, alleviating some of the problems arising from the lack of a clamp system. Initially the ends of the traction beam were not covered with steel, and when the faces became badly splintered the beam was cut in half to provide two new impact surfaces. The resulting arrangement of reversing the ends and leaving a 20 cm gap between them produced no noticeable difference in energy transmitted with the single beam. A 9 kg sledge hammer eventually replaced the lighter one to provide additional shear energy. I also found that the weight drops produced more consistent signals as well as preserved the equipment if done on alluvium or grus rather than over an outcrop.

DATA REDUCTION AND INTERPRETATION

Travel times of the shock waves to various depths in the well were determined by measuring the interval between the time break (TB) and the onset of the signal at the downhole geophone. As mentioned earlier, the TB system consisted of a vertical geophone at the weight drop and a horizontal geophone at the traction beam. It is apparent from the composite seismogram in Figure 5 that uncertainties in the vertical TB would lead to greater error in the travel time, so the horizontal geophone can be used as a more reliable indication of the event initiation time. Before picking P arrivals for a well, I would scan the entire record and compute the time differences for each weight drop between a clear first break on the vertical TB and a peak and trough on the horizontal TB and average the differences. These averages were then used to determine the initiation time of an event for all weight drops, regardless of the quality of the vertical TB. The vertical TB alone was used less than 5% of the time, only when it was found that a particular travel time did not fit the other observations. The horizontal events, on the other hand, could be timed exclusively on the horizontal TB because the generation of shear waves was not accompanied by noise. An additional factor was that the energy imparted by a sledge hammer blow was insufficient to be clearly recorded by the vertical TB.

Measurements of times were aided by a Gerber variable scale stretched to 10 divisions/.01 sec, or 1 division/msec. Assuming maximum precision, the TB was picked to ± .5 msec, and the first arrivals could be determined anywhere from ± .5 to ± 2 msec. Travel time-depth data from all nine wells are listed in Table A1 in the Appendix.

Few corrections, were applied to the data. The distance from the vertical geophone in the borehole package to the first 5 meter mark on the cable was included in determining actual depth in the hole. However, several corrections applied by Gibbs et al (1975, 1976) were not made in this study due to the differences in logging interval and total well depth. Gibbs recorded at 2.5 meter intervals in 30 meter wells and tried to take into consideration the offset of the P and S-wave generators from the well by using an uphole inline geophone which would record the "origin time" as the onset of the wave generated 2 meters away. They then established a "corrected travel time" as the time difference between the uphole and downhole geophone (corresponding to a vertical ray path) plus a timing correction based upon the 2 meter offset. Rather than over-correcting my data, I chose to assume that the energy would travel the shortest time (and approximately the shortest distance) from the energy source to the borehole geophones. Since I was dealing with 100 meter holes recorded every 5 or 10 meters and the weight drop and traction beam were roughly 3 meters offset from the hole, the ray path length for a measurement at a depth of 10 meters would be 10.4 meters, less than a 5% difference. Assuming a travel time of 10-15 msec, it would be impossible to distinguish differences in arrival time between 10 and 10.4 meter ray paths, with the previously stated level of precision of $\pm$ 1 msec. One effect of ignoring this correction is to obtain near surface velocities from time-depth data which are higher than if the correction was applied. However, the error is within the statistical limits imposed by measurement limitations.

P Waves

The standard approach to reducing time-depth data is to determine interval velocities. Assuming layers of uniform velocity, the problem becomes similar to surface refraction analysis. Sets of points appearing to have a linear trend are first chosen by inspection and are then subjected to a linear regression analysis to determine the best fitting straight line segment over that interval in the least-squares sense. If more than one segment is fitted to the entire well, a check must be made to assure that these lines intersect at a value intermediate to the sets of points used in the linear regression. The least-squares program employed for these data incorporated the error in arrival time in the calculations, and computed the time intercept and slope values along with the standard error (s.e.) of the slope. Interval velocities are found by taking the inverse of the slope, with the upper and lower bounds of the velocity being the inverse of (slope ± s.e.). All wells were fitted with either 1 or 2 straight lines segments, and plots showing the data points with the straight lines and velocities are in Figures A9a - A17a in the Appendix. The results are tabulated in Table 3 and displayed in a velocity vs. depth format in Figure 6.

Several observations concerning Figure 6 may be made. First, there does not seem to be any common depth at which there is a change of velocity: it occurs anywhere from 15 meters to nearly 70 meters below the ground surface. There is a rather wide spread in both the near surface and bottom of hole (BOH) velocities, with the greatest top to bottom difference occuring in well FPK of 3.86 km/sec (1.36 to 5.22 km/sec), a nearly 300% increase. Surface velocities range between 1.26 and 4.75 km/sec, while BOH velocities fall between 2.66 and 5.73 km/sec. The median BOH velocity is 4.52 km/sec, and the mean is 4.41 ± .89 km/sec.

Recognizing that the velocity difference from top to bottom ranges from 0 to 284%, it is instructive at this point to consider some of the possible mechanisms influencing seismic velocity variations. An increase in P-wave velocity in crystalline rock with depth can be due to:

1) a transition from weathered to unweathered rock. Little work has been reported dealing with the effect of weathering _in situ_, but at Frenchman's Creek (Gibbs _et al_, 1976) the velocity changed from 2.26 to 3.90 km/sec in the transition from weathered to fresh quartz diorite, an increase of over 70%.

2) a transition from unsaturated to saturated rock. Determining the water table in sediments is a common practice with refraction surveys, but _in situ_ measurements in crystalline rocks are not readily found in the literature. Nur and Simmons' (1969) laboratory work found an increase on the order of 30 to 70% from the dry to saturated state at low confining pressures (<50 bars) normally encountered in near surface rocks. The increase is attributed to water filling the crack and pore spaces in the samples.

3) the presence and closing of macrocracks, defined

by Stierman and Kovach (1979) as "fractures large enough to render a rock sample inappropriate for standard geophysical studies in the laboratory." They postulated that a macrocrack porosity of 5 to 10% could produce a 30 to 50% drop in the P-wave velocity from laboratory values obtained from saturated rock. If these fractures closed under increasing confining stress with depth, an increase in velocity would be observed.

4) a combination of any of these mechanisms.

The question of which process dominates in the Mojave desert wells can best be answered by examining the variation of the S-wave velocities and the associated elastic moduli. The expected effect of the preceding three mechanisms on the S-wave velocities would be as follows:

1) In a transition from weathered to unweathered rock, Vs would increase at the boundary, since the shear modulus would increase as the rock became more rigid. Poisson's ratio would most likely increase if the transition occurred in dry rock, and decrease if it occurred in saturated rock.

2) In a transition from unsaturated to saturated rock, Vs would remain the same across the boundary, since the shear modulus is almost independent of the fluid saturation (Nur and

Simmons, 1969). Poisson's ratio would increase at the boundary.

3) The closing of macrocracks would not be responsible for a sharp change, but there would be an overall gradational increase in Vs associated with the crack closures in response to the increasing confining stresses.

4) If more than one mechanism is responsible for an increase in Vp, additional independent parameters would have to be considered before reaching a conclusion. For example, core samples and drilling rate can identify weathered and fresh rock, determination of the local water table can separate the saturated from unsaturated zones, and well logging techniques such as ultrasonic televiewing (Zoback, 1979) can identify fractures in the borehole walls before the well is cased.

Since it has been shown that Vp alone is insufficient to determine the cause of the velocity increase, this topic will be delayed until S-waves are discussed in the next section.

S waves

The efforts to recognize shear arrivals produced by horizontal traction have not been very successful. A variety of methods were attempted with only limited results.

The most widely accepted technique for determining the onset of an S-wave is to look for a signal polarity reversal between events initiated on opposite ends of the horizontal traction beam (Figure 7a). Because horizontally polarized SH waves are generated, the reversal will be produced on the borehole geophone aligned parallel to the beam. However, several factors can be mentioned which may be responsible for the variation in seismic signature encountered throughout a well. Contributing to the diverse nature of the signals was the absence of a clamping device, such as spring steel or an inflatable diaphragm, to secure the geophone package against the casing. The amplitude of the signal would be strongest when the package rested against the case but weaken considerably when it hung free in the well. Another factor was the inability to orient the downhole package to insure that one geophone was always parallel to the beam. Gibbs et al (1976) used a declinometer to align the geophones, but this technique is expensive. This alignment may not prove as much of a problem if the data are recorded digitally. A parallel trace may be obtained by vector summing the two horizontal traces if the angle between the beam and the axis of a geophone are known. In theory, analog records may be digitized for analysis, but the volume of data in this study, combined with fluctuation in signal amplitude and character, precludes this option.

Many "reversals" were observed which were offset by as much as 5 to 8 msec, or almost a half wavelength (Figure 7b). For example, an easily identifiable sequence of peak - trough - peak would occur in response to an impact on the right side of the beam, and the left side would produce an inverted sequence on the same trace. One sequence would be delayed, however, such that the first breaks would not coincide on the same time line. Precautions were taken to insure that the beam ends were equidistant from the well, so this phenomena cannot be attributed to an asymmetrical set-up. Perhaps it is due to a very localized, near surface delay below one side or the other, but a lag of up to 8 msec is difficult to explain in this manner.

I set aside my attempts at identifying S arrivals by reversal, and next tried to follow consistent peaks or troughs throughout the well on either of the horizontal traces. This method was hampered not only by the same signal variability as before but also by the increased effect of attenuation with depth. Undoubtedly, the maximum energy imparted by my 9 kg sledge hammer is less than the 30 kg slide hammer used by Gibbs et al (1975, 1976). The effects are more noticeable below 50 meters where the signal to noise ratio is greater. An additional problem encountered with this technique was the systematic disappearance or reversal of an arrival with depth. This is attributed to the geophone slowly rotating in the hole between each depth as the cable is lowered. An inherent danger in this phase-following method is to misinterpret a series of picks as S arrivals when they are actually due to something else.

A third method was tried in which I picked shear events recorded on the vertical geophone. I noticed that there was a similar amount of energy arriving at the vertical sensor later than the P-wave recorded by the weight drops and roughly the same time as the S arrivals on the horizontal geophones. I was not intentionally looking for any conversions, either P-S or S-P, which would require an acoustic boundary. That would presuppose an interface such as a water table to be present, which could not be assumed in all cases. The actual mechanism to detect a horizontally polarized shear event on a vertical geophone is not understood, but I believe that in some cases the energy recorded was due to shear waves. The main advantages to this technique were that the arrivals were generally more distinct than those recorded on the horzontal traces, and there was no disappearance or reversal of an event followed down the hole, because the vertical sensor is not affected by any rotation of the geophone package.

Unfortunately, the results were plagued with ambiguities, with the reasonableness varying from well to well. For example, well SMS yielded V_s = 1.84 km/sec for a Poisson's ratio = 0.40, which is to be expected for saturated rocks situated adjacent to and slightly above Soda Lake playa (Figure 3). On the other hand, well YGR yielded a surface velocity of V_s = 1.96 km/sec, higher than the surface V_p of 1.26 km/sec, which is clearly impossible.

Rather than discard all the S-wave data, I made one last attempt to interpret the few wells which showed some promise. If we have a good S arrival time (T_s) and a corresponding P arrival time (T_p) at any depth, along with the intercept time (T_i) at z=0, we may use the equation

$$(1) \qquad V_p/V_s = 1 + (T_s - T_p)/(T_p - T_i),$$

only if we assume that V_p/V_s, and therefore Poisson's ratio, remains constant throughout the well. This assumption will probably be valid in wells displaying minor velocity changes from top to bottom. Large velocity variations are more likely to be the result of a major variation of physical properties or of an encounter with the water table, either of which would be accompanied by a change of Poisson's ratio. I established the following criteria for using individual S arrivals:

1) Arrivals must be definite first breaks

2) Arrivals must display good reversal

3) The difference between surface and BOH P-wave velocities should be less than 100%

4) Poisson's ratio should remain constant if data from more than one depth is evaluated.

The only wells to meet this criteria are LMT, SMS, and TPK. Wells GAR and HHL failed because of the variable character of the S arrivals, while the others were disqualified on the basis of large velocity changes.

Those arrivals meeting the requirements were picked and are listed in Table A2 in the Appendix. I determined mean arrival times and standard errors for both P and S arrivals, and used the means with the intercept time from the upper layer interval velocity to find Vp/Vs. Poisson's ratio is then computed by

(2) [(Vp/Vs)**2 - 2]/[2(Vp/Vs)**2 - 2].

The limits for Vp/Vs and Poisson's ratios are found by substituting the extreme values for Ts and Tp into the equations. Irregularities in Tp which may contribute to fluctuations in the ratios were smoothed by computing a predicted Tp from the P-wave interval velocity. Figures A9a, A15a, and A16a in the Appendix and Table 4 summarize the results.

Well LMT shows significant variations in Poisson's ratio computed from the observed Tp's, but this is due to P arrival times at the bottom of the well (Figure A9a). The predicted Tp's indicate that Poisson's ratio is constant. Well SMS displays a high Poisson's ratio, similar to that obtained from the method mentioned above. Well TPK remains fairly constant within the 20 meter interval of the two measurements, but the fact that it is increasing indicates possible variations throughout the well.

Due to the inconsistency of any one method to work for all wells, the S-wave data have not contributed as much information as I had hoped. Many important clues concerning the physical characteristics of the rocks are not available without this information. For example, no accurate assessment of the nature of the velocity increase discussed earlier is possible, since wells with more than a 30% P-wave velocity difference from top to bottom were not analyzed for S-waves, and the three wells that were analyzed assumed a constant Poisson's ratio with depth. Recommendations for future work are listed in the conclusions.

DISCUSSION

I. Gradational Velocities - Curve Fitting

One objective of this study is to investigate the hypothesis that seismic velocities in crystalline rock increase gradationally with depth. Several curves with different mathematical characteristics were tested and are compared below. In all cases, the velocity-depth function is obtained by taking the inverse of the first derivative of the time-depth function.

Polynomial Curve

A simple quadratic of the form

(3) $$T = A + BZ + C(Z^{**}2)$$

was fitted to data from each well using a generalized least-squares minimization routine. The equation is linear, thus the coefficients obtained by this method assure that the residuals have been minimized. The coefficient A is the intercept time, B is the inverse of the near surface velocity, and C is the rate at which the curve deviates from the straight line A + BZ at greater depths. The resultant curves are shown in Figures A9b through A17b in the

Appendix, while the velocities and coefficients are summarized in Table 5 and Figure 8.

The time-depth plots in themselves appear to be well suited to the quadratic curves. However, it is the character of the first derivative of a polynomial which leads to the divergent velocities in Figure 8. In this case,

$$V(Z) = 1/(B + 2CZ) \tag{4}$$

the velocity continues to increase until the slope of the quadratic is zero, corresponding to an infinite velocity at $Z = -B/2C$. Values in Table 5 indicate infinite velocities would be encountered at depths ranging from 82 meters in CBL to 268 in GAR. Well LMT did not posses sufficient curvature to be reliably fitted to a quadratic, hence the straight line on the velocity plot.

In spite of the polynomial's simplicity, the sole fact that the velocity goes to infinity for any polynomial renders it inappropriate as a time-depth or velocity-depth function. This example has been included primarily as a reference for the next functions.

Exponential Curve - Minimum Residual

An exponential decay curve of the form

(5) $$T = A + BZ + C\exp(GZ)$$

was next applied to the time-depth data. The associated velocity function is

(6) $$V = 1/\{B + CG\exp(GZ)\}.$$

A significant difference between these formulas and equations 3 and 4 is that these equations are non-linear. The coefficients A, B, C, and G cannot all be determined by a least-squares minimization. The procedure used in this case was to assume an initial value for G (values between 0 and -.35), whereupon the remaining three coefficients could be obtained by regression. The residual would be computed for these coefficients, G would be incremented by a small amount, and the process repeated. If the new residual was smaller than the previous, the iteration would continue; otherwise the best value of G (i.e., the one which would minimize the residual) would be between the previous and current values of G. The process terminated when two consecutive residuals differed by less than 1%, and the coefficients determined with this value for G were selected as the "best" exponential curve which represented the data. An additional difference between polynomial and exponential decay functions is that the exponential fits the slope of the straight line to arrival times at greater depths. Thus, the physical significance of B is that it represents the inverse of the BOH velocity, rather than near surface velocities as in the polynomial. Coefficient A is the time intercept for the straight line, A+C is the intercept of the actual curve, and the term Cexp(GZ) determines the rate at which the curve deviates from the straight line at shallow depths. The time-depth curves are shown in Figures A9c through A17c in the Appendix and the velocities and coefficients are summarized in Figure 9 and Table 6.

A quick glance at the time-depth curves indicates qualitatively that the fit to the data is acceptable in all cases except for GAR and YGR, which display negative intercept times. However, Figure 9 reveals that while 4 of the wells converge to a reasonable BOH velocity, the others appear to be diverging from valid BOH velocities at different rates. A clue may be found in Table 6 where the coefficients for LMT, CBL, and SMS are markedly different from the others, especially the negative values for B. No other obvious relationship between the coefficients appeared to exist that would distinguish between those wells which converge to or diverge from a realistic final velocity, and again I had fallen into the trap of assuming a mathematically proper time-depth function would always produce a physically reasonable velocity function.

At this point several other functions were applied to the data, including a logarithmic equation of the form

(7) $$T = A + BZ + C\{LN(Z+G)\}$$

and what I have designated a "pseudopolynomial" of the form

(8) $$T = A + BZ + C(Z**G).$$

Both of these are nonlinear equations, requiring the value of G to be determined by iteration. Typical choices for G ranged from 1 to 15 for the logarithmic equation to between 1 and 2 for the pseudopolynomial. These curves proved inappropriate either because they failed to posess an asymptotic velocity or the asymptotic velocity was physically improbable. I decided the best course of action would be to analyze the mathematical properties of the various functions I was applying to the data to determine if the velocity would behave properly throughout the well. The second derivative of the velocity function provided the necessary insight by revealing whether there was an inflection point in the velocity curve. An inflection would denote a depth at which the rate of change in velocity would reverse sign, and either increase to an infinite velocity or decrease asymptotically to a fixed value. I have designated this depth the "slowdown depth", indicating the desirable nature of deceleration at this point in order to approach a reasonable velocity at greater depths.

All functions have been checked for slowdown depths.

Keep in mind that it is not the third derivative of the original time-depth function which is analyzed, but instead the second derivative of the velocity function obtained from the time-depth curve. In summary:

1) The quadratic possesses neither a slowdown depth nor an asymptotic value;
2) The logarithmic does not possess a slowdown depth, but has an asymptotic velocity = 1/B;
3) The pseudopolynomial possesses an inflection point, but it is the depth at which acceleration occurs. It does not approach a final velocity;
4) The exponential has both a slowdown depth at

$$Z^{*} = \{\ln B - \ln|G| - \ln|C|\}/G \tag{9}$$

as well as an asymptotic velocity = 1/B.

In light of this information, the unusual behavior of the exponential curve may now be understood. Those wells which possessed reasonable velocity curves were characterized by slowdown depths which were near the interval velocity breaks, while the others had slowdown depths which were either undefined (the coefficient B was negative) or much deeper than the interval velocity break.

The concept of a slowdown depth makes sense. The velocity must be allowed to increase with depth, even to the extent of accelerating with depth, and yet still not exceed a physically limited velocity at some greater depth. Also, an inflection point in the velocity curve should be expected if the travel-time data indicates an abrupt change in velocity at some depth. With this information at hand, an additional attempt was made at fitting the time-depth data to an exponential curve.

Exponential Curve - Subjective Fit

In this case, it was not required that the coefficient G in the equation

$$T = A + BZ + C\exp(GZ) \tag{5}$$

be obtained by minimizing the residual, but instead was determined by a subjective process which took many factors into account. A least-squares technique was still used, and a wide range of values for G (0 to -.35) was tried for each well. The final values of G were selected based upon the following criteria:

1) the rate of change of velocity with depth (obtained by differentiating the velocity function) at the top of the hole must be greater than at the bottom, indicating that the velocity is asymptotically approaching the value 1/B;
2) The time intercept (A+C) must be a positive number;
3) The slowdown depth should occur as near the

interval velocity break as possible, or at least at some point below the ground surface;

4) The BOH velocity from the curve should approximate the BOH interval velocity, within the standard errors if possible;

5) The residuals should be as close to minimum as allowable, subject to the other criteria.

As an observation, values of |C| less than .005 indicate that the exponential term Cexp(GZ) is not greatly significant in the curve fitting process, and that most values chosen for G would be satisfactory, assuming the five conditions were met.

The results of this subjective fitting are shown in Figures A9d through A17d in the Appendix, while the velocities and coefficients are summarized in Figure 10 and Table 7. Quantitatively, the fit is generally better than the polynomial curves but poorer than the exponential curve obtained by minimizing the residuals. However, increasing the residuals by a slight amount is a small price to pay to avoid physically meaningless values for slopes and intercept times.

There is a significant comparability of velocity-depth profiles between the interval velocities in Figure 6 and the exponential velocities in Figure 10. The lowest and highest velocity wells, GAR and CBL respectively, maintain their relative ranking. There is some interchange of rank among the intermediate velocity wells, based upon the asymptotic velocities. SPH has moved from the second lowest interval velocity to the mode by increasing from 3.8 to 5.1 km/sec, which is the result of the curve being fit to the apparent high velocities in the bottom 10 meters of the hole. SMS has advanced 2 places, also due to the effect of data points near the bottom of the hole. The downward shift of LMT can be attributed to the general overall trend toward higher velocities. The mean BOH velocity is 4.62 $\pm$ 0.86 km/sec, up 0.2 km/sec from the mean BOH interval velocity, while the mean asymptotic velocity is 4.80 $\pm$ 0.90 km/sec.

An obvious question must now be asked - are these velocity gradients a realistic representation of the true velocities encountered in the well, or are they simply a product of the mathematical properties of the exponential curve? To answer this question, the physical significance of the four coefficients must be firmly established. The equations again are:

(5) $$T = A + BZ + C\exp(GZ), \text{ and}$$

(6) $$V = 1/\{B + GC\exp(GZ)\}.$$

First, let us assume that G is negative in our case; this will be shown later. At very large values of Z the exponential term will vanish, leaving $T = A + BZ$, which represents a straight line through arrival times at great depths. Coefficient A is the intercept time of this asymptotic straight line, B is its slope, and from the lower equation we see that 1/B is the asymptotic velocity value. When Z=0, the equations reduce to

(10) $$To = A + C$$

(11) $$Vo = 1/(B + GC)$$

Coefficient C is the correction to intercept time A which takes into account the near surface velocities so that C = To - A. The product GC is the maximum deviation at the surface from the asymptotic slope B, so that the slope of the time-depth curve at the surface is equal to B + GC. Solving for G,

(12) $$G = (\text{near surface slope} - B)/C$$

If we call the near surface slope Bo and substitute To - A for C, we obtain the expression

(13) $$G = (Bo - B)/(To - A)$$

which reveals G as the ratio of the difference in slopes to the difference in intercept times between the surface and great depths. Since G has the units of (1/meters), it is also a depth dependent factor in the exponential, and indicates the sensitivity of the velocity variation with depth. In all cases where the velocity increases with depth, either abruptly or gradually, Bo will be greater than B while To will be less than A, resulting in a negative value for G.

This raises a subsidiary question - can the coefficients A, B, C, and G be determined empirically from interval velocities such that they both fit the time-depth data and yield reasonable velocities within acceptable statistical limits? To answer this, the original slopes and times intercepts from the seven wells which displayed an interval velocity difference between the top and bottom were used to calculate the coefficients. These are tabulated in Table 8, with the empirical curves in Figures A9e through A17e and the velocity-depth functions plotted in Figure 11.

In general, the empirical curves predict earlier arrival times near the velocity break than do the interval velocities. This should be expected, because the starting and ending slopes of the curve are constrained to those of the straight line segments. Qualitatively, the curves do not appear to fit the data closely except for FPK, TPK, and perhaps YGR. Quantitatively, however, we run into difficulty in applying statistical criteria. The ineffectiveness of the correlation coefficient was noticed and therefore deleted from Table 8 since the values computed were greater than the theoretical maximum of 1. This disparity is due to the requirement that the coefficients be the result of a linear regression analysis in which the residuals have been minimized, and that was not the case here. The correlation coefficient is defined (Romano, 1977, p 164) as

$$(14) \quad = \sqrt{\frac{\text{sum of (predicted value - mean value)**2}}{\text{sum of (observed value - mean value)**2}}}$$

and if the predicted values are consistently farther from the mean than the observed values, the correlation coefficient exceeds the limit of 1. A potential measure of "goodness of fit" is to compare the minimum residual obtained by the first pass with the exponential curve with the empirical residual, expressed as a percent increase. As seen in Table 8, the percent increase ranges between 38% and 178%.

What constitutes an acceptable fit? Based upon inspection of the plots and of Table 8, some admittedly arbitrary guidelines may be established for an acceptable empirical fit:

1) The curve should not substantially <u>overestimate</u> the near-surface velocity beyond the upper layer interval velocity value.
2) The residuals should increase by no more than 50% over the minimum residual obtainable by an exponential curve.
3) The correlation coefficient for the original minimum residual curve should exceed 0.99, indicating a good exponential fit is possible.

Likewise, arbitrary guidelines may be established for an acceptable subjective fit:

1) The criteria enumerated on page 28 must be satisfied.
2) The curve should not substantially <u>underestimate</u> the near-surface velocity below reasonable values, such as those obtained from short refraction surveys.
3) The residuals should increase by no more than 5 - 10% over the minimum residual obtainable by an exponential curve.
4) The correlation coefficient for the original minimum residual curve should exceed 0.99.

The initial question remains to be answered: are the velocity gradients real or apparent? The mere fact that an exponential curve may fit the data to within certain statistical limits does not prove the presence of a velocity gradient, but a satisfactory fit both subjectively and empirically strongly supports its existence. On the other hand, the ability to make velocities "behave", such as shown between Figures 9 and 10, implies that the gradients are as probably a product of mathematics as of reality. This "taming" is especially evident in the criteria for subjective fitting on page 28, which permits some freedom to choose the asymptotic velocity to be close to the interval BOH velocity, inferring that this velocity is both accurate and the maximum permissible. In any attempt to derive a velocity-depth relationship from the data, the results are always sensitive to the assumed functional form. For example, variations in G of around 10% may change the residual by less than 1%, but the near surface velocity can fluctuate by 4% and the asymptotic velocity may change by up to 10%. Hence, when the minimum residual requirement is abolished, there is no absolute standard to verify the accuracy of the velocities obtained.

II. Surface Refraction - Crustal Studies

The application of downhole velocity measurements to both short refraction surveys and crustal studies should be considered. In theory, surface refraction results interpreted as velocity-depth relationships should be directly correlatable to velocity-depth functions determined from downhole studies. However, surface refraction possesses several inherent ambiguities which might place limitations on these comparisons. Weathering and elevation corrections, as well as delay times (Dobrin, 1960), must be considered to account for near surface inhomogeneities. More importantly, it is unlikely that both techniques sample the same regions of rock. It is not always appropriate to assume that the velocities and physical properties will be uniform over the extent of a refraction spread large enough to interrogate to depths comparable to a well. Nevertheless, the two techniques have been used to determine velocities independently, primarily in engineering geology. Warrick (1974), for example, measured P and S-waves in San Francisco Bay muds with surface and downhole methods and found satisfactory agreement of velocities.

Surface refraction could be used to verify the velocity breaks detected by downhole measurements.

Straightforward horizontal layered interpretation for both P and S-waves would be more difficult in those locations where the downhole velocity displayed only minor variations. In these cases a gradational velocity increase with depth analysis could be applied, such as the Wiechert - Herglotz - Bateman, or WHB, integral method (i.e., Grant and West, 1965; Leet, 1938; Slichter, 1932). An intrinsic drawback of this method follows from the inversion process of working from the surface downwards, yielding the highest velocity possible at any depth (Healy, 1970). The data must be smoothed to eliminate any apparent inhomogeneities, but the resultant velocity-depth function should be comparable with those found by well measurements.

The WHB integral method has been successfully tested with data from a trial velocity model. Stierman (oral communication) assumed a velocity-depth function and, with the help of a ray tracing program, computed the travel time, horizontal distance, and depth of penetration for a number of rays with different take-off angles from the source. I wrote a WHB integral program to convert the travel time-distance data into velocity-depth data, and the computed velocities agreed to within 3% of the values from the original velocity-depth function. This example estimates the degree of correlation which might be expected between velocity data from well measurements and that inferred from surface refraction surveys.

The Stone Canyon well has been the site for investigations of _in situ_ velocities in the quartz diorite of central California's Gabilan range, adjacent to the San Andreas fault. Stierman and Kovach (1979) conducted sonic logs and downhole travel time measurements in the 600 meter deep well. Velocities ranging from 2.8 to 3.5 km/sec were encountered between 50 and 580 meters down the hole, with an increase to around 4 km/sec at the bottom. Surface refraction surveys were conducted in the area by Stierman _et al_ (1979). Short profiles were used to determine the overburden thickness, while an intermediate length (6 km) refraction line supplied data for a complex model of the upper 1 km of the crust. The velocity in the vicinity of the well is 3.08 km/sec, while near the bottom of the hole it is set at 3.98 km/sec. These velocities are in good agreement with those obtained from well logs.

Crustal studies are often extensions of the seismic refraction method, employing either large explosions with profiles from 100 to 400 km long, or earthquakes and seismometer arrays. However, before continuing this comparison between velocities in shallow boreholes and crustal velocities, let us first contemplate some observations by Healy (1970) concerning crustal models. A ray path between the source and receiver passes through rocks with a broad spectrum of physical properties. These properties may be averaged for any depth or range of depths, resulting in the typical model consisting of "layers". However, we must remember that these properties and thicknesses must be treated as statistical figures with varying degrees of reliability, rather than absolute layers of uniform character. Despite the remarkable consistency of these average properties throughout North America, attempts to obtain greater detail are usually rewarded with greater complexity than the data are capable of resolving. For example:

> "The surface of the earth is composed of a great variety of rocks with low seismic velocity and complex structure. These rocks are either sedimentary rocks, whose velocity may increase rather regularly with depth, or fractured crystalline rocks, which may have an extremely erratic velocity structure. Although this uppermost layer is not very thick, its low velocity and its extreme complexity produce effects that can be compared to a frost on the surface of an optical system which scatters the wave energy and makes it difficult to focus precisely on the details below" (Healy, 1970).

With these thoughts in mind, let us now turn to some of the crustal studies conducted in the Mojave Desert.

Kanamori and Hadley (1975) recorded quarry blasts to compute a representative velocity structure for southern California. The principal profile establishing the upper crustal structure stretched 100 km across the western Mojave towards Los Angeles. The model deduced from this data consists partly of a top layer 4 km thick with Vp = 5.5 km/sec underlain by 6.3 km/sec material extending to a depth of 27.4 km. In light of the previous paragraph, how does this model fit the P-wave velocities in this report? If we consider the subjective and interval BOH velocities of the 5 western wells, we find that only CBL and FPK approach the 5.5 km/sec value for Kanamori and Hadley's upper layer (1975). What are some of the explanations for the rest of the wells falling considerably short of this value?

Both Kanamori and Hadley (1975) and Stierman and Kovach (1979) discuss dilatancy as a possible mechanism for lower than average velocities, while Stierman and Kovach (1979) prefer the failure of macrocracks to close at depth. Both of these conditions may be initiated or maintained by a deviatoric stress field, usually associated with a tectonically active setting such as a fault zone and adjacent regions. Upon comparing the various velocity models developed in each well from Tables 3 and 5 through 8 with distances from the Garlock fault in Table 2, a correlation between velocity and distance from the fault becomes evident. Let us therefore examine the five western Mojave wells situated within Kanamori and Hadley's (1975) study area for a velocity dependence upon distance from a fault. We will exempt the four eastern Mojave wells from this analysis since the tectonic setting here is not as clear as in the western half.

What type of relationship might be expected if the near-surface velocity increases with distance from a fault? The function must be constrained both on the low and high ends, corresponding to the velocity at the fault and the velocity at some distance beyond the influence of the fault. An inverse or inverse-square relationship might be suggested, but these fail to behave near the fault where the distance x is small. The ideal function is the simple exponential,

(15) $$V(x) = Vf - V\{exp(-ax)\}$$

ich satisfies the condition for well defined initial and final velocities. In this case, at x = 0,

(16) $$Vo = Vf - V$$

and at x = great distance,

(17) $$V = Vf.$$

As was the situation in the previous curve fitting efforts, the value of "a" must be determined iteratively.

A significant decision must be made concerning which velocities to use in the curve fitting. Obvious candidates are the lower interval velocities, the velocities of the subjectively fitted exponential curves evaluated at a common depth, and the asymptotic velocities. All three groups of velocities have been modeled individually as well as compositely. The results are displayed in Table 9 and Figure 12.

The interpretation of these results must be approached with caution since the small sample size (5 wells) and the one degree of freedom reduces the significance of the correlation coefficient. The lower interval velocity yields the poorest fit while the asymptotic velocity of the subjective exponential displays the best correlation. Both of these have final velocities Vf = 5.7 km/sec, slightly higher than Kanamori and Hadley's (1975) model of 5.5 km/sec. This is influenced by the high velocities encountered in the bottom of CBL, velocities which have a greater margin of error than in other wells (i.e., Table 3). I decided to keep the data from CBL, rather than eliminate it and thereby reduce my sample size by 20%.

The last column in Table 9 denotes the distance at which the velocity is within 1% of the final velocity. The distances vary between 22 and 38 km, with 3 out of 4 wells in the 20-30 km range. These values are perhaps affected by the last two data points from CBL and FPK occurring at distances of 24 and 24.4 km, respectively. But on the basis of available data, I believe the evidence indicates that an active (Quaternary) strike-slip fault such as the Garlock reduces the seismic velocities of rocks up to 20 or 30 km from the fault trace. This could very well be one of the contributing factors towards the "extremely erratic velocity structure" of crystalline rocks (Healy, 1970). However, the evidence is unclear if there is a similar relationship between velocity and distance from the Blackwater fault, where the motion has been primarily dip-slip (Hewett, 1954b).

A shallow crustal velocity study of an eastern Mojave site was conducted by Hileman (1979). 20 aftershocks were used in a maximum likelihood, least-squares inversion to minimize hypocenter location uncertainties. A number of velocity models were employed in which the layer boundaries were fixed and the velocities were allowed to vary in the minimization process. He found each of the trials indicated upper layer (1.5 km) velocities on the order of 4.5 to 4.9 km/sec, somewhat lower than those of the usual velocity models. The velocities are not greatly constrained by the data, but are in general agreement with those of the eastern Mojave wells reported here. The mean BOH interval velocity for HHL, SMS, TPK, and YGR is 4.40 ± 0.37 km/sec, while the mean asymptotic velocity from the subjectively fitted exponential is 4.70 ± 0.68 km/sec. In fact, the averages for all wells mentioned earlier also agree with these slower near-surface crustal velocities.

It is difficult to determine the standard error for Hileman's (1979) velocities, but Kanamori and Hadley (1975) included the travel time data for velocity computations. Working through their values, the standard error for the upper layer places the velocity between 5.42 and 5.57 km/sec, based upon 3 data points and the origin. This is not enough error to state that the two crustal models are similar, and so we are faced with the likelihood that the velocity structure in the eastern Mojave is significantly different from that in the western Mojave. In spite of the fact that the mean velocities in the 5 western wells are comparable to the means in the eastern, my conclusion is that the velocity characteristics indeed differ. The western Mojave velocities measured in this study are dominated by the influence of the Garlock fault, lowering the near fault well velocities enough to drop the mean below the regional average of 5.5 km/sec.

III. Comparison of Laboratory and Field Studies

Let us now turn to a comparison between *in situ* studies and laboratory measurements of seismic velocities. Table 10 is a summary of laboratory work on granitic rocks by Nur and Simmons (1969) and Feves *et al* (1977), showing Vp and Vs for both dry and saturated states at near-surface confining pressures. There are various standard errors which arise from averaging velocities, both within a study group by an author and between study groups by different authors. Significant differences between the two sets of data occur for dry and saturated Vp values at zero pressure. These could be due to different measurement techniques or variations between individual samples of the same rock type, as indicated by differences for Vp in dry Westerly granite of over 20% (Nur and Simmons, 1969; Feves *et al*, 1977). Thus, laboratory values cannot be used as absolutes in determining velocities, but instead should be viewed statistically when a sufficient number of samples are included.

Laboratory results can be compared to field studies if pressures are converted to depths. Assuming the external stress to be equal to lithostatic pressures (= 262 bar/km) and the pore pressure to be equal to hydrostatic pressure (

= 98 bar/km), the depth at which the effective stress (= external pressure - pore pressure) is equal to 100 bars is 380 meters for dry rock and 610 meters for saturated. We should definitely expect velocities from the Mojave wells to come within the ranges in Table 10, probably closer to values for 0 bar. Thus, the predicted P-wave velocities should fall between 3.64 and 5.50 km/sec for dry rocks and 5.40 to 6.06 km/sec for saturated rocks.

Compare these velocity ranges with results by other workers in Table 1. If the setting for each of these studies is known, then all velocities are lower than predicted by laboratory values. The first 3 entries by Leet and Ewing (1932) are the products of seismic waves generated by shots usually located in quarry ponds, a likely indication of saturated rocks. The depth of penetration was around 20 meters, so comparing these velocities with the laboratory values for 0 bar reveals _in situ_ velocities 10% lower than expected. Carrol _et al_ (1966) and (most likely) Nicholls (1961) conducted their studies in deep tunnels, where the pressures would be expected to approach 100 bars. These velocities match the mean laboratory value for dry rocks, but if the tunnels are saturated (as might be expected at depth), the velocities are 10% below the predicted values.

Other studies comparable to this report (Gibbs _et al_, 1975, 1976; Stierman and Kovach, 1979) have also reported lower than predicted velocities in wells. One feature common to these efforts is the location of the field areas in tectonically active regions.

Consider now the BOH interval velocities for the Mojave wells, listed in Table 3. All but GAR fall within the predicted range for dry surface rock, while only CBL is within the limits for saturated rock if we overlook its large standard error. But are these rocks really dry? In terms of hydrology, these granitic rocks would probably be classified as aquicludes (Ward, 1975), indicating the characteristic of being porous and capable of absorbing water slowly, but not able to transmit it in appreciable quantities. It seems reasonable to assume that if the rocks are situated below the water table, they should be saturated. Evidence of clear velocity breaks most likely caused by the water table and occasional notes in the driller's logs indicate the wells penetrate the water table. The concept of "dry" rocks is the product of laboratory procedures which for many years would thoroughly vacuum dry a sample at high temperatures for hours before measurements. Thus, if we conclude the rocks at the bottom of the wells are saturated, we must speculate on other mechanisms to account for the disparity between laboratory and downhole velocities.

Weathering cannot be eliminated from consideration. Sharp (1954) stated that the coarse-grained quartz monzonite of Cima Dome near well TPK disintegrates more rapidly and uniformly under desert conditions than a nearby medium-grained granite. Weathering undoubtedly contributes toward some of the near surface velocities less than 2 km/sec (wells YGR, FPK; also Digges Canyon and North Peak in Table 1, Gibbs et al, 1975). But inspection of surface outcrops and chip samples reveals only slight to moderate alteration of the feldspars to clay minerals. Chemical weathering in a hot dry climate such as the Mojave Desert is probably the least significant factor affecting velocities of deeper rocks.

Fracturing appears to be the most probable mechanism for lower than expected velocities. To understand why, let us review the theoretical basis, laboratory evidence, and confirmation by in situ measurements.

Walsh (1965) developed the theoretical framework for the effect of fractures on P-wave velocity. He found that flat cracks are more efficient at increasing the compressibility of a rock than spherical (ie, intergranular) pores of the same total volume. He explained the pressure dependence of the bulk modulus by showing that flat cracks close much more readily and completely than spherical pores. Since compressional wave velocities are directly related to the bulk modulus, lower velocities would be expected for rocks with greater crack volume.

Nur and Simmons (1969) produced the laboratory evidence supporting this theory, forming the basis of the microcrack hypothesis. They determined the need to measure both the pore and crack porosity in low porosity rocks such as granites, and reported a direct correlation between the difference in dry and saturated P-wave velocities versus crack porosity. Thus, the microcrack hypothesis appears a suitable explanation for the effect of saturation and pressure on seismic velocities.

Major drawbacks of laboratory studies should be mentioned. The sample size is often too small when compared to the relative heterogeneity which might be expected in any area. Measuring a great number of small samples is not comparable to measuring a few large samples. Another problem is that only the more competent cores may be used for analysis. Either the less competent cores are not recovered from the well or contain large fractures which preclude them from laboratory analysis. On the basis of theoretical evidence, we would expect larger fractures to increase the compressibility even more, but the laboratory has proven an impractical setting for testing this idea.

The field appears a better laboratory in this case, and has confirmed the effect of larger fractures on compressional velocity. Stierman and Kovach (1979) interpreted the difference between the core density and the in situ density inferred from a borehole gravity survey as arising from a significant fracture porosity rather than pore porsity. The fractures were thought to be responsible for a 30 to 50% reduction of seismic velocities. Sjogren et al (1979) related P-wave velocity to the number of cracks per meter encountered in core samples from a suite of igneous and metamorphic rocks. Seismic velocities appear to have the potential for yielding estimates as to the extent of fracturing of rock formations. The reliability of the estimate increases when Poisson's ratio is also considered, which of course entails the measurement of S-wave velocities.

Fractures occur naturally for a variety of reasons. Zoback (1979) reported the fracture distribution of a well in granite located 3.7 km from the San Andreas fault near Palmdale, California. In this well the distribution averaged 8 to 12 cracks/10 m above 150 meters, with a sharp decrease in occurrence below that to 2 or 3 cracks/10 m around 250 meters. The presence of these fractures could be explained as the result of weathering, cooling after emplacement, or uplift. They could also be the product of shear motion associated with strike-slip or thrust faulting (Zoback, 1979).

Finally, what is the application of this information to the Mojave wells? In the western wells, I expect greater fracturing in strike-slip regions than in normal dip-slip regions, based upon the evidence by Hewett (1954b) for limited displacement on the dip-slip faults and that for great lateral displacement on the Garlock by Smith (1962). I believe a domain with a vertical maximum principal stress, such as near a normal fault, would be less likely to exhibit a regional fracture distribution than a domain with either a vertical minimum principal stress (thrusting) or intermediate principal stress (strike-slip). This idea has been confirmed by the dependence of velocity upon distance from the Garlock fault stated in the previous section, whereas the Blackwater fault fails to display a similar influence.

The eastern Mojave is a more complex setting, but extensive thrust faulting subsequent to the igneous intrusion (Hewett, 1954a, 1954b) may have caused widespread regional fracturing, resulting in both a homogenization of the physical properties of the crustal rocks and a relative lowering of crustal velocities. This speculation is supported by velocities in the eastern wells being more uniform and not being influenced by any one fault. However, fractures in tectonically dormant areas will heal if given sufficient time, and thus it does not appear likely that fracturing is the only mechanism responsible for the lower velocities encountered here. A suitable explanation for the difference in crustal velocities between the eastern and western Mojave as well as the hypothesis of extensive fracturing in the eastern Mojave deserves additional research.

CONCLUSIONS

Downhole velocity surveys are an efficient and unambiguous method for investigating the near surface velocity structure of crystalline rocks. The average total time for 2 people to conduct a complete survey of a 100 meter well is approximately 5 hours from setup to packing up and relocating. This method necessitates drilling in crystalline rocks at a cost in the neighborhood of $4000 to $5000 for a 100 to 250 meter well (Zoback, 1979; Tien Lee, oral communication). The expense of drilling encourages logging of existing holes and multiple use of new ones.

This survey of the near surface velocity structure of the Mojave Desert reveals that the western and eastern sections have different velocities due to their associated tectonic environments. The western regional near surface velocity is 5.5 km/sec, with the major factor lowering the measured velocities being the compressional fractures arising from strike-slip faults such as the Garlock. P-wave velocity is reduced exponentially with greater proximity to the fault, with a projected lowest velocity at 2 km/sec. The eastern regional near surface velocity is around 4.7 km/sec, which is probably due to a more complex tectonic setting. I postulate that fracturing is more widespread in the east since the regional thrusting was contemporaneous with emplacement of the igneous bodies.

The data was not recorded with sufficient resolution to firmly establish a velocity gradient. However, an exponential decay curve with subjectively determined coefficients appears to be best suited to both fit the original time-depth data and yield an appropriate velocity-depth relationship.

Recommendations for future work are as follows:

1) Replace the current amplifier/camera setup by a signal enhancement system with both hard copy and digital recording capabilities. This should improve resolution with a smaller sampling interval and allow the stacking of several events into one record per depth. The digital recorder would permit analytical determination of the geophone orientation for shear events.

2) Install a clamping device on the downhole geophone. An inflatable diaphragm looks promising, since it only requires a bladder, compressed air, and a large amount of tubing. There should be no problems with getting stuck in the hole, and difficulties encountered with over-buoyancy in water-filled holes could be

overcome by replacing the air with a fluid.

3) Replace the timing system with something less susceptible to noise. Inertia or impact related switches would be suitable.

4) Investigate the need for a larger shear wave generator. It is unclear if a larger device is required, because other problems in this survey nullified the effect of a heavier hammer. Possibilities include a slide hammer similar to Gibbs et al, (1975, 1976), or a massive pendulum with a short, rigid arm to fully utilize the conversion of potential to kinetic energy.

REFERENCES

Birch, F. (1960), The velocity of compressional waves in rocks to 10 Kb, part I, J. Geophys. Res., vol 65, 1083+.

Carroll, Roderick D., J. H. Scott, and D. R. Cunningham (1966), Elastic moduli of granitic rock from in situ measurement of seismic velocity, U. S. Geological Survey Professional Paper 550-C, pp C25 - C28.

Dibblee, T. W. Jr., and D. F. Hewett (1970), Geology of the Mojave Desert, Calif Div. Mines and Geol., Mineral Information Service, Vol. 23, no. 9, pp 180 - 185.

Dobrin, Milton B., (1960), Introduction to Geophysical Prospecting, McGraw-Hill, New York.

Feves, M., G. Simmons, and R. W. Siegfried (1977), Microcracks in crustal igneous rocks: Physical properties, in J. G. Heacock, ed., The earth's crust; Its natural and physical properties, American Geophysical Union Geophysical Monograph 20, pp 95 - 117.

Gibbs, James F., T. E. Fumal, and R. D. Borcherdt (1975), In situ measurements of seismic velocities at twelve locations in the San Francisco Bay region, U. S. Geological Survey Open File Report 75-564.

Gibbs, James F., T. E. Fumal, and R. D. Borcherdt (1976), In situ measurements of seismic velocities in the San Francisco Bay region, Part II, U. S. Geological Survey Open File Report 76-731.

Gogonenkov, G. N., and P. D. Shlychkin (1969), Seismic properties of a crystalline basement in the light of deep borehole measurements, Izvestiya (Physics of the Solid Earth), vol 8, August, pp 486 - 490.

Grant, F. S. and G. F. West (1965), Interpretation Therory in Applied Geophysics, McGraw-Hill, New York.

Healy, J. H. (1970), A comment on the evidence for a worldwide zone of low siesmic velocity at shallow depths in the earth's crust, in Heacock, J. H., ed., The structure and physical properties of the earth's crust, American Geophysical Union Geophysical Monograph 14, pp 35 - 40.

Hewett, D. F. (1954a), General geology of the Mojave Desert region, California, in Jahns, R. H., ed., Geology of Southern California: Calif. Div. Mines Bull. 170, vol II, p 5 - 20.

Hewett, D. F. (1954b), A fault map of the Mojave Desert region, in Jahns, R. H., ed., Geology of Southern California: Calif. Div. Mines Bull 170, Vol IV, p 15 - 18.

Hileman, James A. (1979), Inversion of phase times for hypocenters and shallow crustal velocities, Mojave Desert, California, Bull. Seismol. Soc. Amer., vol 69, pp 387 - 396.

Kanamori, Hiroo, and David Hadley (1975), Crustal structure and temporal velocity change in southern California, Pageoph, vol 113, pp 257 - 280.

Kobayashi, N. (1959), A method of determining the underground structure by means of SH waves, Zisin, ser. 2, vol 12, no. 1, pp 19 - 24.

Leet, L. Don, and W. Maurice Ewing (1932), Velocity of elastic waves in granite, Early Geophysical Papers, vol 1, pp 202 - 215.

Leet, L. Don (1938), Practical Seismology and Seismic Prospecting, Appleton-Century-Crofts, New York

Nicholls, Harry, R. (1961), In situ determination of the dynamic constants of rock, U. S. Bureau of Mines, Report of Investigations, 5888, 13 pages.

Nur, Amos, and G. S. Simmons (1969), The effect of saturation on velocity in low porosity rocks, Earth and Planetary Sci. L., vol 7, pp 183 - 193.

Romano, Albert (1977), Applied Statistics for Science and Industry, Allyn and Bacon, Inc., Boston.

Sass, J. H., S. P. Galanis, Jr., B. V. Marshall, A. H. Lachenbruch, R. J. Munroe, and T. H. Moses, Jr. (1978), Conductive heat flow in the Randsburg area, California, U. S. Geological Survey Open File Report 78-756.

Sharp, Robert P. (1954), The nature of Cima Dome, in Jahns, R. H., ed., Geology of Southern California: Calif. Div Mines Bull. 170, vol V, pp 49 - 52.

Simmons, Gene, and A. Nur (1968), Granites: relation of properties in situ to laboratory measurements, Science, vol 162, pp 789 - 791.

Sjogren, B., A. Ofsthus, and J. Sandberg (1979), Seismic classification of rock mass qualities, Geophysical Prospecting, vol 27, pp 409 - 442.

Slichter, L. B. (1932), Interpretation of seismic travel-time curves in horizontal structures, Physics, vol 3, pp 273 - 295.

Smith, G. I. (1962), Large lateral displacement on the Garlock fault, California, as measured from an offset dike swarm, Amer. Assoc. Petrol. Geol. Bull., vol 46, pp 85 - 104.

Stierman, D. J., J. H. Healy, and R. L. Kovach (1979), Pressure induced velocity gradient: an alternative to a Pg refractor in the Gabilan Range, central California, Bull. Seismol. Soc. Amer., vol 69, pp 397 - 415.

Stierman, D. J., and R. L. Kovach (1979), An in situ study: The Stone Canyon well, J. Geophys. Res., vol 84, pp 672 - 678.

Swain, R. J. (1962), Recent techniques for determination of in situ elastic properties and measurement of motion amplification in layered media, Geophysics, vol 28, pp 237 - 241.

Walsh, J. B. (1965), The effect of cracks on the compressibility of rock, J. Geophys, Res., vol 70, pp 381 - 389.

Ward, R. C. (1975), Principles of Hydrology, McGraw-Hill, London.

Warrick, Richard E. (1974), Seismic investigation of a San Francisco Bay mud site, Bull. Seismol. Soc. Amer., vol 64, no. 2, pp 375 - 385.

Zoback, Mark D. (1979), Measurement of in situ stress, natural fracture distribution, and fracture permeability in a well near Palmdale, California, submitted to Workshop on Measurement of Ground Strain Phenomena Related to Earthquake Prediction.

TABLE 1 - SUMMARY OF PREVIOUS IN SITU VELOCITY WORK IN GRANITIC ROCKS

LOCATION AND ROCK TYPE	Vp KM/SEC	Vs KM/SEC	POISSON'S RATIO	DENSITY GM/CC	BULK MODULUS x10**10 DYNE/SQ CM
Quincy Granite 1/	4.96	2.48	.33	2.65	43.5
Westerly Granite 1/	5.00				
Rockport Granite 1/	5.08				
Lithonia Granite Gneiss 2/	5.56	3.15	.26	2.63	46.5
Silver Plume Granite, Col. 3/	5.43	2.71	.33	2.67	52.4
Climax Stock, NTS 3/	5.49	2.74	.33	2.74	54.9
El Granada Q. Diorite 4/	3.85	1.64	.39	2.53	28.4
Digges Can Q. Diorite Grus 4/	1.06	0.55	.32	2.19	1.6
North Pk. Q. Diorite Grus 4/	1.26	0.64	.32	2.30	2.4
Frenchman's Cr. Q. Diorite 5/	3.90	1.94	.34	2.52	25.7
Stone Canyon Q. Monzonite 6/	3.98				

1/ Leet and Ewing (1932)
2/ Nicholls (1961)
3/ Carroll et al (1966)
4/ Gibbs et al (1975)
5/ Gibbs et al (1976)
6/ Stierman et al (1979)

TABLE 2 - WELL DESCRIPTIONS

WELL NAME	NORTH LAT	WEST LON	ELEV M	DEPTH M	ROCK TYPE	DISTANCE FROM (KM) GARLOCK F.	BLACKWATER F.
GAR	37 27.8′	117 33.4′	1164	152	Q. Monzonite	1.8	13.3
LMT	35 31.8′	117 39.2′	1012	106	Granodiorite	7.9	*
SPH	35 33.6′	117 35.1′	1006	101	Granodiorite	9.1	*
CBL	35 18.9′	117 20.2′	1146	76	Q. Monzonite	24.0	4.6
FPK	35 15.5′	117 32.3′	936	102	Granodiorite	24.4	24.1
HHL	35 24.8′	116 03.8′	561	138	Q. Monzonite	**	**
SMS	35 07.6′	116 09.2′	366	107	Granodiorite(?)	**	**
TPK	35 17.3′	115 33.4′	1606	102	Q. Monzonite	**	**
YGR	35 22.2′	115 53.6′	890	102	Q. Monzonite	**	**

* - Located on opposite side of Garlock fault from Blackwater fault.

** - Not applicable to eastern Mojave wells.

TABLE 3 - P-WAVE INTERVAL VELOCITIES

WELL NAME	SURFACE VELOCITY KM/SEC	BOH VELOCITY KM/SEC	DIFFERENCE	% INCREASE	VELOCITY BREAK METERS
GAR	1.33 (1.20, 1.48)*	2.66 (2.59, 2.74)	1.33	100	34
LMT	4.75 (4.50, 5.03)	4.75 (4.50, 5.03)	0	0	--
SPH	1.74 (1.61, 1.89)	3.79 (3.49, 4.15)	2.05	118	47
CBL	2.14 (1.88, 2.47)	5.73 (4.54, 7.78)	3.59	168	39
FPK	1.36 (1.12, 1.73)	5.22 (4.95, 5.53)	3.86	284	15
HHL	2.19 (2.14, 2.25)	4.37 (4.16, 4.61)	2.18	100	67
SMS	4.52 (4.34, 4.71)	4.52 (4.34, 4.71)	0	0	--
TPK	3.09 (2.91, 3.29)	3.91 (3.56, 4.33)	0.82	27	55
YGR	1.26 (1.09, 1.48)	4.82 (4.62, 5.04)	3.56	283	17
mode	2.14	4.52			39
mean	2.49 ± 1.34	4.41 ± 0.89			39

* Numbers in parentheses represent standard errors for velocities

TABLE 4 - Vp/Vs AND POISSON'S RATIO FOR SELECTED WELLS, ASSUMING CONSTANT POISSON'S RATIO WITH DEPTH

WELL NAME	INTERCEPT TIME (SEC)	DEPTH (M)	S ARRIVAL TIME (SEC)	P ARRIVAL TIME (SEC)	Vp/Vs*	POISSON'S RATIO **	PREDICTED P ARRIVAL	Vp/Vs*	POISSON'S RATIO **	INFERRED Vs (KM/S)
LMT	.0143	81.1	.0446	.0315	1.76	.26	.0313	1.78	.27	2.67
			(.0013)	(.0010)	[1.59, 1.95]	[.17, .32]				
		106.1	.0538	.0345	1.95	.32	.0366	1.77	.27	2.68
			(.0020)	(.0021)	[1.68, 2.29]	[.23, .38]				
SMS	.0037	25.7	.0160	.0093	2.20	.37	.0094	2.16	.36	2.09
			(.0012)	(.0014)	[1.59, 3.23]	[.17, .45]				
TPK	.0087	45.7	.0358	.0236	1.82	.28	.0235	1.83	.29	1.69
			(.0012)	(.0011)	[1.62, 2.05]	[.19, .34]				
		65.7	.0477	.0290	1.92	.31	.0292	1.90	.31	2.06
			(.0019)	(.0011)	[1.73, 2.13]	[.25, .36]				

* Vp/Vs = 1 + (Ts - Tp)/(Tp - Ti)
** Poisson's ratio = [(Vp/Vs)**2 - 2]/[2*(Vp/Vs)**2 - 2]
Numbers in parentheses represent standard errors for arrival times
Numbers in braces represent extreme values possible

TABLE 5 - P-WAVE VELOCITIES AND COEFFICIENTS FOR A POLYNOMIAL OF THE FORM T = A + BZ + CZ**2 FITTED TO TIME-DEPTH DATA

WELL NAME	COEFFICIENTS A	B	C	CORRELATION COEFFICIENT	RESIDUAL	VELOCITY Z=0	Z=BOH	ROLLOVER DEPTH(M)
GAR	.0066	.5836 E-3	-109 E-8	.9960	.000280	1.71	4.07	268*
LMT	.0144	.2059 E-3	0	.9851	.000237	4.86	4.86	**
SPH	.0072	.6752 E-3	-268 E-8	.9920	.000291	1.48	8.90	126
CBL	.0065	.6150 E-3	-376 E-8	.9872	.000234	1.63	19.61	82
FPK	.0157	.2960 E-3	- 84 E-8	.9839	.000162	3.38	8.36	176
HHL	.0035	.5406 E-3	-143 E-8	.9916	.000195	1.85	7.13	189
SMS	.0022	.3291 E-3	-131 E-8	.9864	.000123	3.04	9.40	126
TPK	.0080	.3705 E-3	- 73 E-8	.9938	.000126	2.70	4.45	254
YGR	.0059	.3386 E-3	- 94 E-8	.9752	.000211	2.95	6.64	180

* Rollover depth - depth at which velocity is infinite: Z = -B/2C

** Straight line, no rollover depth

TABLE 6 – P-WAVE VELOCITIES AND COEFFICIENTS FOR AN EXPONENTIAL OF THE FORM T = A + BZ + C{exp(GZ)} FITTED TO TIME-DEPTH DATA

*** (MINIMUM RESIDUAL) ***

WELL NAME	COEFFICIENTS A	B	C	G	CORRELATION COEFFICIENT	RESIDUAL	VELOCITY Z=0	Z=BOH	SLOWDOWN DEPTH(M)
GAR	.016755	.000361	-.022369	-.06745	.9973	.000232	0.54	2.77	21*
LMT	572.089	-.013219	-572.075	-.00002	.9853	.000236	4.45	5.26	**
SPH	.041693	.000112	-.036418	-.02075	.9925	.000282	1.15	5.07	92
CBL	.041112	-.000035	-.036030	-.0225	.9878	.000229	1.29	8.71	**
FPK	.018845	.000186	-.015084	-.16225	.9887	.000136	0.38	5.39	16
HHL	.054839	.000063	-.053190	-.01056	.9919	.000193	1.63	5.30	207
SMS	1321.14	-.058549	-1321.14	-.00004	.9864	.000123	3.05	9.31	**
TPK	.010741	.000277	-.005166	-.1	.9942	.000121	1.26	3.61	30
YGR	.010144	.000207	-.019572	-.186	.9872	.000152	0.26	4.83	15

* Slowdown depth defined as Z = {lnB - ln|G| - ln|C|}/G

** Undefined slowdown for negative values of B

TABLE 7 - P-WAVE VELOCITIES AND COEFFICIENTS FOR AN EXPONENTIAL
OF THE FORM T = A + BZ + C{exp(GZ)} FITTED TO TIME-DEPTH DATA
*** (SUBJECTIVE FIT) ***

WELL NAME	COEFFICIENTS A	B	C	G	CORRELATION COEFFICIENT	RESIDUAL	% ABOVE MIN RES	VELOCITY Z=0	Z=BOH	SLOWDOWN DEPTH(M)
GAR	.020189	.000335	-.019421	-.037	.9971	.000240	4	0.95	2.96	21
LMT	.014484	.000205	-.001101	-.181	.9851	.000237	1	2.47	4.87	0
SPH	.030060	.000196	-.025908	-.031	.9924	.000284	1	1.00	4.40	45
CBL	.019908	.000168	-.017655	-.058	.9867	.000239	4	0.84	5.52	31
FPK	.019085	.000182	-.012491	-.134	.9886	.000136	1	0.54	5.49	17
HHL	.022992	.000216	-.021368	-.024	.9915	.000197	2	1.37	4.27	36
SMS	.005620	.000190	-.003860	-.071	.9818	.000142	16	2.15	5.23	5
TPK	.011618	.000266	-.004763	-.056	.9940	.000123	1	1.88	3.74	0
YGR	.011231	.000194	-.011195	-.089	.9844	.000168	10	0.84	5.16	18

TABLE 8 - P-WAVE VELOCITIES AND COEFFICIENTS FOR AN EXPONENTIAL OF THE FORM T - A +BZ + C{exp(GZ)} FITTED TO TIME-DEPTH DATA

*** (EMPIRICAL FIT) ***

WELL NAME	COEFFICIENTS A	B	C	G	RESIDUAL	% ABOVE MIN RES	VELOCITY Z=0	Z=BOH	SLOWDOWN DEPTH
GAR	.015202	.000356	-.012984	-.0292	.000414	78	1.32	2.63	0
LMT*									
SPH	.022197	.000264	-.014542	-.0215	.000682	141	1.73	3.34	8
CBL	.018930	.000174	-.011354	-.0259	.000639	178	2.13	4.52	20
FPK	.018388	.000192	-.008448	-.0645	.000222	64	1.36	5.20	16
HHL	.019800	.000229	-.015299	-.0149	.000390	60	2.19	3.86	0
SMS*									
TPK	.012381	.000256	-.003722	-.0183	.000167	38	3.09	3.74	-72
YGR	.010128	.000207	-.009770	-.0600	.000224	47	1.26	4.78	-17

* Wells LMT and SMS exhibited only one interval velocity

TABLE 9 - P-WAVE VELOCITY AS A FUNCTION OF DISTANCE FROM THE GARLOCK FAULT
FUNCTION OF THE FORM $V(x) = Vf - V\exp(-ax)$

VELOCITY SOURCE*	Vf KM/SEC	V KM/SEC	a 1/KM	CORRELATION COEFFICIENT	RESIDUAL	V(x)=0.99Vf, x IN KM
Interval velocity, lower layer	5.712	3.668	.110	.9305	.179	38
Asymptotic velocity, subjective exponential	5.768	3.915	.190	.9896	.065	22
Velocity at z = 70m, subjective exponential	5.568	3.427	.155	.9763	.091	27
Composite, all data	5.647	3.626	.151	.9435	.089	28

* Data from wells GAR, LMT, SPH, CBL, and FPK only.

TABLE 10 - SUMMARY OF SELECTED SEISMIC VELOCITIES FROM LABORATORY STUDIES OF GRANITIC ROCKS

ROCK TYPE	Vp DRY 0 BAR	Vp DRY 100 BAR	Vp SAT 0 BAR	Vp SAT 100 BAR	Vs DRY 0 BAR	Vs DRY 100 BAR	Vs SAT 0 BAR	Vs SAT 100 BAR
Casco Granite 1/	3.30	5.05	5.30	6.02	2.32	2.79	2.42	3.00
Westerly Granite 1/	3.80	4.98	5.48	5.70	2.80	3.07	3.00	3.10
Troy Granite 1/	4.50	5.91	5.70	6.22	2.90	3.33	2.90	3.33
AVERAGE 1/	3.86 (.60)*	5.31 (.51)	5.49 (.20)	5.98 (.26)	2.67 (.31)	3.06 (.27)	2.77 (.31)	3.14 (.16)
Wausau Granite 2/	5.91	6.03	6.25	6.30	3.39	3.59	3.39	3.43
Red River Q. Monz. 2/	5.11	5.48	5.84	5.88	4.44	4.45?	4.35	4.37
Graniteville Gran. 2/	4.80	5.37	5.85	5.94	3.84	4.03	3.97	4.05
AVERAGE 2/	5.27 (.57)	5.62 (.35)	5.98 (.23)	6.04 (.22)	3.89 (.52)	4.02 (.43)	3.90 (.48)	3.95 (.47)
TOTAL AVERAGE	4.57 (.93)	5.47 (.43)	5.73 (.33)	6.01 (.22)	3.28 (.77)	3.54 (.61)	3.33 (.71)	3.54 (.54)

1/ Nur and Simmons (1969)
2/ Feves *et al* (1977)

* Numbers in parentheses represent standard errors for velocities

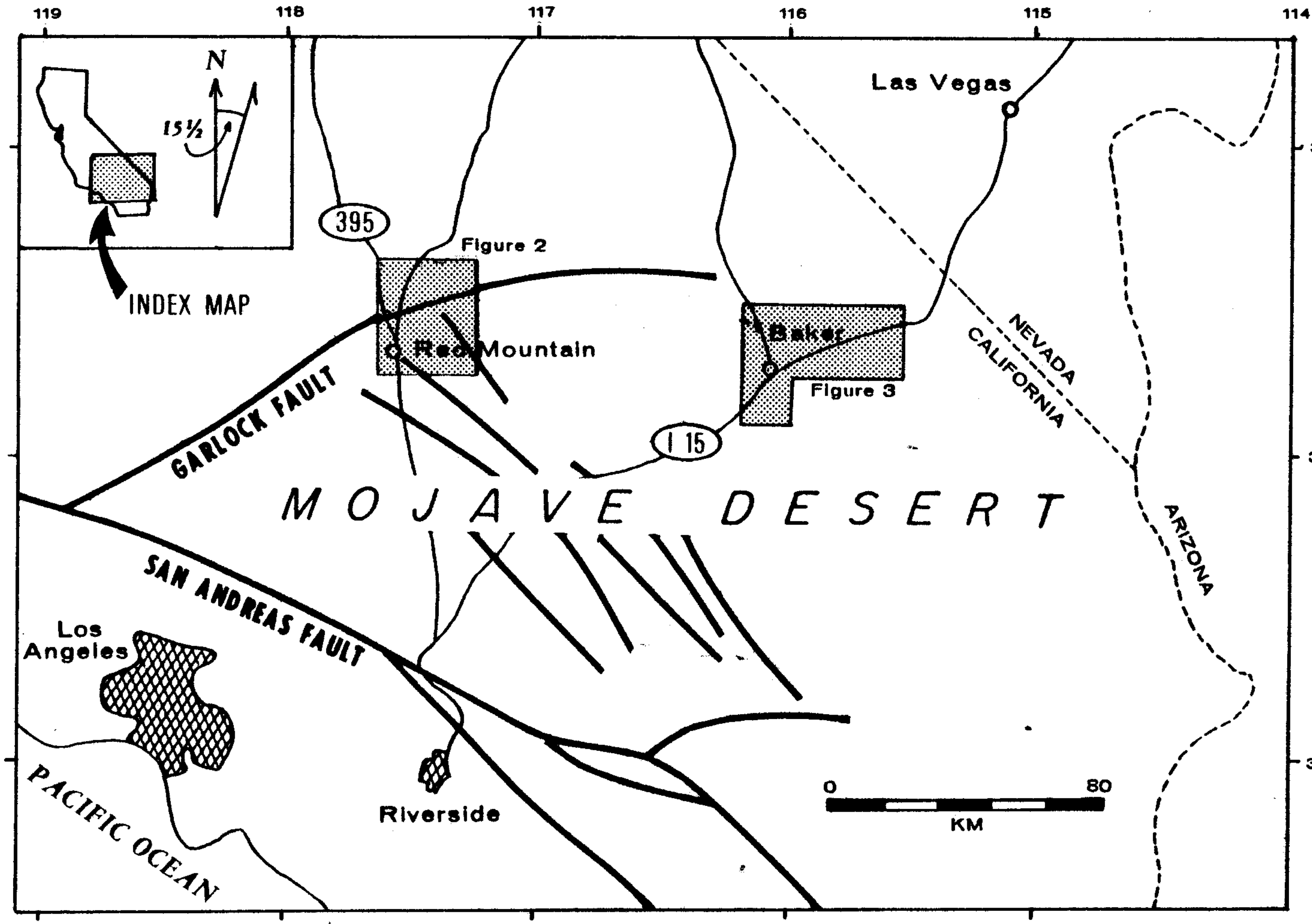

Figure 1 - Index map showing the location of the western and eastern Mojave study areas (enlarged in Figures 2 and 3), their position relative to major quaternary faults, and principal access routes.

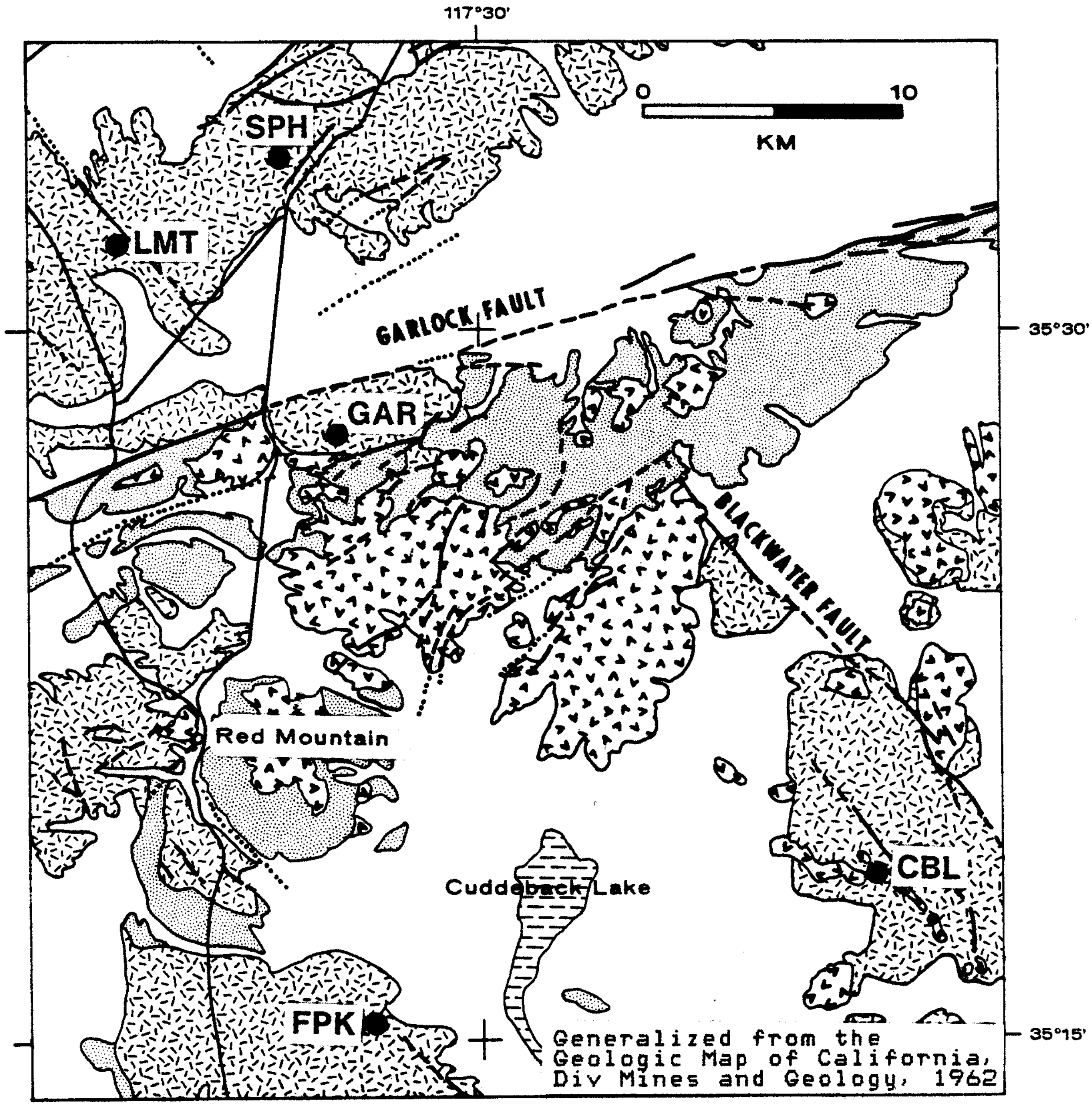

Figure 2 - General geology and location map for western Mojave wells

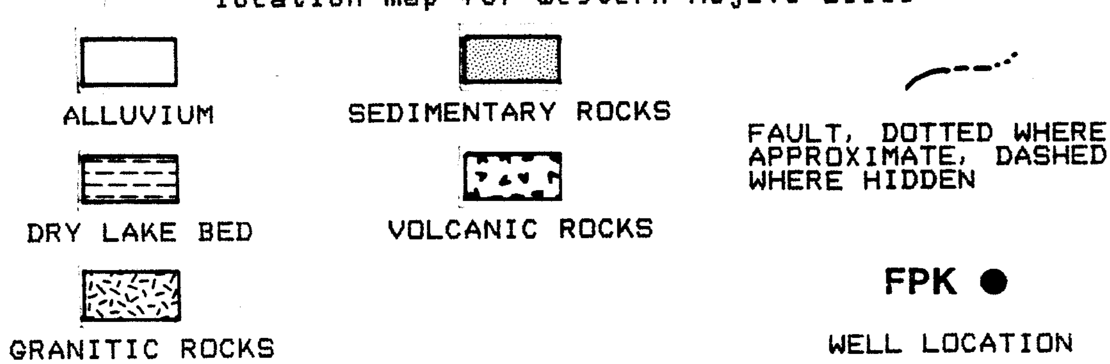

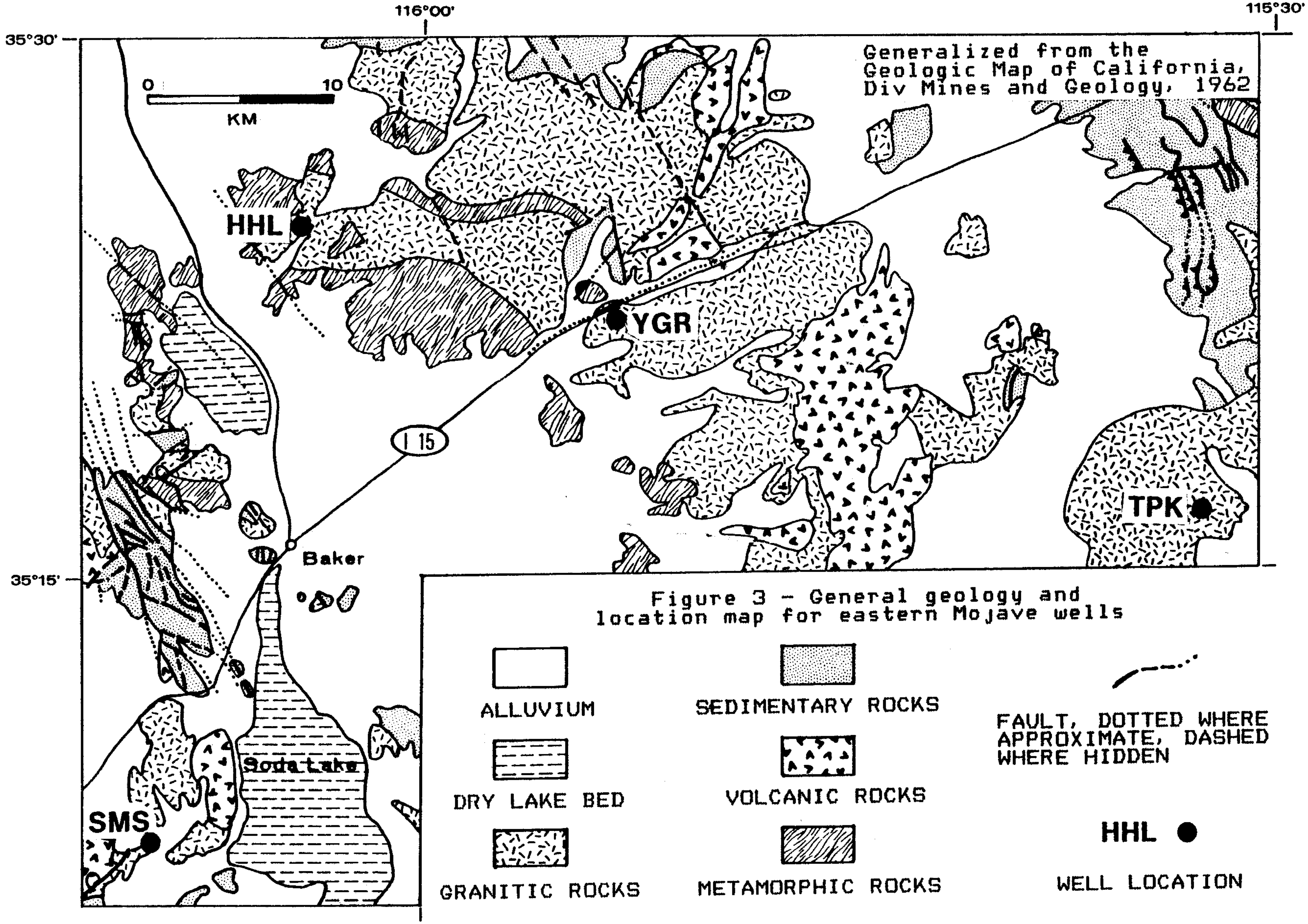

Figure 3 - General geology and location map for eastern Mojave wells

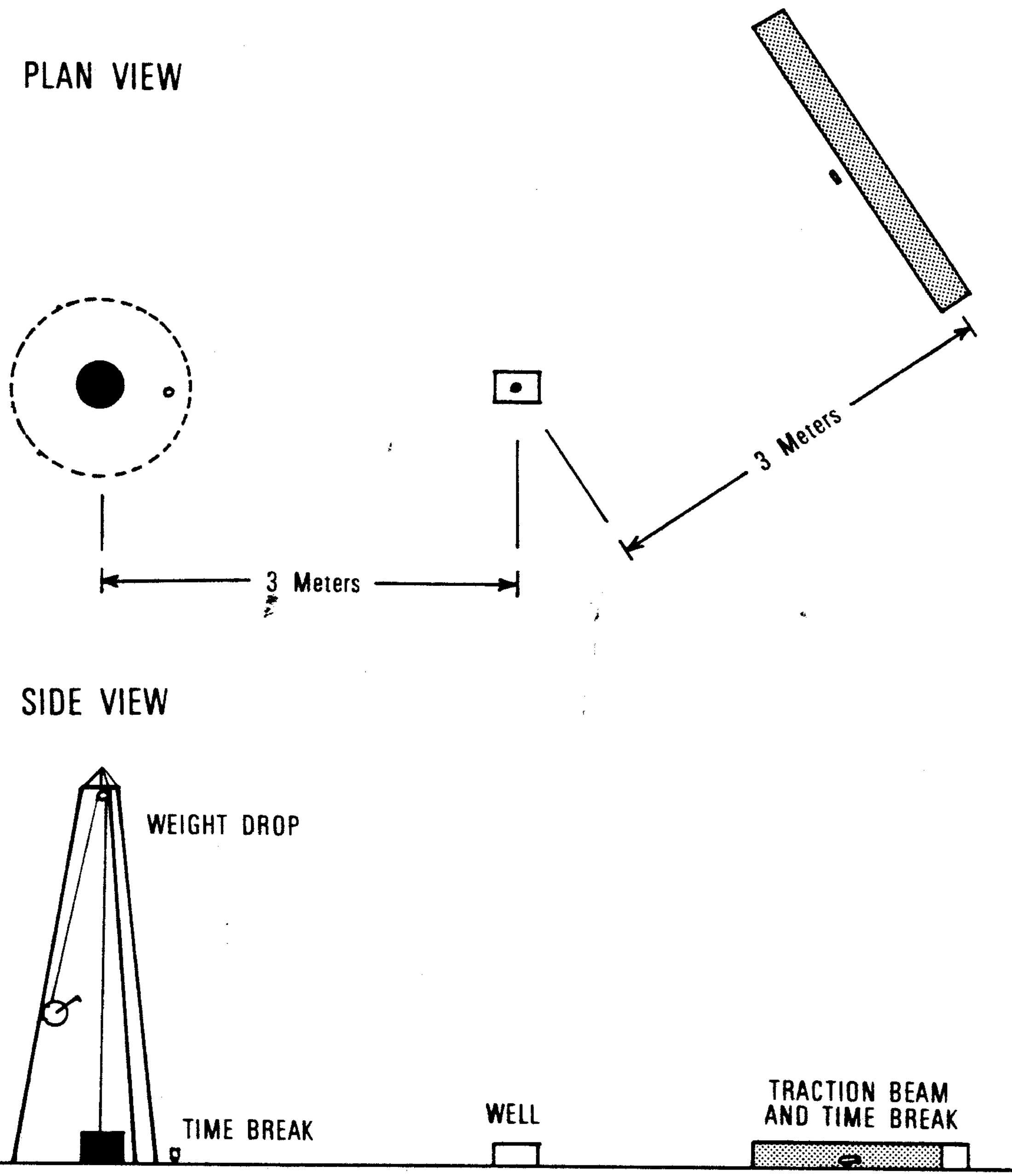

Figure 4 – Idealized layout of equipment at a typical well, showing the location of the weight drop, horizontal traction beam, and time breaks relative to the well.

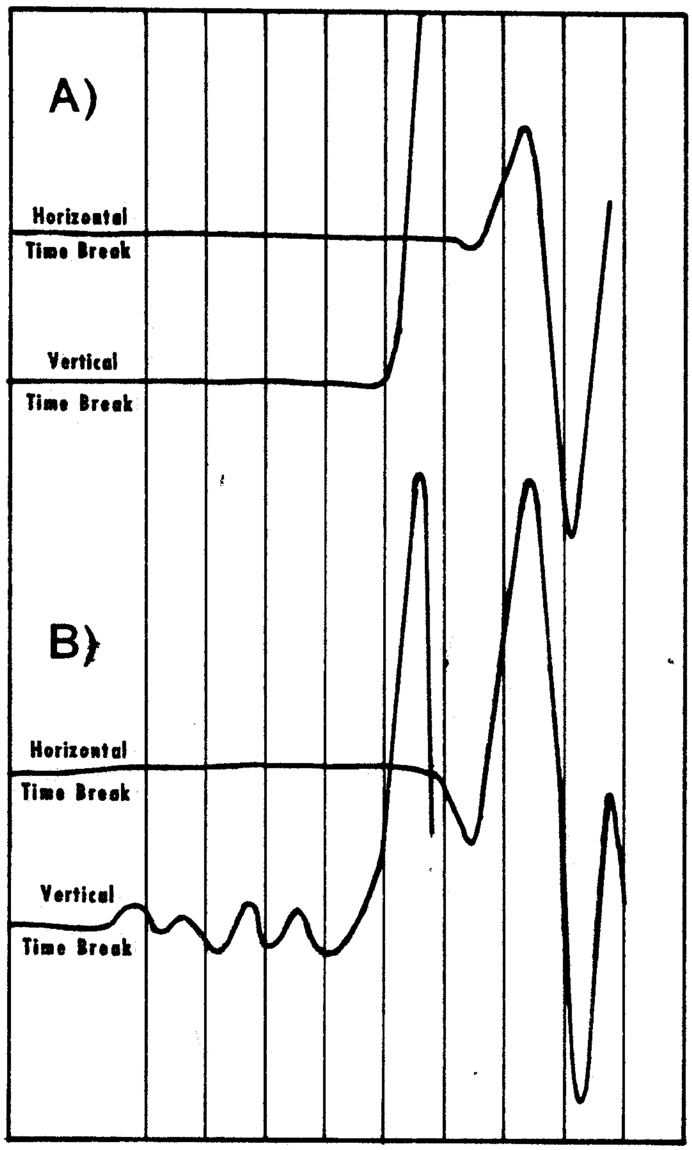

Figure 5 - Detailed seismograms comparing A) clean and B) noisey first breaks on the vertical time break, with the regular wave packet recorded on the horizontal time break. A) and B) are aligned so that the first breaks coincide. Timing line interval is 10 msec.

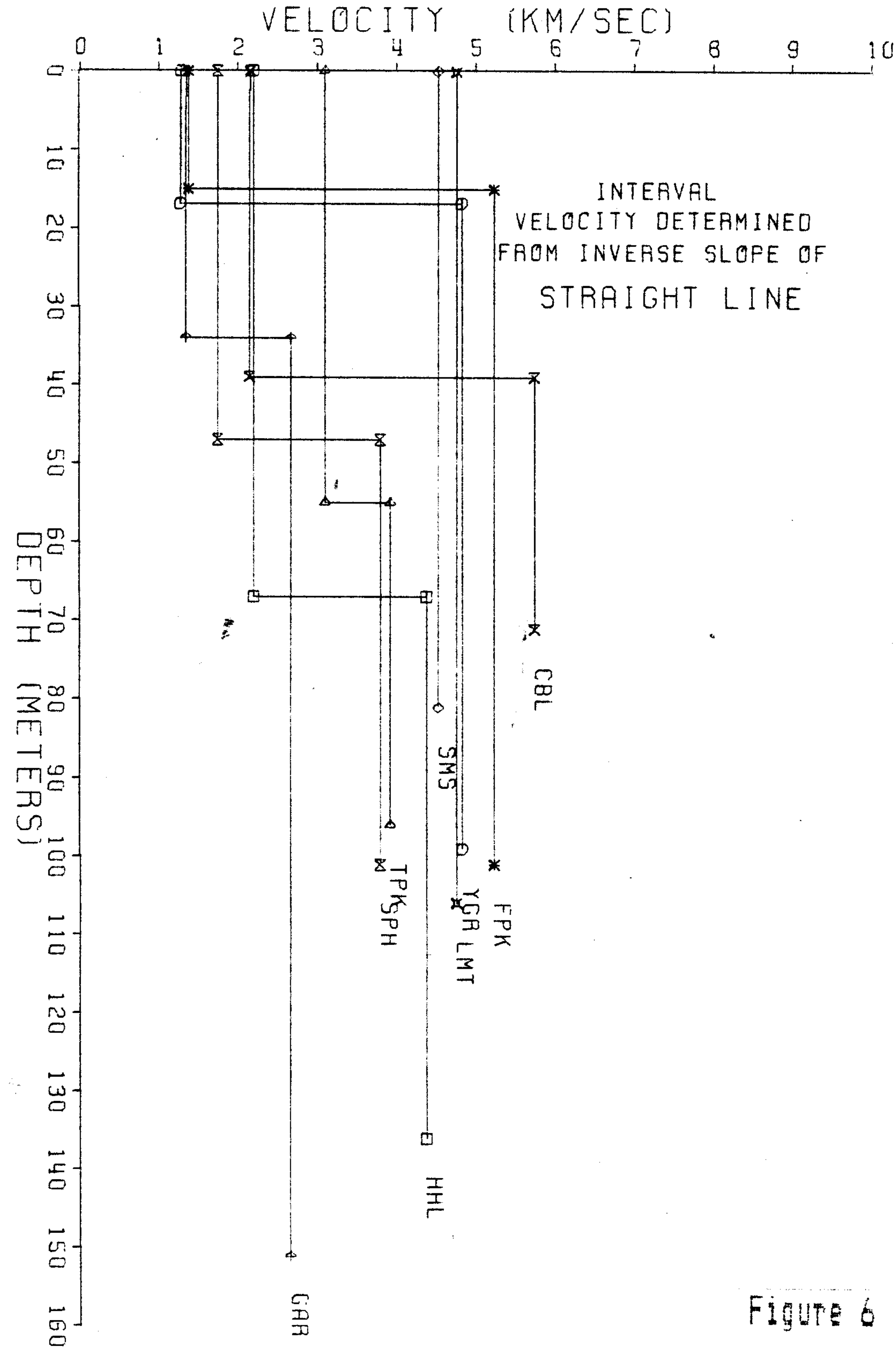
VELOCITY (KM/SEC)
0 1 2 3 4 5 6 7 8 9 10
DEPTH (METERS)
0 10 20 30 40 50 60 70 80 90 100 110 120 130 140 150 160
INTERVAL
VELOCITY DETERMINED
FROM INVERSE SLOPE OF
STRAIGHT LINE
CBL
SMS
FPK
YGR
LMT
TPK
SPH
HHL
GAR

Figure 6

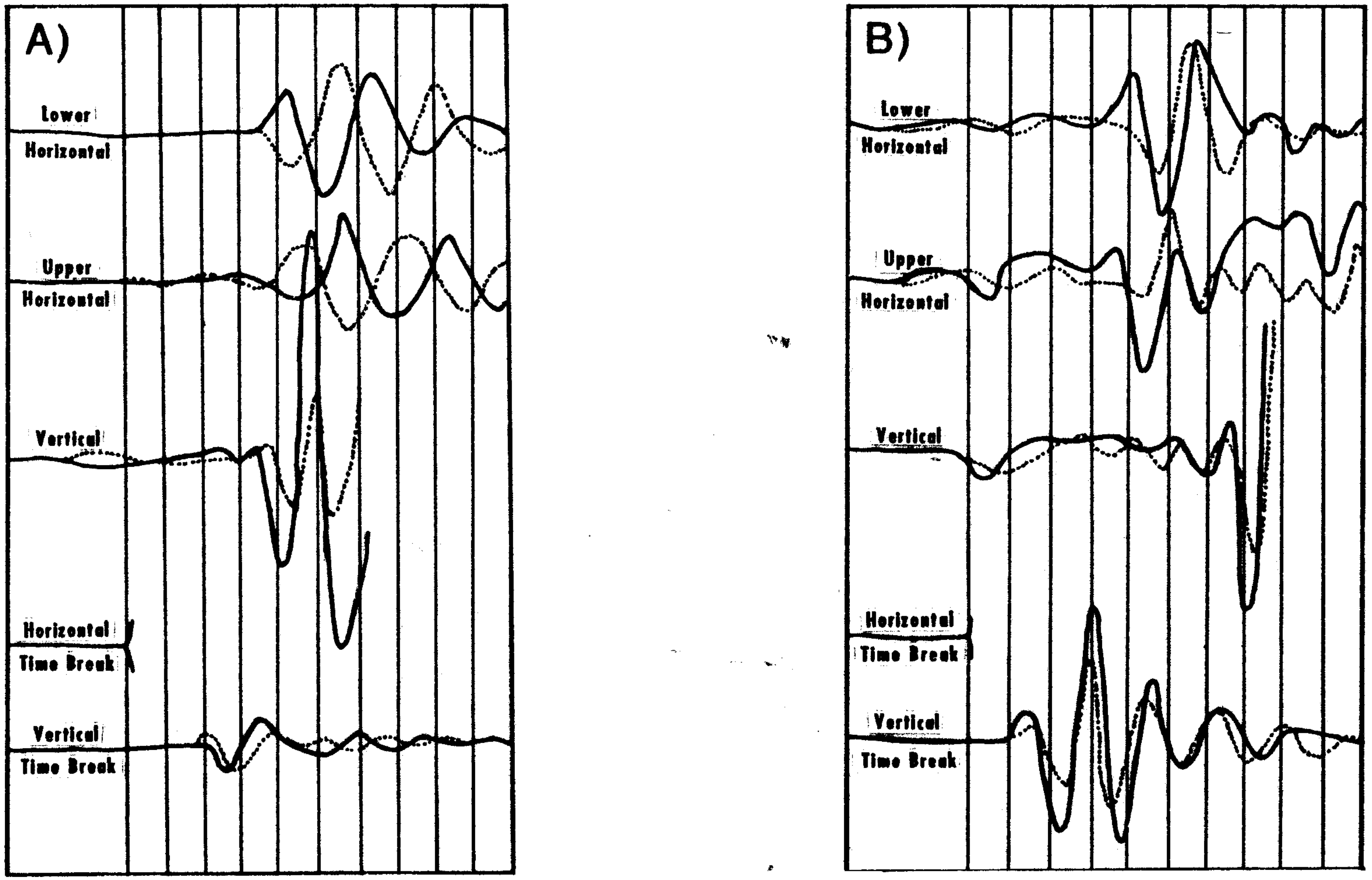

Figure 7 – Seismograms from impacts on opposite ends of the horizontal traction beam drafted onto a common time line. A) displays good reversal while B) displays offset reversal of shear energy recorded on the lower horizontal borehole geophone. The onset of shear energy occurs when the signals reverse polarity. A) was recorded in well TPK, B) in well YGR. Timing line interval is 10 msec.

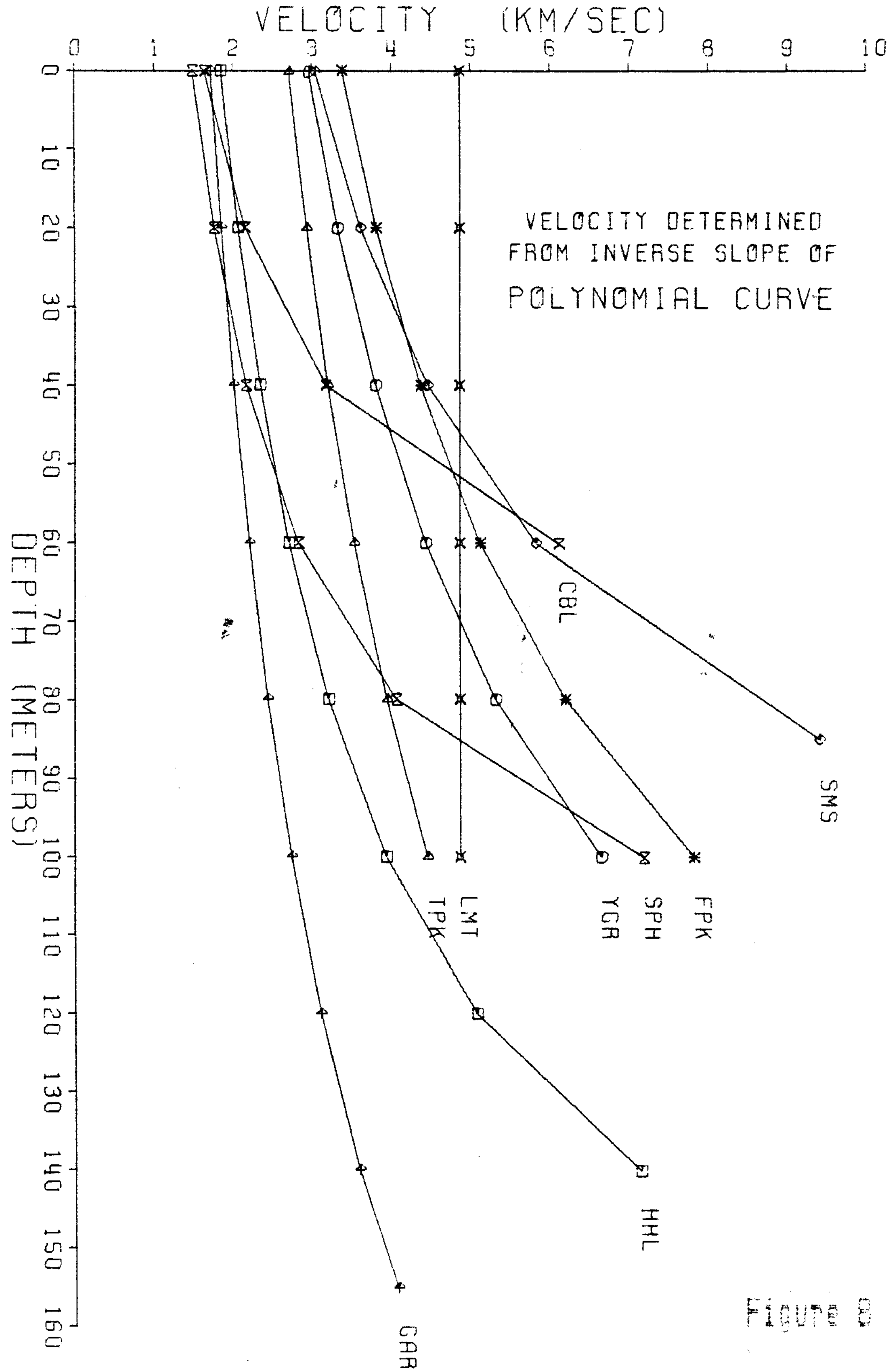
VELOCITY (KM/SEC)
0 1 2 3 4 5 6 7 8 9 10
DEPTH (METERS)
0 10 20 30 40 50 60 70 80 90 100 110 120 130 140 150 160
VELOCITY DETERMINED FROM INVERSE SLOPE OF POLYNOMIAL CURVE
CBL
SMS
FPK
SPH
YGR
LMT
TPK
HHL
GAR

Figure 8

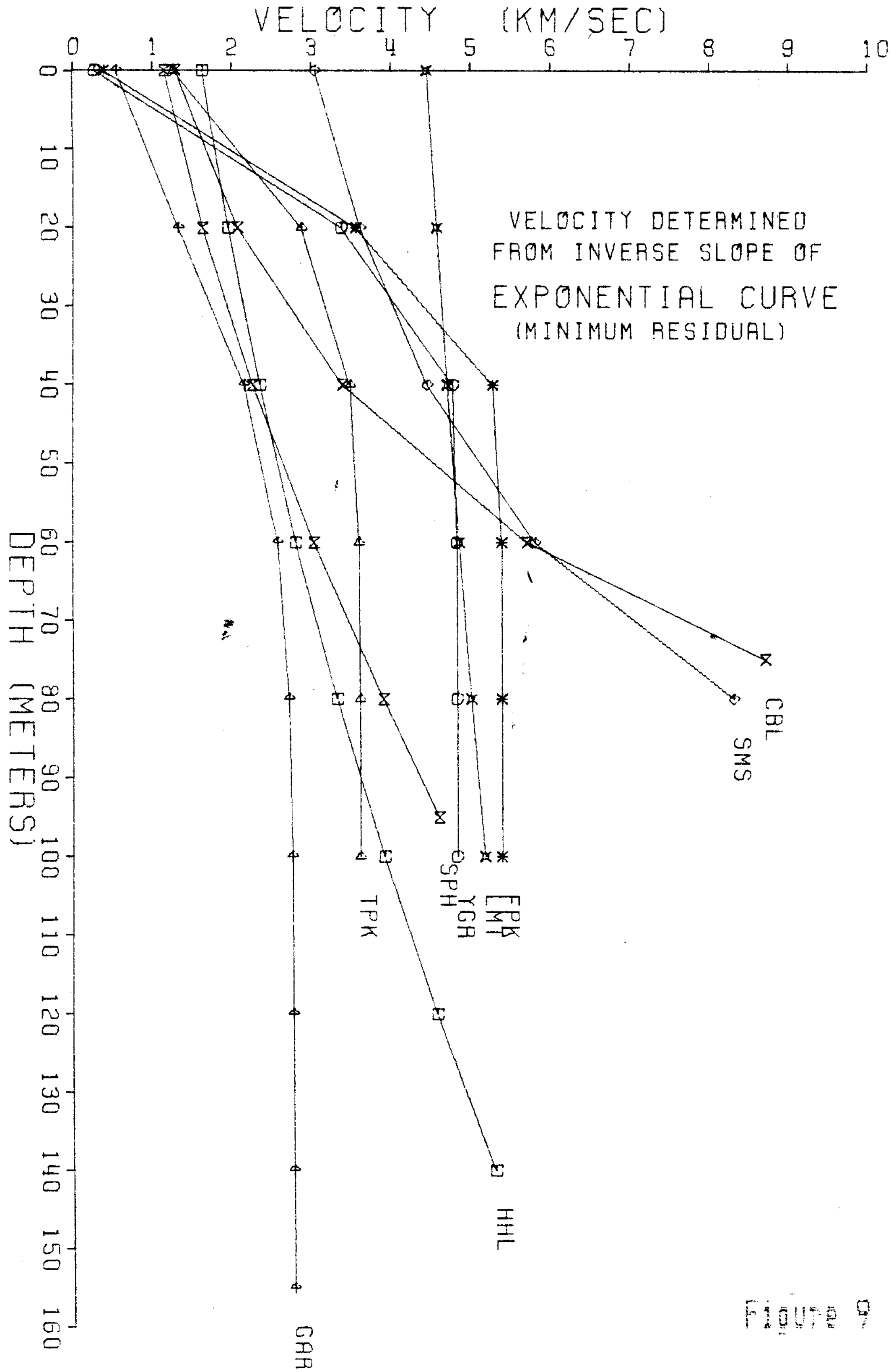
VELOCITY (KM/SEC)
0 1 2 3 4 5 6 7 8 9 10
DEPTH (METERS)
0 10 20 30 40 50 60 70 80 90 100 110 120 130 140 150 160
VELOCITY DETERMINED
FROM INVERSE SLOPE OF
EXPONENTIAL CURVE
(MINIMUM RESIDUAL)
CBL
SMS
TPK
SPH
YGR
EMT
EPK
HHL
GAR

Figure 9

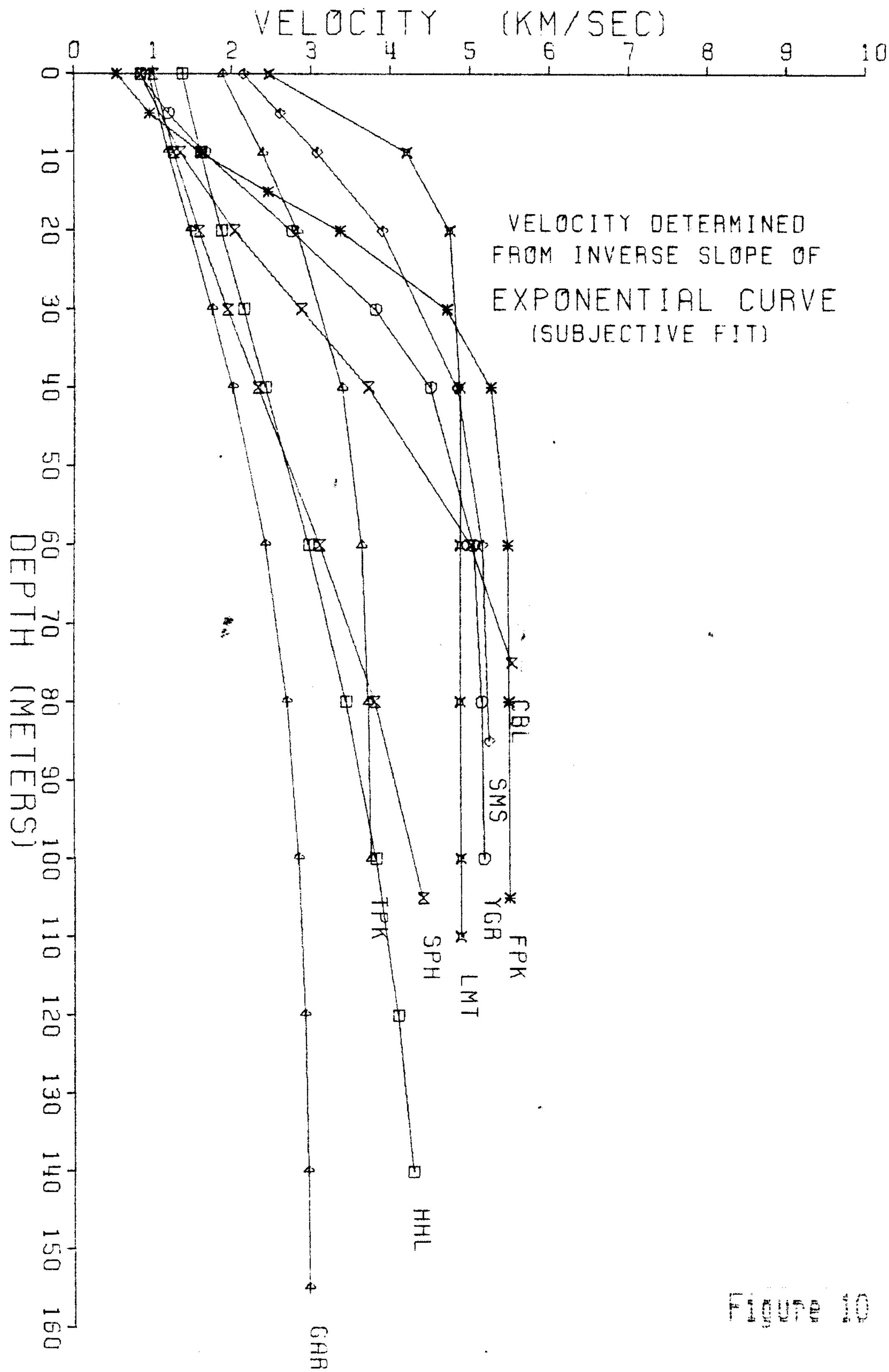
VELOCITY (KM/SEC)
0 1 2 3 4 5 6 7 8 9 10
VELOCITY DETERMINED
FROM INVERSE SLOPE OF
EXPONENTIAL CURVE
(SUBJECTIVE FIT)
DEPTH (METERS)
0 10 20 30 40 50 60 70 80 90 100 110 120 130 140 150 160
CBL
SMS
YGR
FPK
LMT
SPH
TPK
HHL
GAR

Figure 10

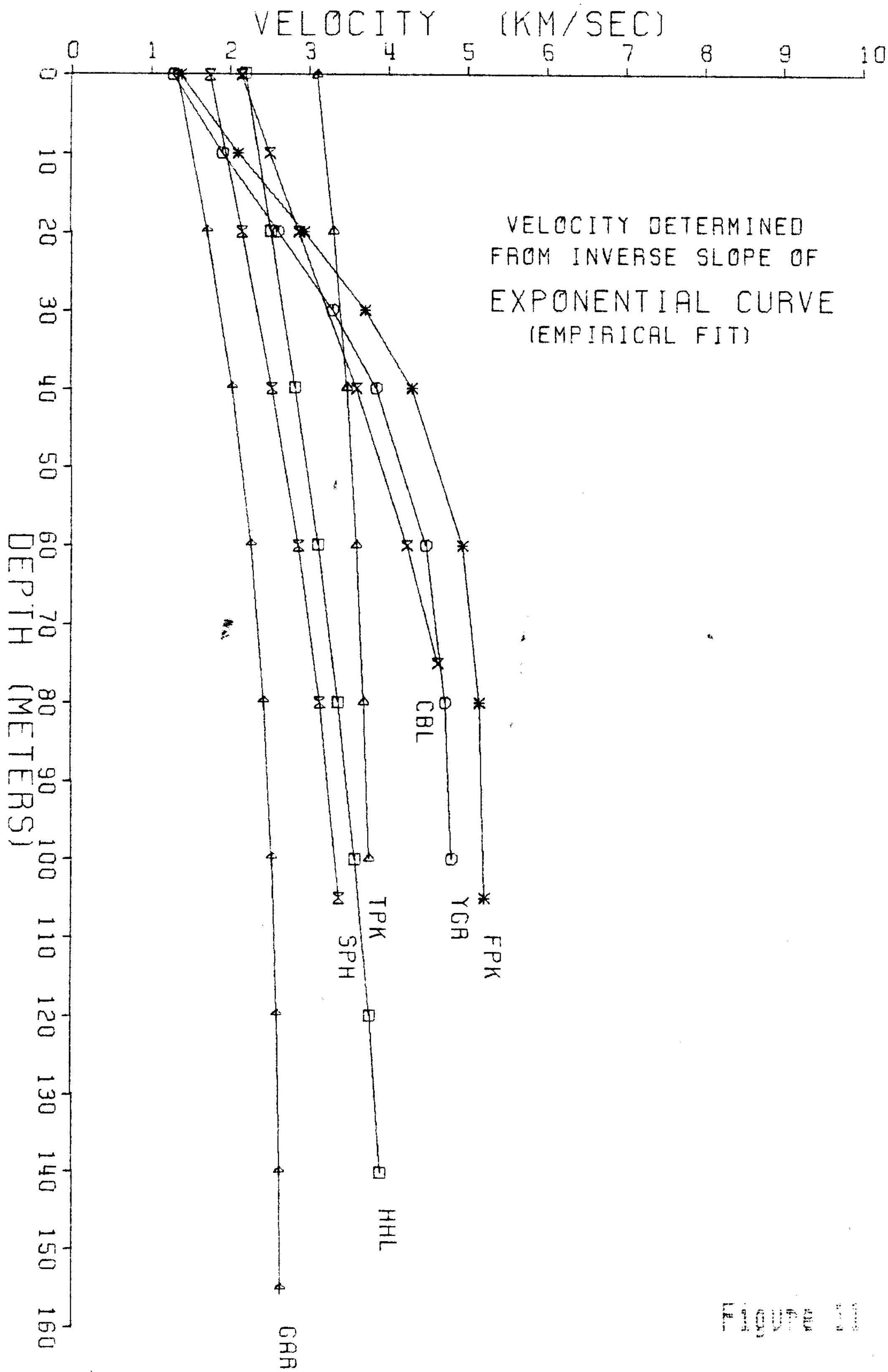
VELOCITY (KM/SEC)
0 1 2 3 4 5 6 7 8 9 10
DEPTH (METERS)
0 10 20 30 40 50 60 70 80 90 100 110 120 130 140 150 160
VELOCITY DETERMINED
FROM INVERSE SLOPE OF
EXPONENTIAL CURVE
(EMPIRICAL FIT)
CBL
TPK
YGA
FPK
SPH
HHL
GAR

Figure 11

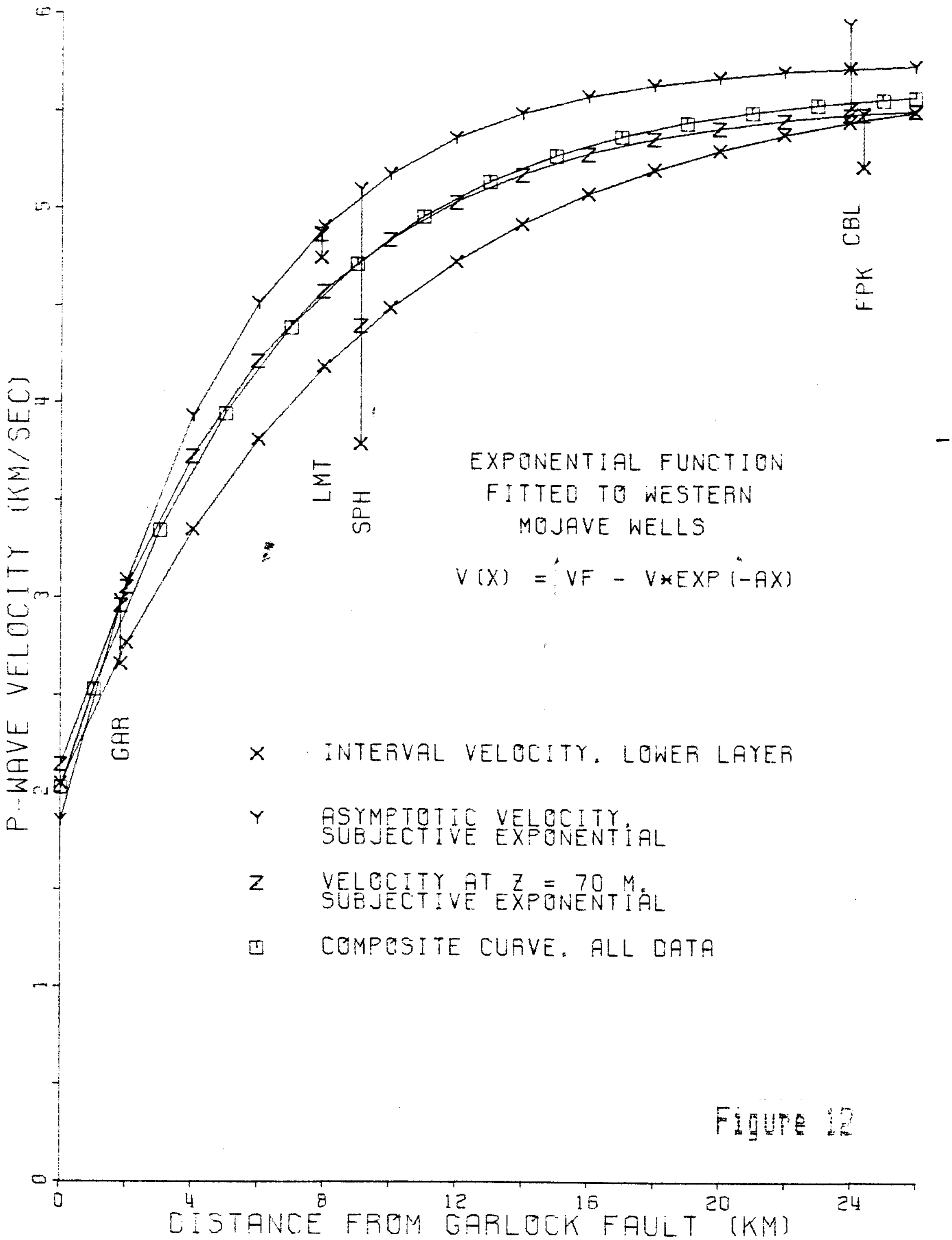
EXPONENTIAL FUNCTION
FITTED TO WESTERN
MOJAVE WELLS
V(X) = VF - V*EXP(-AX)
INTERVAL VELOCITY, LOWER LAYER
ASYMPTOTIC VELOCITY, SUBJECTIVE EXPONENTIAL
VELOCITY AT Z = 70 M, SUBJECTIVE EXPONENTIAL
COMPOSITE CURVE, ALL DATA
GAR
LMT
SPH
FPK
CBL
P-WAVE VELOCITY (KM/SEC)
DISTANCE FROM GARLOCK FAULT (KM)
0
1
2
3
4
5
6
0
4
8
12
16
20
24

Figure 12

APPENDIX

TABLE A1 - TIME-DEPTH DATA FOR P ARRIVALS

*** P-WAVE ARRIVAL TIMES FOR WELL GAR ***

DEPTH (M)	TIME (SEC)	ERROR (SEC)	DEPTH (M)	TIME (SEC)	ERROR (SEC)
11.1	0.0090	0.0015	81.0	0.0450	0.0020
11.1	0.0110	0.0020	91.0	0.0480	0.0020
21.1	0.0190	0.0015	91.0	0.0500	0.0020
21.1	0.0200	0.0015	101.0	0.0550	0.0015
31.1	0.0250	0.0015	101.0	0.0560	0.0020
31.1	0.0250	0.0015	111.0	0.0560	0.0020
41.0	0.0310	0.0020	111.0	0.0590	0.0020
41.0	0.0300	0.0015	121.0	0.0600	0.0020
41.0	0.0300	0.0020	121.0	0.0610	0.0020
51.0	0.0340	0.0015	131.0	0.0650	0.0025
51.0	0.0330	0.0020	131.0	0.0650	0.0020
61.0	0.0380	0.0015	141.0	0.0680	0.0020
61.0	0.0400	0.0015	141.0	0.0680	0.0020
71.0	0.0420	0.0020	141.0	0.0680	0.0020
71.0	0.0410	0.0020	151.0	0.0670	0.0030
81.0	0.0440	0.0020	151.0	0.0710	0.0025

*** P-WAVE ARRIVAL TIMES FOR WELL LMT ***

DEPTH (M)	TIME (SEC)	ERROR (SEC)	DEPTH (M)	TIME (SEC)	ERROR (SEC)
11.1	0.0170	0.0015	61.1	0.0270	0.0020
11.1	0.0160	0.0015	71.1	0.0290	0.0015
21.1	0.0190	0.0020	71.1	0.0310	0.0015
21.1	0.0200	0.0020	81.1	0.0310	0.0015
31.1	0.0220	0.0015	81.1	0.0320	0.0015
31.1	0.0200	0.0025	91.1	0.0340	0.0015
41.1	0.0220	0.0020	91.1	0.0340	0.0015
41.1	0.0210	0.0015	101.1	0.0360	0.0020
51.1	0.0250	0.0015	101.1	0.0360	0.0015
51.1	0.0240	0.0020	106.1	0.0350	0.0025
61.1	0.0270	0.0015	106.1	0.0360	0.0015

TABLE A1 - TIME-DEPTH DATA FOR P ARRIVALS (CONT)

*** P-WAVE ARRIVAL TIMES FOR WELL SPH ***

DEPTH (M)	TIME (SEC)	ERROR (SEC)	DEPTH (M)	TIME (SEC)	ERROR (SEC)
11.1	0.0150	0.0020	51.1	0.0350	0.0015
11.1	0.0120	0.0015	61.1	0.0370	0.0020
11.1	0.0160	0.0020	61.1	0.0350	0.0020
21.1	0.0180	0.0020	71.1	0.0410	0.0015
21.1	0.0210	0.0015	71.1	0.0410	0.0015
31.1	0.0260	0.0015	81.1	0.0450	0.0015
31.1	0.0260	0.0015	81.1	0.0440	0.0015
41.1	0.0300	0.0015	91.1	0.0470	0.0020
41.1	0.0320	0.0015	91.1	0.0460	0.0015
51.1	0.0370	0.0015	101.1	0.0490	0.0015
51.1	0.0350	0.0015	101.1	0.0480	0.0015
51.1	0.0370	0.0015			

*** P-WAVE ARRIVAL TIMES FOR WELL CBL ***

DEPTH (M)	TIME (SEC)	ERROR (SEC)	DEPTH (M)	TIME (SEC)	ERROR (SEC)
11.1	0.0120	0.0015	41.1	0.0270	0.0015
11.1	0.0140	0.0015	51.1	0.0270	0.0015
21.1	0.0170	0.0015	51.1	0.0280	0.0015
21.1	0.0170	0.0015	61.1	0.0290	0.0015
31.1	0.0220	0.0015	61.1	0.0290	0.0015
31.1	0.0220	0.0015	71.1	0.0320	0.0015
31.1	0.0210	0.0015	71.1	0.0310	0.0015
31.1	0.0240	0.0015	71.1	0.0320	0.0015
41.1	0.0260	0.0020			

TABLE A1 - TIME-DEPTH DATA FOR P ARRIVALS (CONT)

*** P-WAVE ARRIVAL TIMES FOR WELL FPK ***

DEPTH (M)	TIME (SEC)	ERROR (SEC)	DEPTH (M)	TIME (SEC)	ERROR (SEC)
6.2	0.0150	0.0015	51.2	0.0290	0.0015
11.2	0.0160	0.0025	51.2	0.0280	0.0015
11.2	0.0180	0.0015	56.2	0.0290	0.0015
16.2	0.0220	0.0015	56.2	0.0300	0.0015
16.2	0.0220	0.0015	61.2	0.0290	0.0015
16.2	0.0220	0.0015	61.2	0.0300	0.0015
16.2	0.0220	0.0015	61.2	0.0300	0.0015
21.2	0.0210	0.0025	66.2	0.0310	0.0015
21.2	0.0220	0.0015	66.2	0.0310	0.0015
26.2	0.0240	0.0015	71.2	0.0330	0.0015
26.2	0.0230	0.0015	71.2	0.0320	0.0015
26.2	0.0230	0.0015	76.2	0.0330	0.0015
31.2	0.0240	0.0015	81.2	0.0340	0.0025
31.2	0.0230	0.0015	81.2	0.0340	0.0015
31.2	0.0250	0.0015	81.2	0.0340	0.0015
36.2	0.0250	0.0015	91.2	0.0360	0.0015
36.2	0.0250	0.0015	91.2	0.0380	0.0015
41.2	0.0260	0.0015	96.2	0.0360	0.0015
41.2	0.0270	0.0015	96.2	0.0360	0.0015
46.2	0.0290	0.0015	101.2	0.0370	0.0015
46.2	0.0280	0.0015	101.2	0.0370	0.0015

TABLE A1 - TIME-DEPTH DATA FOR P ARRIVALS (CONT)

*** P-WAVE ARRIVAL TIMES FOR WELL HHL ***

DEPTH (M)	TIME (SEC)	ERROR (SEC)
5.7	0.0085	0.0010
5.7	0.0070	0.0015
5.7	0.0070	0.0025
5.7	0.0065	0.0015
10.7	0.0100	0.0010
10.7	0.0110	0.0020
10.7	0.0080	0.0030
15.7	0.0100	0.0030
15.7	0.0125	0.0020
15.7	0.0115	0.0015
20.7	0.0135	0.0025
20.7	0.0125	0.0020
20.7	0.0115	0.0020
25.7	0.0160	0.0020
25.7	0.0140	0.0020
30.7	0.0175	0.0020
30.7	0.0180	0.0020
30.7	0.0165	0.0020
35.7	0.0225	0.0015
35.7	0.0225	0.0015
35.7	0.0230	0.0015
40.7	0.0210	0.0015
40.7	0.0215	0.0015
40.7	0.0225	0.0020
45.7	0.0235	0.0015
45.7	0.0220	0.0015
45.7	0.0240	0.0015
50.7	0.0285	0.0015
50.7	0.0285	0.0015
50.7	0.0285	0.0015
55.7	0.0305	0.0015
55.7	0.0305	0.0015
55.7	0.0310	0.0015
60.7	0.0305	0.0015
60.7	0.0315	0.0010
60.7	0.0315	0.0010
65.7	0.0355	0.0010
65.7	0.0350	0.0010
65.7	0.0355	0.0010
70.7	0.0380	0.0015
70.7	0.0375	0.0015
70.7	0.0365	0.0015
75.7	0.0400	0.0015
75.7	0.0400	0.0015
75.7	0.0380	0.0020
80.7	0.0390	0.0015
80.7	0.0390	0.0015
80.7	0.0380	0.0015
85.7	0.0395	0.0015
85.7	0.0390	0.0015
85.7	0.0385	0.0015
90.7	0.0380	0.0015
90.7	0.0380	0.0015
90.7	0.0400	0.0015
95.7	0.0390	0.0025
95.7	0.0390	0.0015
95.7	0.0395	0.0015
100.7	0.0425	0.0015
100.7	0.0415	0.0015
100.7	0.0430	0.0015
105.7	0.0430	0.0015
105.7	0.0435	0.0015
105.7	0.0430	0.0015
110.7	0.0445	0.0020
110.7	0.0455	0.0015
110.7	0.0455	0.0015
115.7	0.0460	0.0015
115.7	0.0460	0.0010
115.7	0.0460	0.0015
120.7	0.0465	0.0010
120.7	0.0465	0.0015
120.7	0.0475	0.0020
125.7	0.0480	0.0015
125.7	0.0480	0.0015
125.7	0.0480	0.0015
130.7	0.0515	0.0015
130.7	0.0525	0.0020
130.7	0.0515	0.0015
135.7	0.0530	0.0015
135.7	0.0525	0.0020
135.7	0.0525	0.0015

TABLE A1 - TIME-DEPTH DATA FOR P ARRIVALS (CONT)

*** P-WAVE ARRIVAL TIMES FOR WELL SMS ***

DEPTH (M)	TIME (SEC)	ERROR (SEC)
5.7	0.0040	0.0010
5.7	0.0040	0.0010
5.7	0.0050	0.0010
10.7	0.0060	0.0015
10.7	0.0065	0.0015
10.7	0.0065	0.0015
10.7	0.0060	0.0015
15.7	0.0080	0.0015
15.7	0.0070	0.0015
15.7	0.0070	0.0015
20.7	0.0080	0.0015
20.7	0.0080	0.0025
20.7	0.0070	0.0015
25.7	0.0090	0.0025
25.7	0.0100	0.0020
25.7	0.0090	0.0015
30.7	0.0095	0.0015
30.7	0.0100	0.0020
30.7	0.0105	0.0015
35.7	0.0130	0.0020
35.7	0.0110	0.0015
35.7	0.0120	0.0025
40.7	0.0130	0.0020
40.7	0.0120	0.0015
40.7	0.0125	0.0015
45.7	0.0145	0.0025
45.7	0.0145	0.0020
45.7	0.0160	0.0010
50.7	0.0165	0.0015
50.7	0.0160	0.0015
50.7	0.0165	0.0015
55.7	0.0175	0.0015
55.7	0.0185	0.0015
55.7	0.0180	0.0015
60.7	0.0180	0.0015
60.7	0.0180	0.0015
60.7	0.0180	0.0025
65.7	0.0180	0.0015
65.7	0.0180	0.0015
65.7	0.0180	0.0015
75.7	0.0195	0.0015
75.7	0.0190	0.0015
75.7	0.0190	0.0015
80.7	0.0195	0.0015
80.7	0.0205	0.0015
80.7	0.0195	0.0015

TABLE A1 - TIME-DEPTH DATA FOR P ARRIVALS (CONT)

*** P-WAVE ARRIVAL TIMES FOR WELL TPK ***

DEPTH (M)	TIME (SEC)	ERROR (SEC)	DEPTH (M)	TIME (SEC)	ERROR (SEC)
5.7	0.0080	0.0020	50.7	0.0245	0.0015
5.7	0.0095	0.0015	50.7	0.0265	0.0015
5.7	0.0085	0.0015	55.7	0.0270	0.0015
10.7	0.0140	0.0015	55.7	0.0270	0.0015
10.7	0.0130	0.0015	60.7	0.0285	0.0015
10.7	0.0125	0.0015	60.7	0.0265	0.0015
15.7	0.0145	0.0015	60.7	0.0270	0.0020
15.7	0.0145	0.0010	65.7	0.0285	0.0020
15.7	0.0140	0.0015	65.7	0.0290	0.0015
20.7	0.0155	0.0015	65.7	0.0295	0.0015
20.7	0.0155	0.0015	70.7	0.0310	0.0015
20.7	0.0165	0.0015	70.7	0.0300	0.0015
25.7	0.0190	0.0020	70.7	0.0310	0.0015
25.7	0.0160	0.0015	75.7	0.0325	0.0015
25.7	0.0170	0.0015	75.7	0.0315	0.0015
30.7	0.0170	0.0015	75.7	0.0310	0.0015
30.7	0.0175	0.0015	80.7	0.0330	0.0015
30.7	0.0175	0.0015	80.7	0.0330	0.0015
35.7	0.0205	0.0015	80.7	0.0335	0.0015
35.7	0.0220	0.0015	85.7	0.0340	0.0015
35.7	0.0200	0.0015	85.7	0.0355	0.0020
40.7	0.0215	0.0020	85.7	0.0340	0.0015
40.7	0.0210	0.0015	90.7	0.0360	0.0015
40.7	0.0210	0.0015	90.7	0.0365	0.0020
45.7	0.0245	0.0015	95.7	0.0360	0.0015
45.7	0.0235	0.0020	95.7	0.0370	0.0015
45.7	0.0230	0.0010	95.7	0.0365	0.0015

TABLE A1 - TIME-DEPTH DATA FOR P ARRIVALS (CONT)

*** P-WAVE ARRIVAL TIMES FOR WELL YGR ***

DEPTH (M)	TIME (SEC)	ERROR (SEC)	DEPTH (M)	TIME (SEC)	ERROR (SEC)
5.7	0.0050	0.0015	55.7	0.0220	0.0015
5.7	0.0040	0.0020	60.7	0.0215	0.0015
5.7	0.0055	0.0015	60.7	0.0220	0.0015
10.7	0.0075	0.0020	60.7	0.0235	0.0015
10.7	0.0095	0.0015	65.7	0.0230	0.0015
10.7	0.0085	0.0015	65.7	0.0230	0.0020
15.7	0.0130	0.0010	65.7	0.0230	0.0015
15.7	0.0120	0.0015	70.7	0.0240	0.0010
15.7	0.0140	0.0020	70.7	0.0235	0.0015
20.7	0.0145	0.0020	70.7	0.0245	0.0015
20.7	0.0155	0.0010	75.7	0.0245	0.0020
25.7	0.0175	0.0015	75.7	0.0265	0.0015
25.7	0.0165	0.0015	75.7	0.0245	0.0015
25.7	0.0170	0.0015	80.7	0.0275	0.0010
35.7	0.0170	0.0015	80.7	0.0280	0.0015
35.7	0.0175	0.0020	80.7	0.0265	0.0015
35.7	0.0175	0.0015	85.7	0.0290	0.0015
40.7	0.0170	0.0015	85.7	0.0300	0.0015
40.7	0.0185	0.0015	85.7	0.0275	0.0015
40.7	0.0175	0.0010	90.7	0.0285	0.0020
45.7	0.0175	0.0015	90.7	0.0305	0.0015
45.7	0.0170	0.0015	90.7	0.0285	0.0015
45.7	0.0190	0.0020	95.7	0.0310	0.0015
50.7	0.0200	0.0015	95.7	0.0320	0.0015
50.7	0.0215	0.0020	95.7	0.0295	0.0015
50.7	0.0210	0.0015	98.9	0.0300	0.0015
55.7	0.0240	0.0015	98.9	0.0300	0.0015
55.7	0.0225	0.0015	98.9	0.0305	0.0015

TABLE 42 - TIME-DEPTH DATA FOR S ARRIVALS

*** S-WAVE ARRIVAL TIMES FOR WELL LMT ***

DEPTH (M)	TIME (SEC)	ERROR (SEC)	DEPTH (M)	TIME (SEC)	ERROR (SEC)
81.1	0.0445	0.0020	106.1	0.0565	0.0010
81.1	0.0440	0.0010	106.1	0.0525	0.0015
81.1	0.0445	0.0010	106.1	0.0530	0.0020
81.1	0.0455	0.0015	106.1	0.0535	0.0020
106.1	0.0535	0.0020			

*** S-WAVE ARRIVAL TIMES FOR WELL SMS ***

DEPTH (M)	TIME (SEC)	ERROR (SEC)	DEPTH (M)	TIME (SEC)	ERROR (SEC)
25.7	0.0170	0.0010	25.7	0.0155	0.0010
25.7	0.0160	0.0010	25.7	0.0155	0.0010
25.7	0.0175	0.0010	25.7	0.0150	0.0010

*** S-WAVE ARRIVAL TIMES FOR WELL TPK ***

DEPTH (M)	TIME (SEC)	ERROR (SEC)	DEPTH (M)	TIME (SEC)	ERROR (SEC)
45.7	0.0370	0.0010	45.7	0.0350	0.0010
45.7	0.0365	0.0010	65.7	0.0460	0.0010
45.7	0.0365	0.0010	65.7	0.0490	0.0010
45.7	0.0350	0.0015	65.7	0.0480	0.0030
45.7	0.0350	0.0010	65.7	0.0470	0.0030

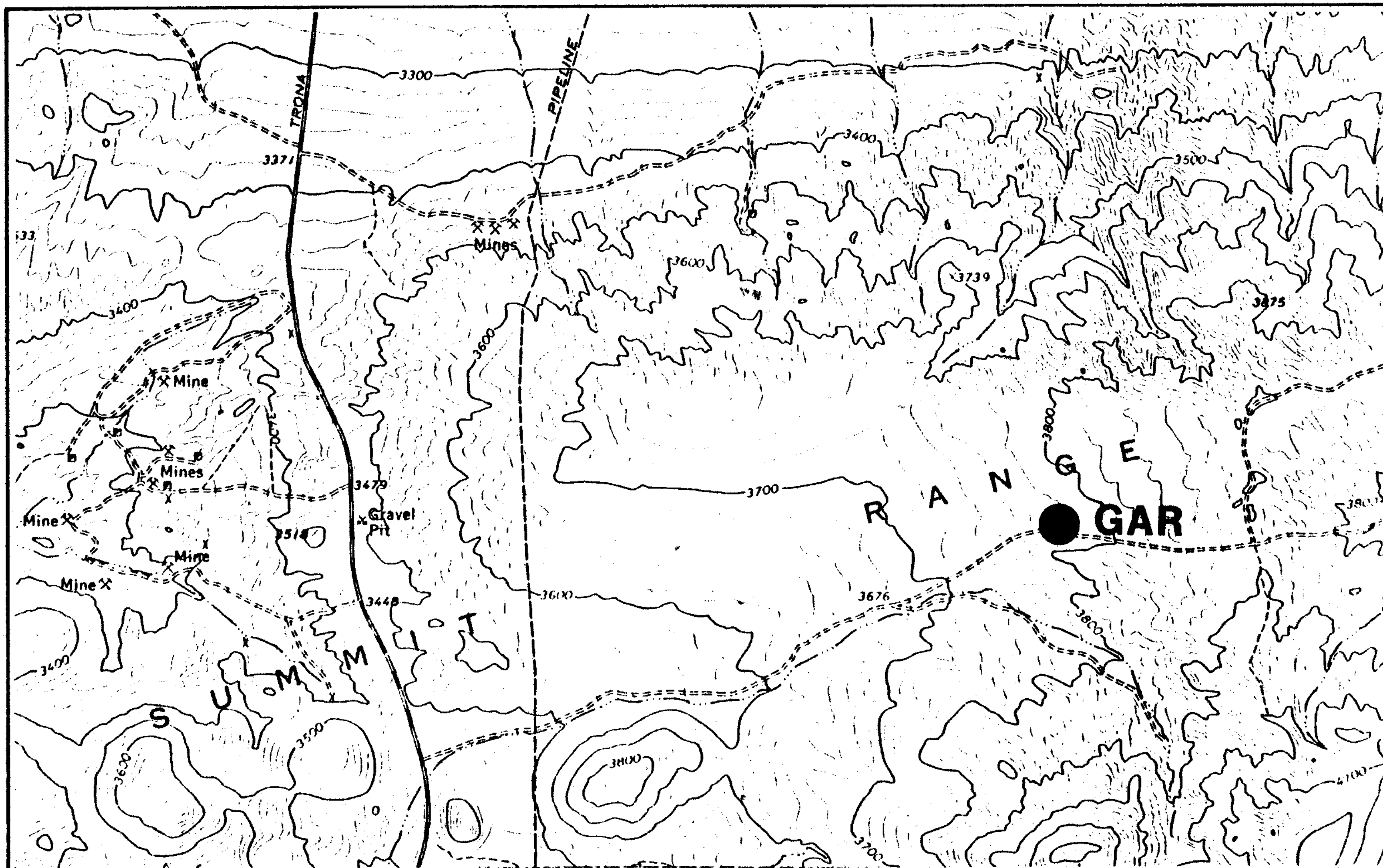

1 .5 0 1 KILOMETER

CONTOUR INTERVAL 20 FEET
DATUM IS MEAN SEA LEVEL

KLINKER MTN., CALIF.
NE/4 RANDSBURG 15' QUADRANGLE
N3522.5—W11730/7.5
1967

Figure A1

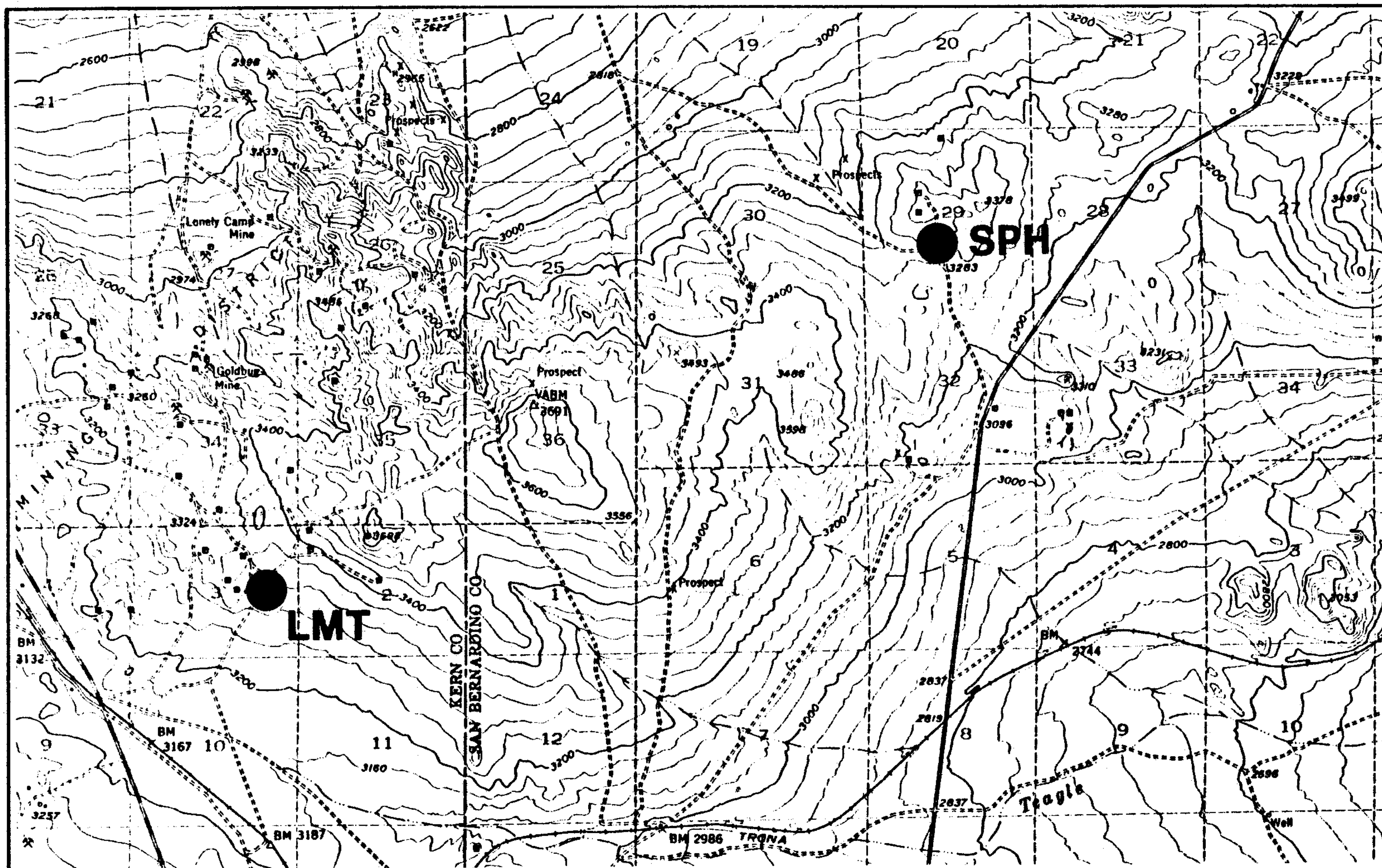

Figure A2

CONTOUR INTERVAL 40 FEET
DOTTED LINES REPRESENT HALF-INTERVAL CONTOURS
DATUM IS MEAN SEA LEVEL

1 .5 0 1 2 3 4 5 KILOMETERS

RIDGECREST, CALIF.
N3530—W11730/15
1953
AMS 2455 II—SERIES V795

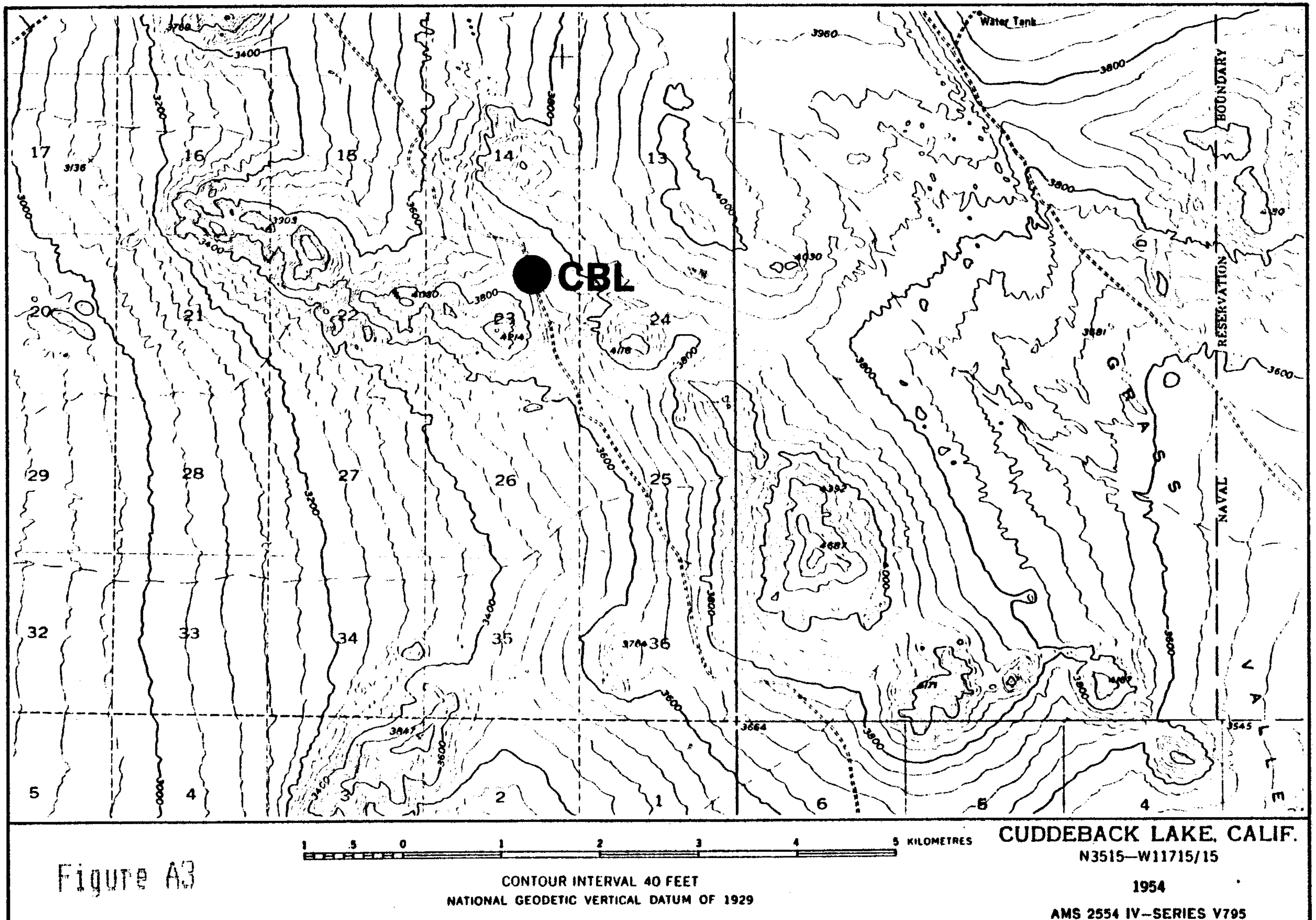
CBL
Water Tank
NAVAL RESERVATION BOUNDARY
G R A S S V A L L E
1 .5 0 1 2 3 4 5 KILOMETRES
CONTOUR INTERVAL 40 FEET
NATIONAL GEODETIC VERTICAL DATUM OF 1929
CUDDEBACK LAKE, CALIF.
N3515—W11715/15
1954
AMS 2554 IV—SERIES V795

Figure A3

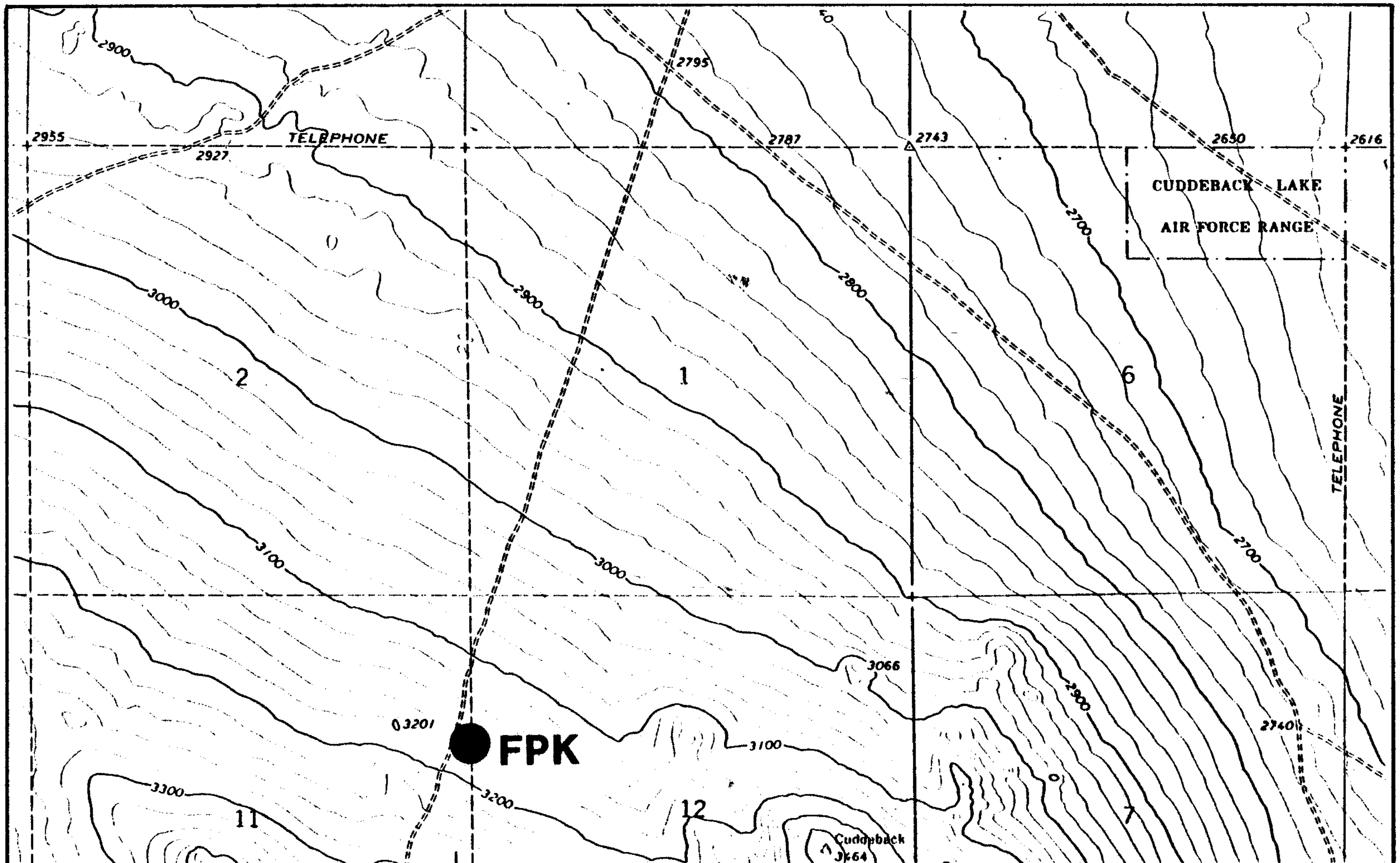

Figure A4

1 5 0 1 KILOMETER

CONTOUR INTERVAL 20 FEET
NATIONAL GEODETIC VERTICAL DATUM OF 1929

RED MOUNTAIN, CALIF.
N3515—W11730/7.5
1967

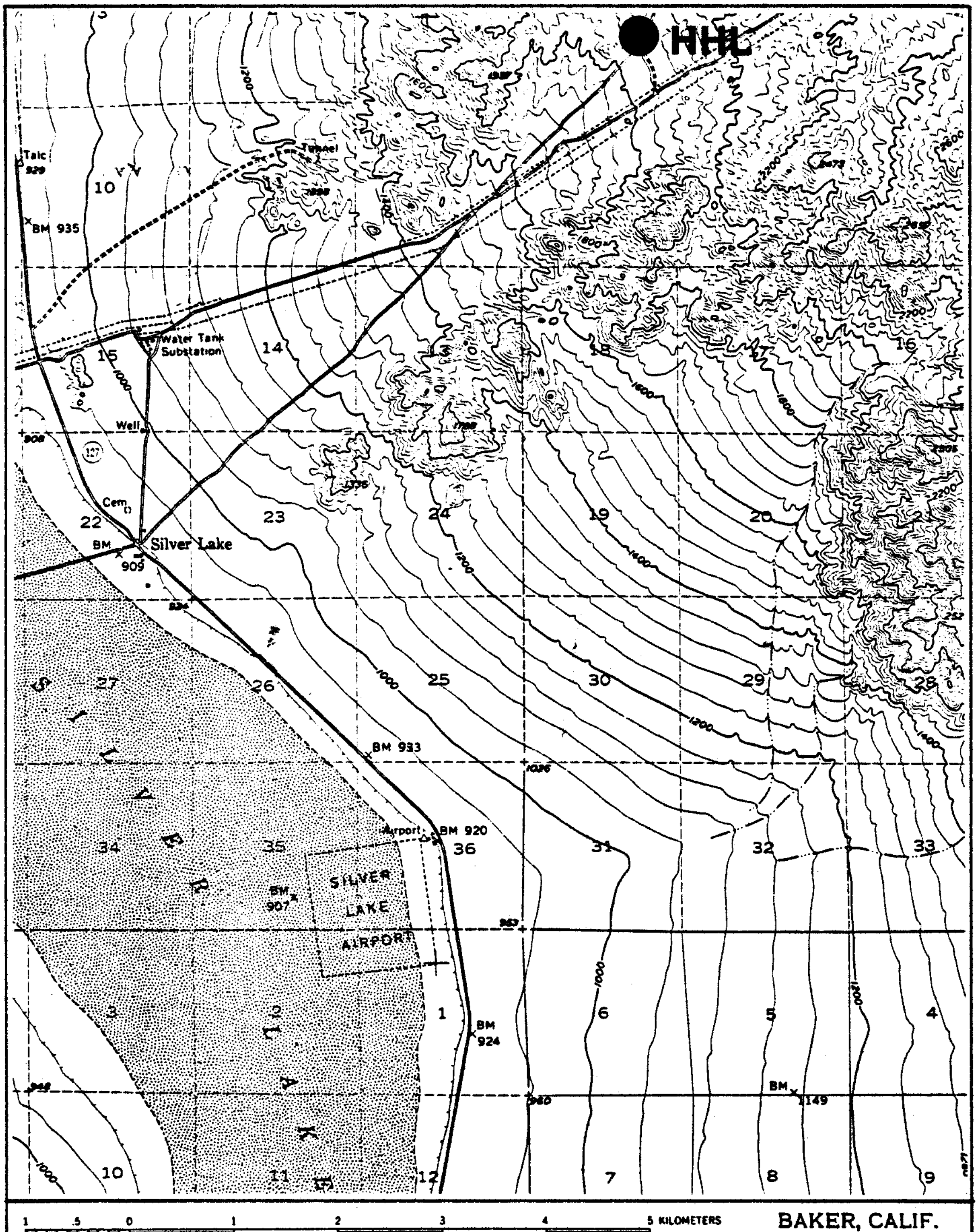

CONTOUR INTERVAL 40 FEET
NATIONAL GEODETIC VERTICAL DATUM OF 1929

BAKER, CALIF.
N3515—W11600/15
1956
AMS 2754 I—SERIES V795

Figure A6

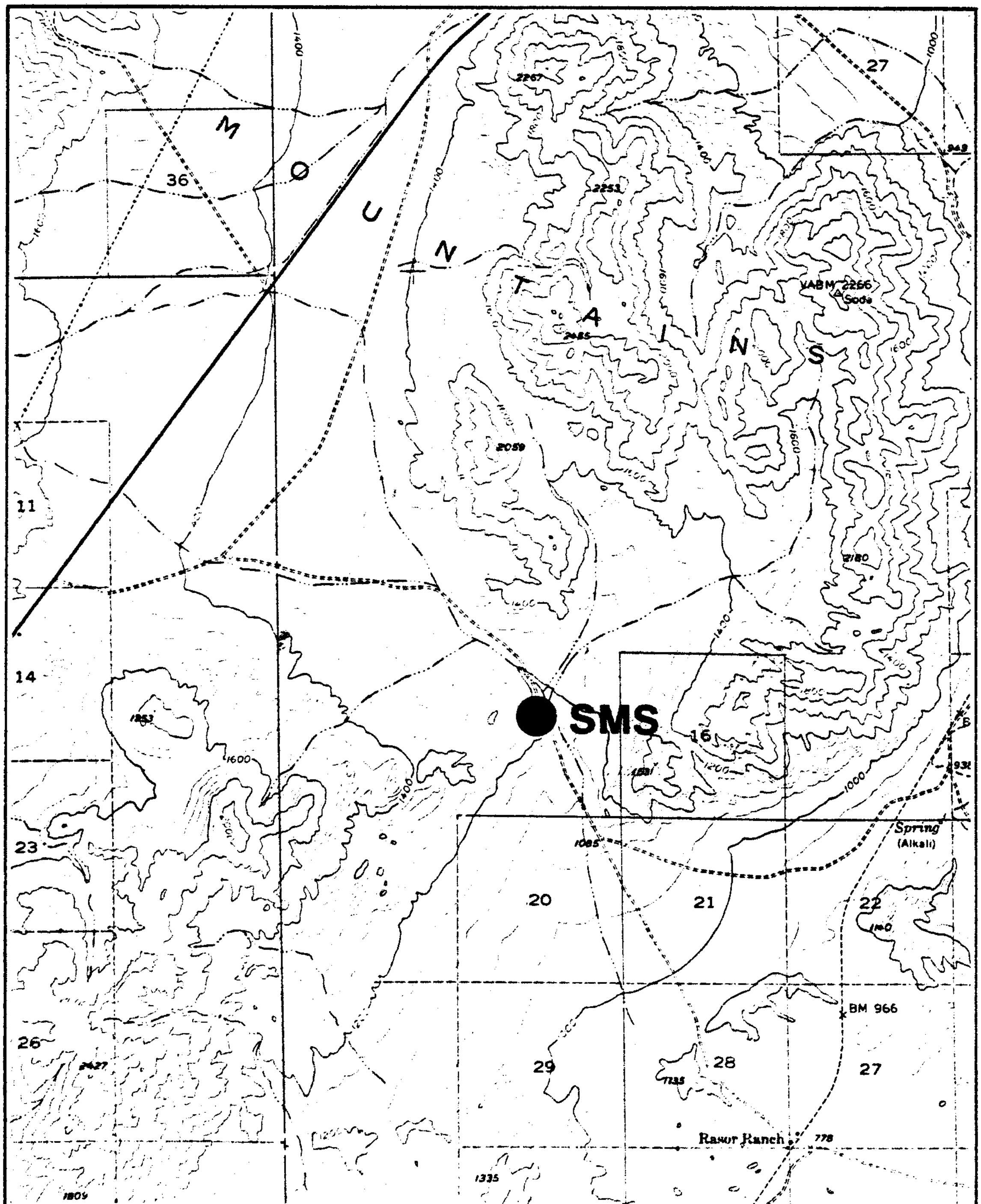

1 .5 0 1 2 3 4 5 KILOMETERS

CONTOUR INTERVAL 40 FEET
DASHED LINES REPRESENT 20-FOOT CONTOURS
NATIONAL GEODETIC VERTICAL DATUM OF 1929

SODA LAKE, CALIF.
N3500—W11600/15

1956

AMS 2754 II—SERIES V796

Figure 46

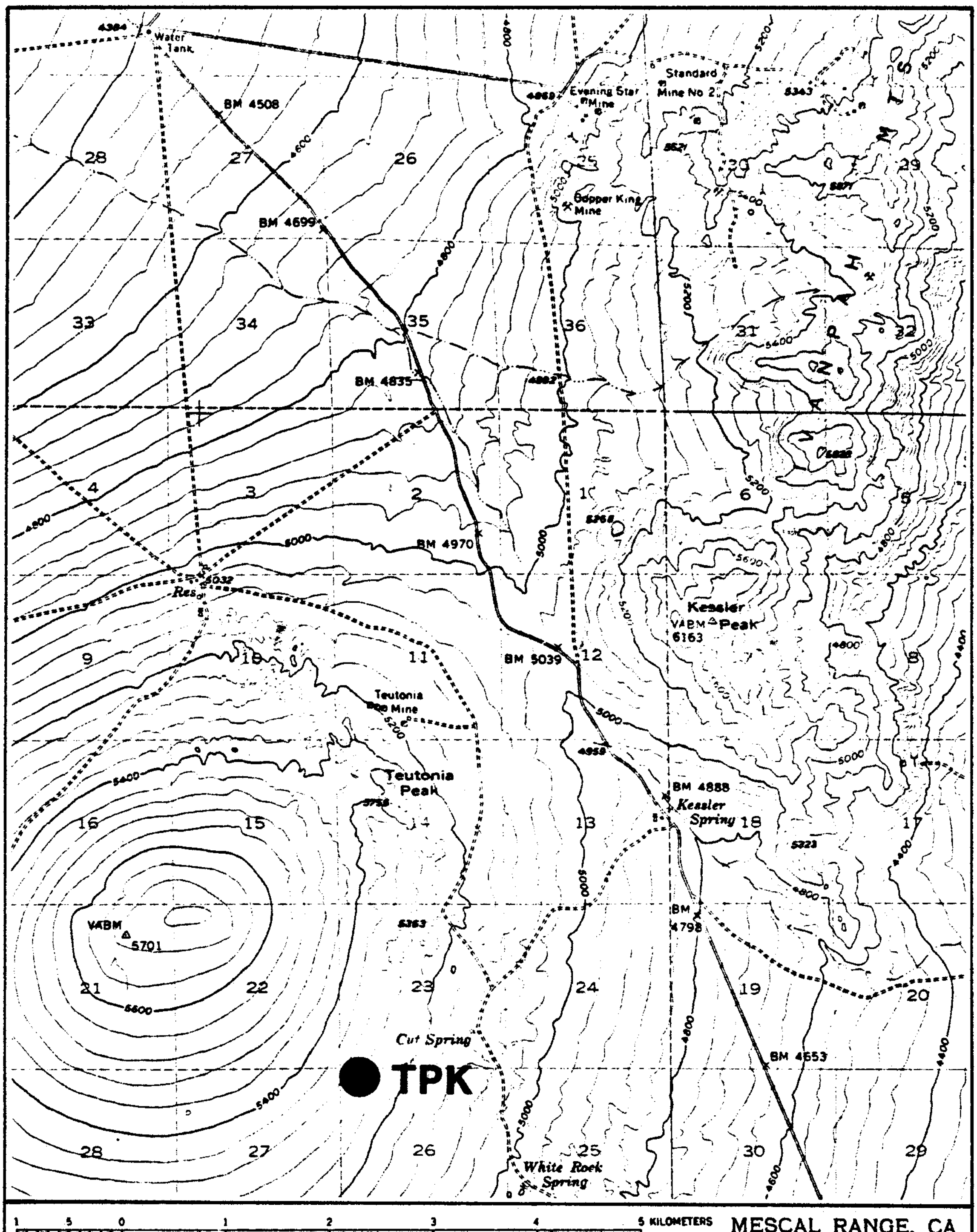

CONTOUR INTERVAL 40 FEET
DATUM IS MEAN SEA LEVEL

MESCAL RANGE, CA.
N3515—W11530/15
1955

AMS 2854 I—SERIES V795

Figure A7

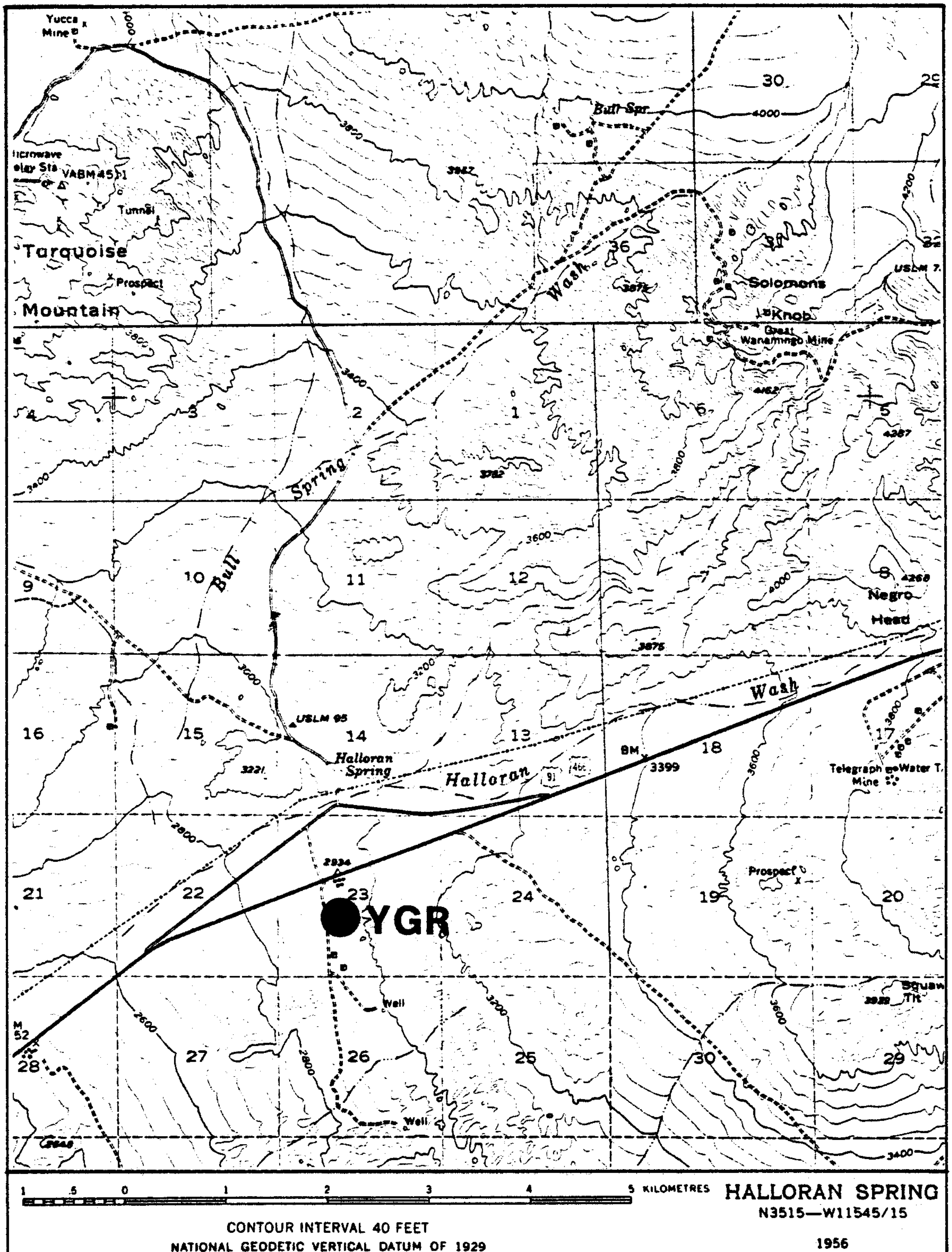
Yucca Mine
Torquoise Mountain
Tunnel
Prospect
VABM 4551
Bull Spr.
Wash
Solomons Knob
Great Wanamingo Mine
Spring
Bull
Negro Head
USLM 95
Halloran Spring
Halloran
Wash
BM 3399
Telegraph Mine
Water T.
Prospect
YGR
Well
Well
1 .5 0 1 2 3 4 5 KILOMETRES
CONTOUR INTERVAL 40 FEET
NATIONAL GEODETIC VERTICAL DATUM OF 1929
HALLORAN SPRING
N3515—W11545/15
1956
AMS 2854 IV—SERIES V795

Figure A8

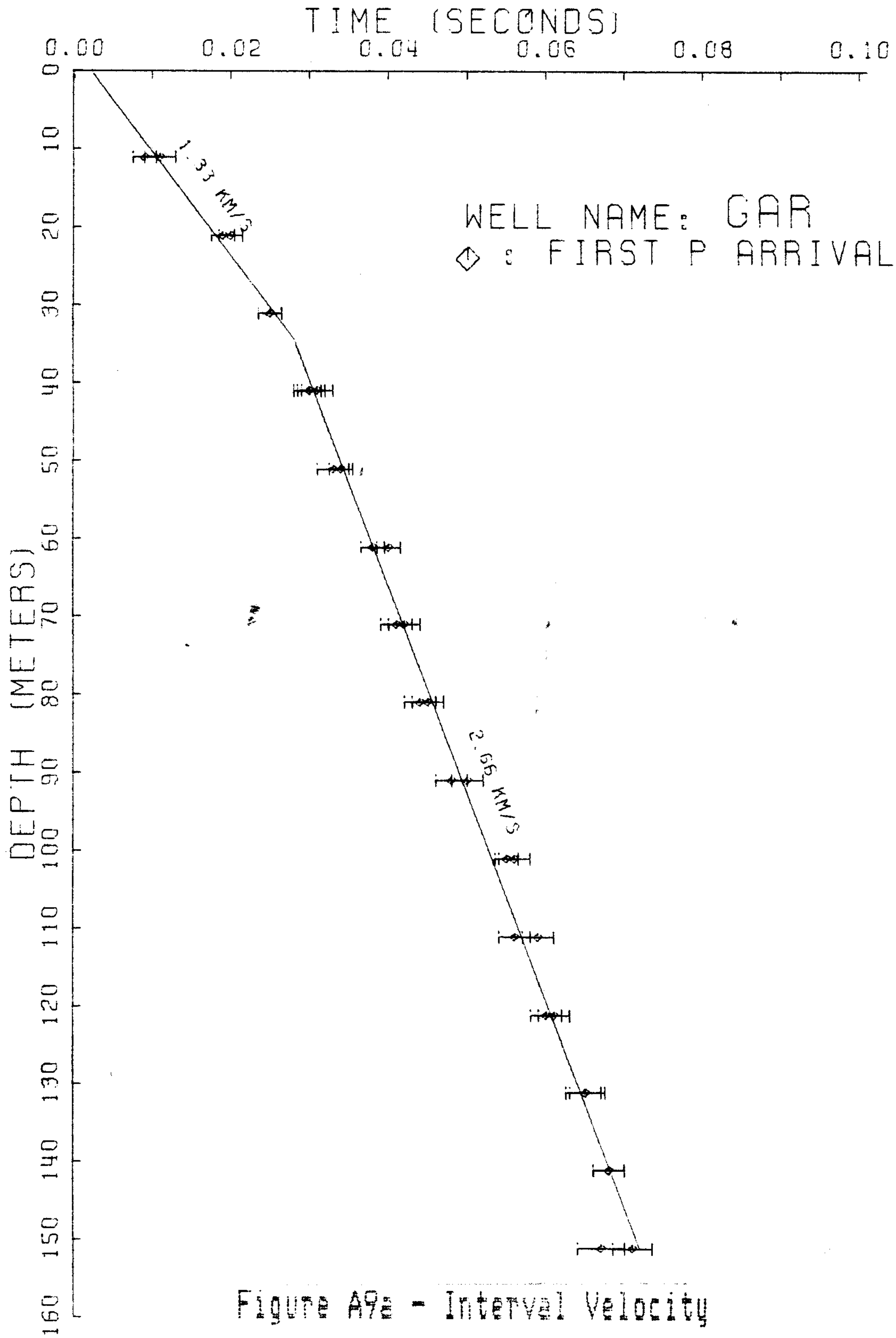

Figure A9a - Interval Velocity

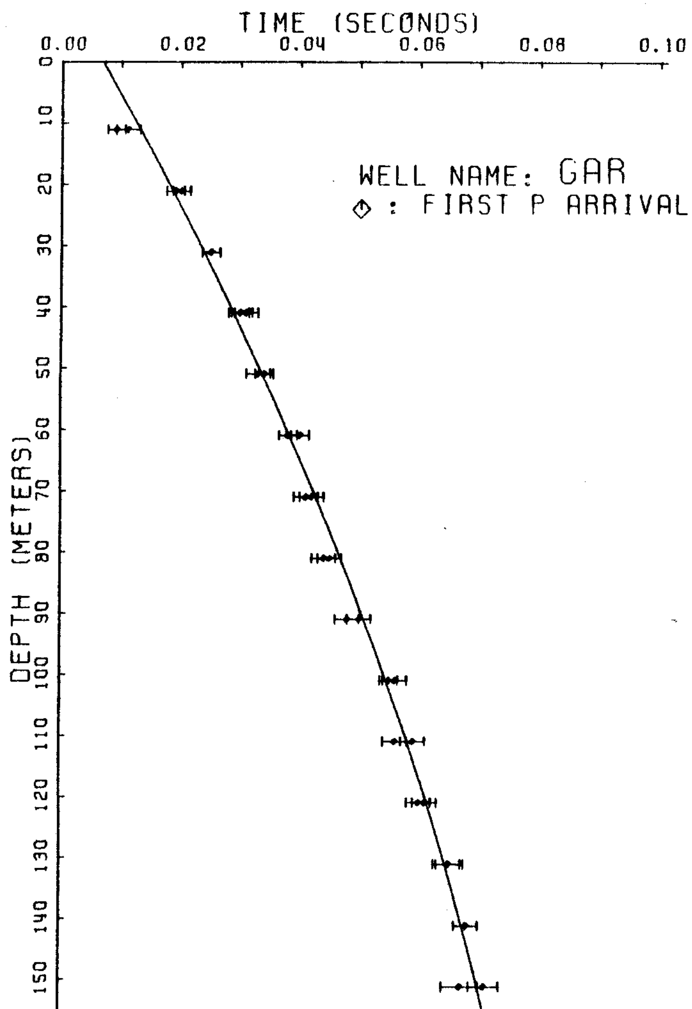

Figure A9b - Polynomial Fit

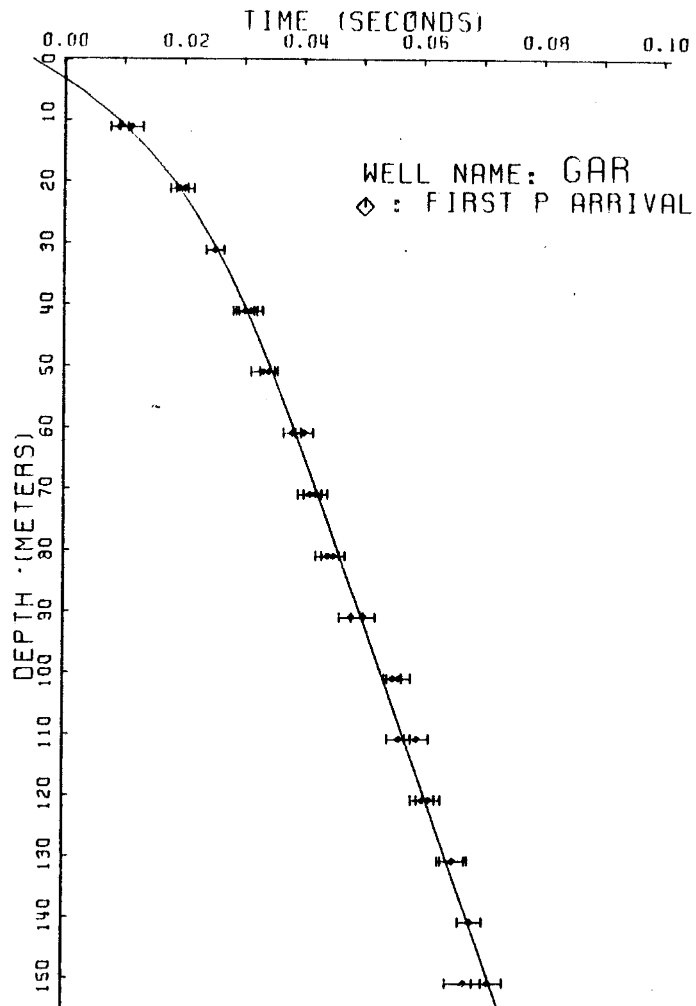

Figure A9c - Exponential, Minimum Residual

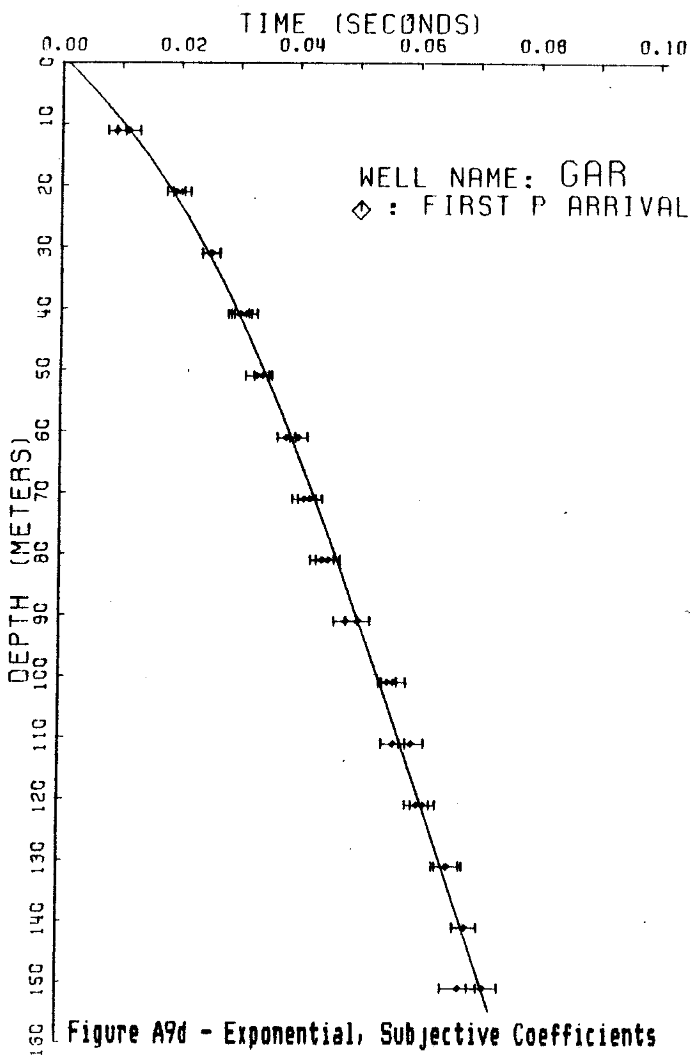

Figure A9d - Exponential, Subjective Coefficients

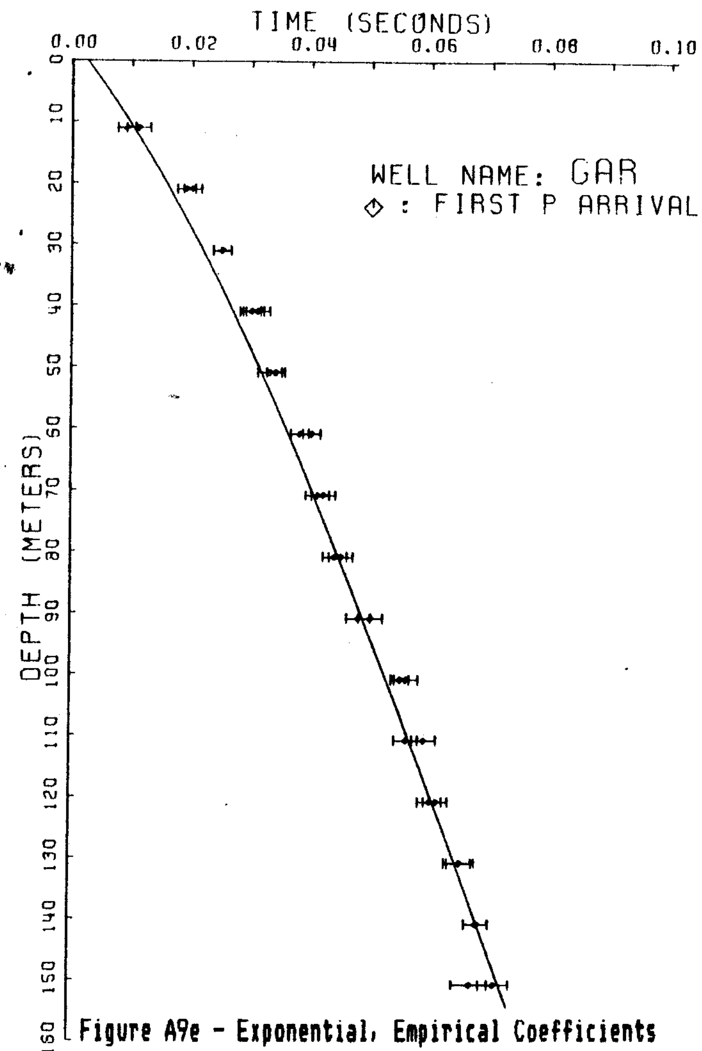

Figure A9e - Exponential, Empirical Coefficients

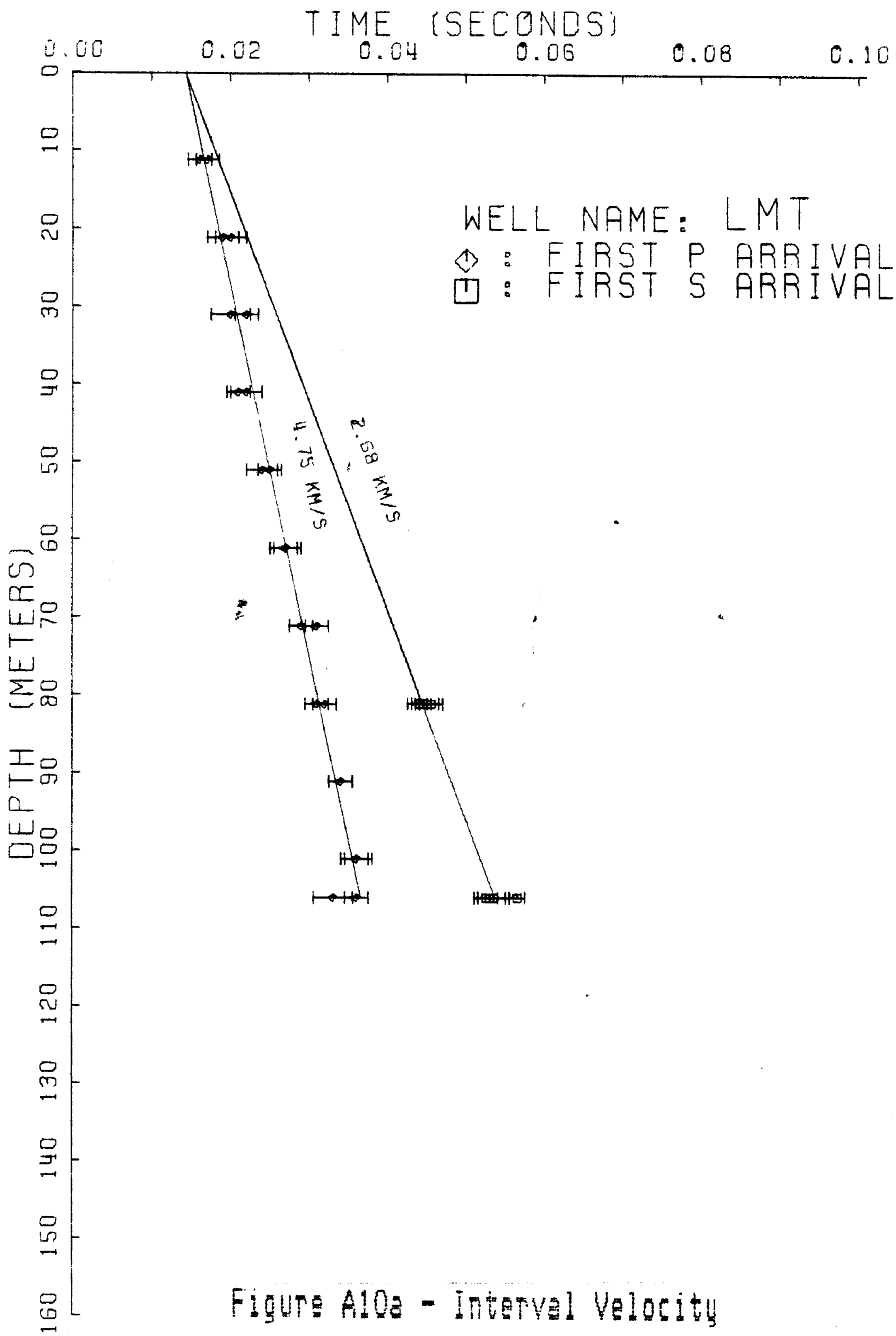

Figure A10a - Interval Velocity

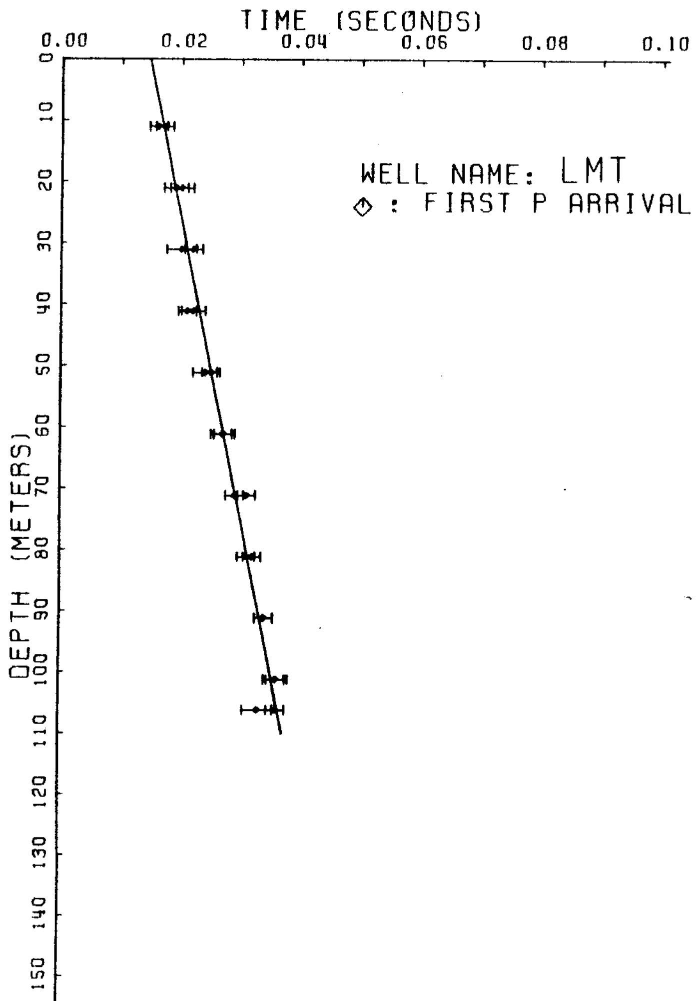

Figure A10b - Polynomial Fit

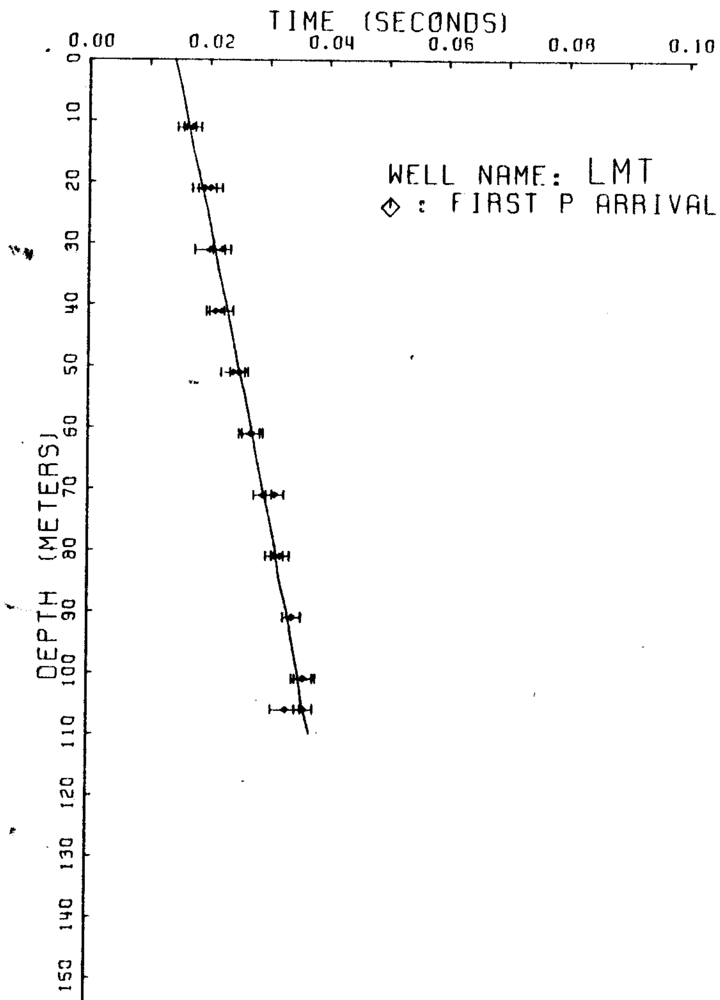

Figure A10c - Exponential, Minimum Residual

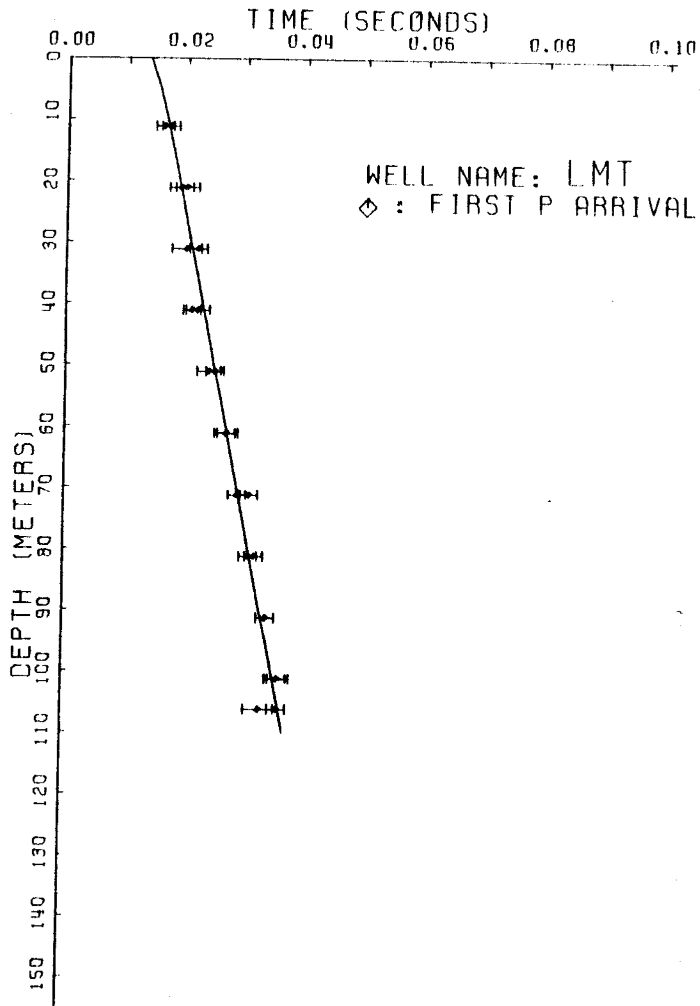

Figure A10d - Exponential, Subjective Coefficients

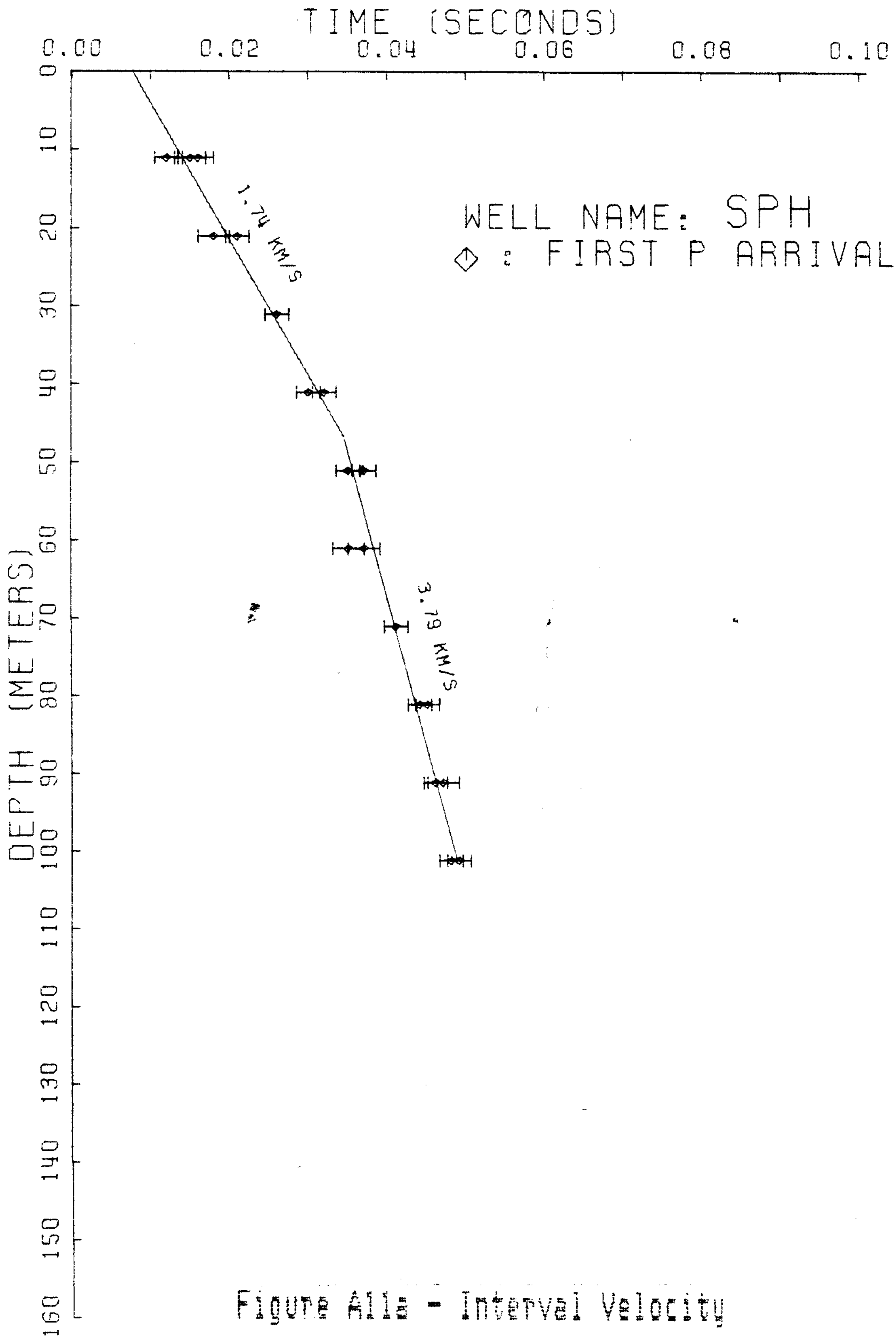

Figure A11a - Interval Velocity

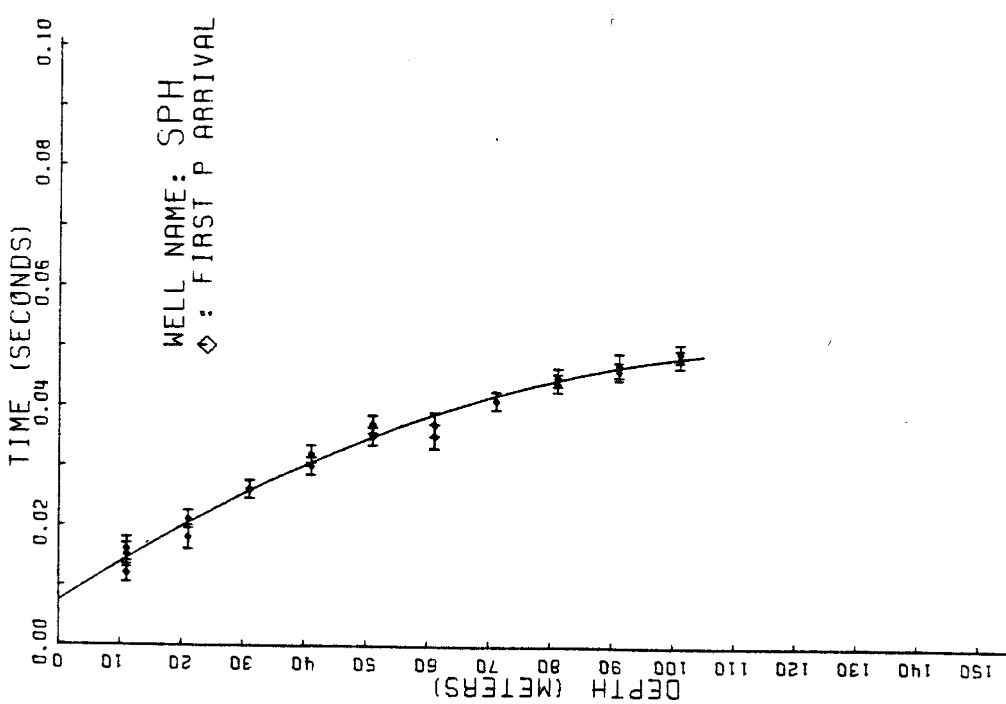

Figure A11b - Polynomial Fit

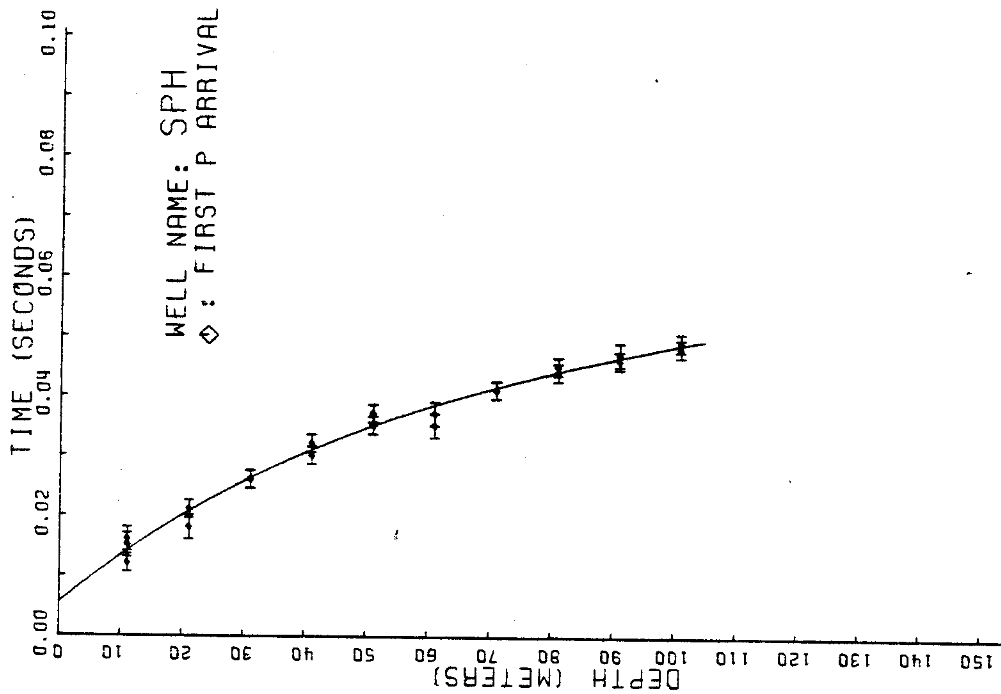

Figure A11c - Exponential, Minimum Residual

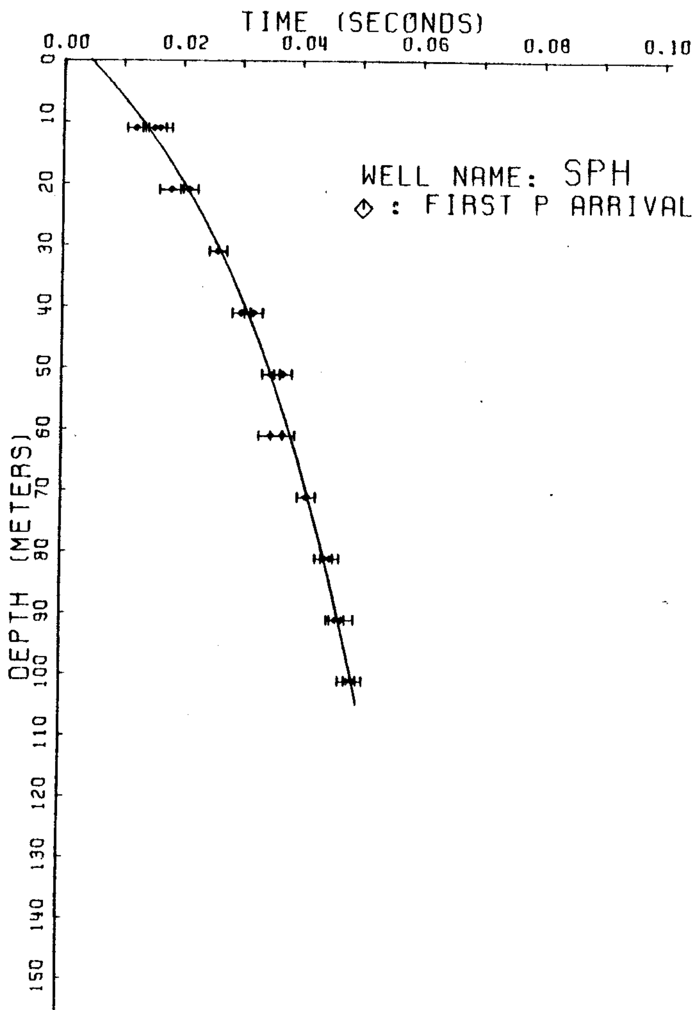

Figure A11d - Exponential, Subjective Coefficients

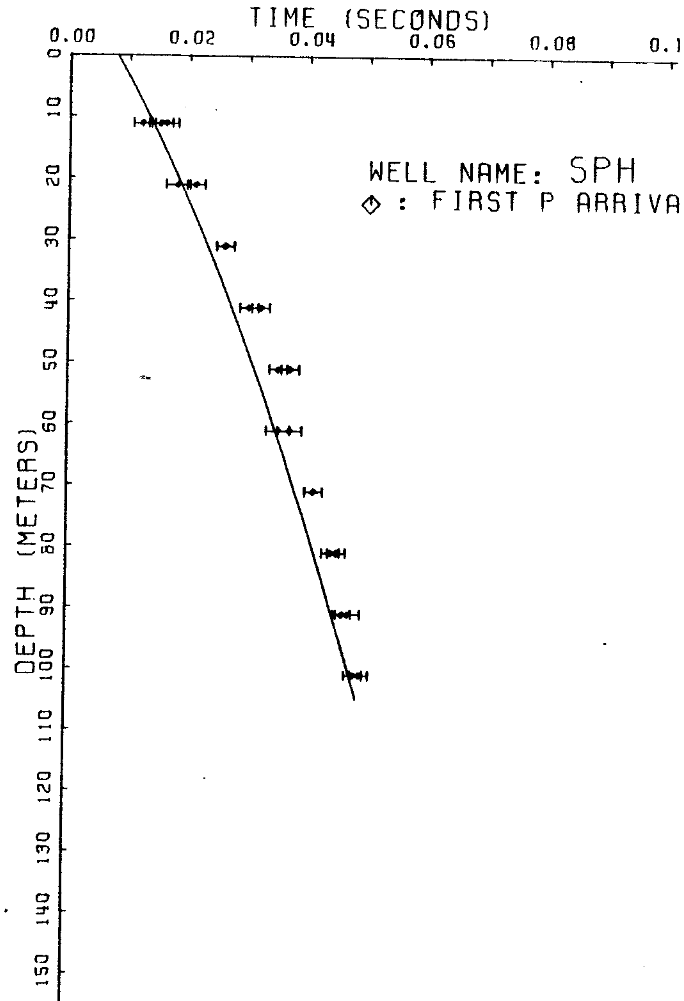

Figure A11e - Exponential, Empirical Coefficients

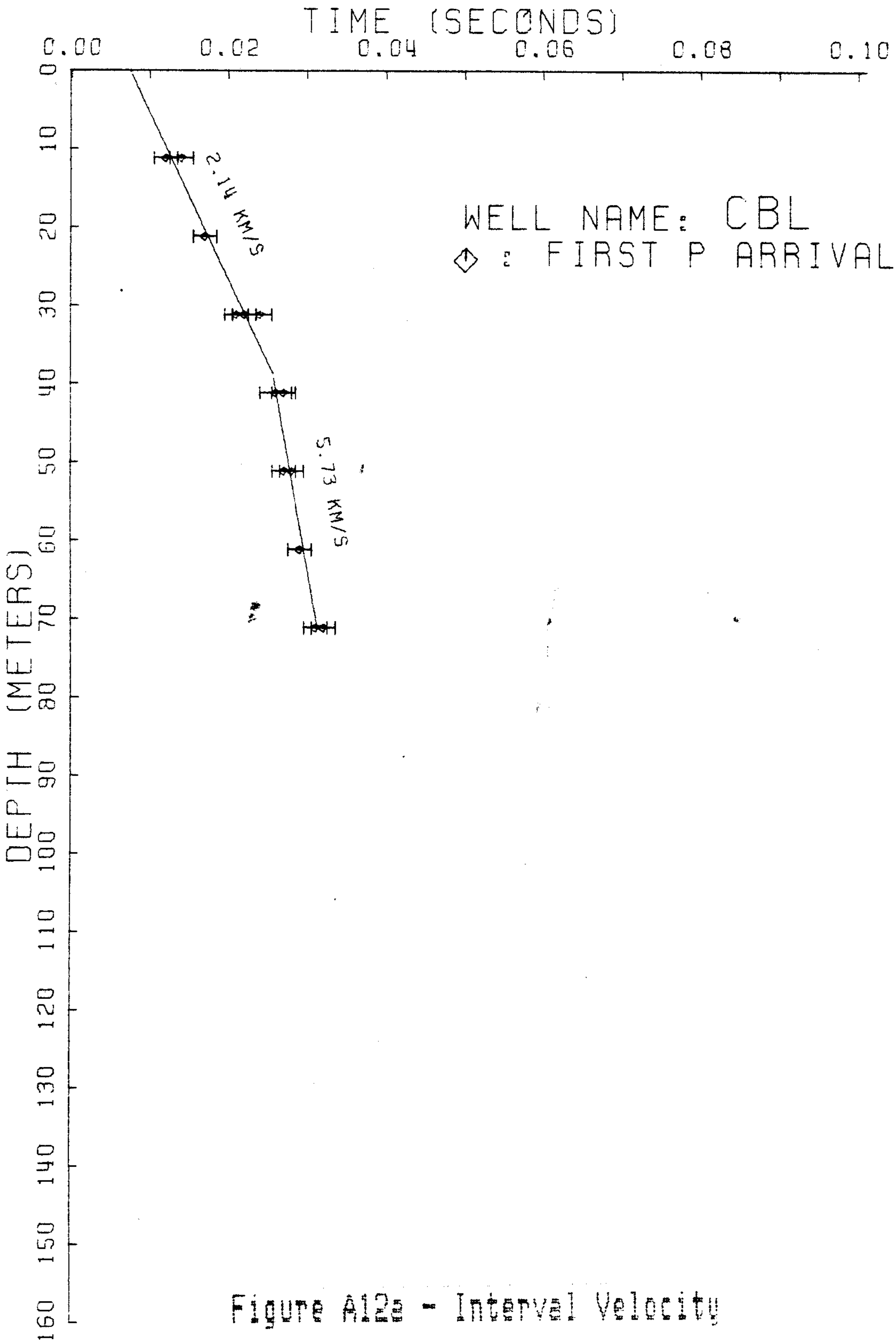

Figure A12a - Interval Velocity

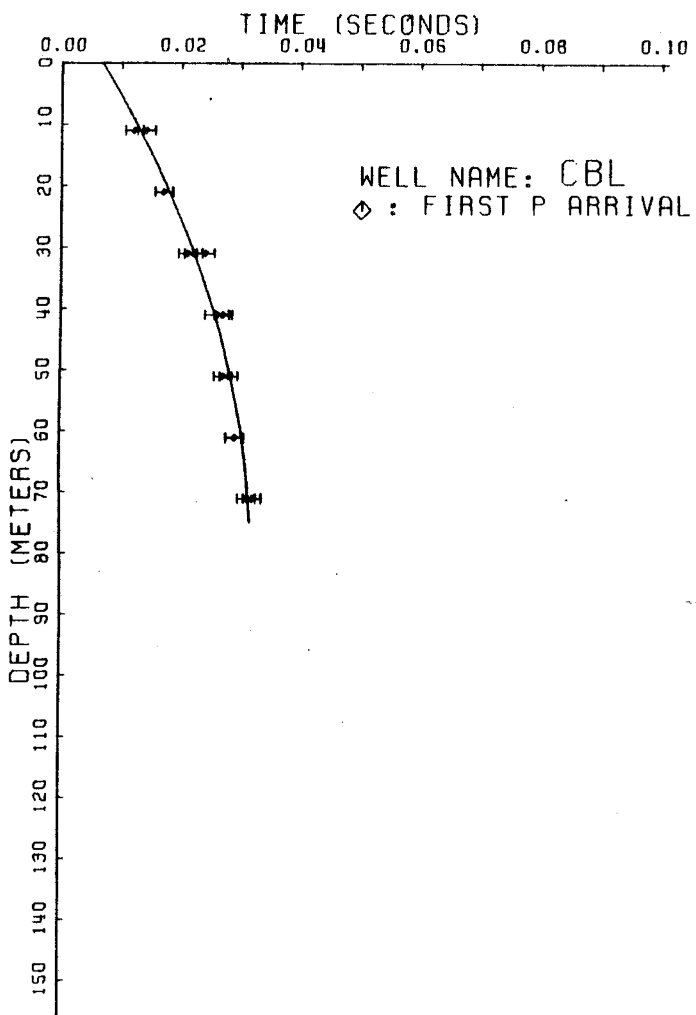

Figure A12b - Polynomial Fit

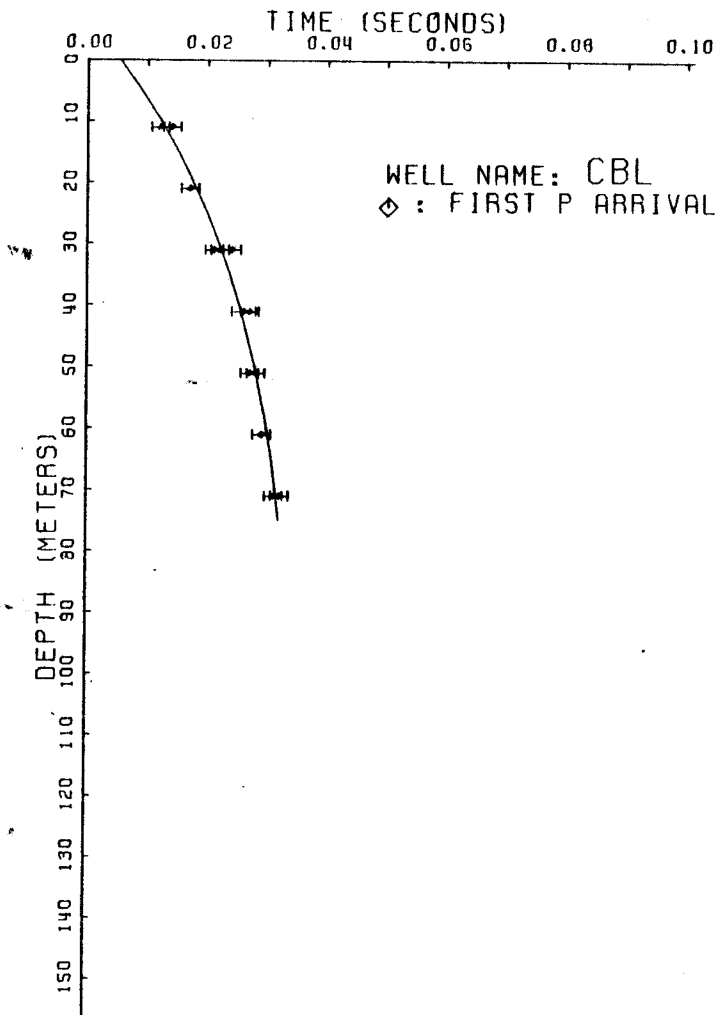

Figure A12c - Exponential, Minimum Residual

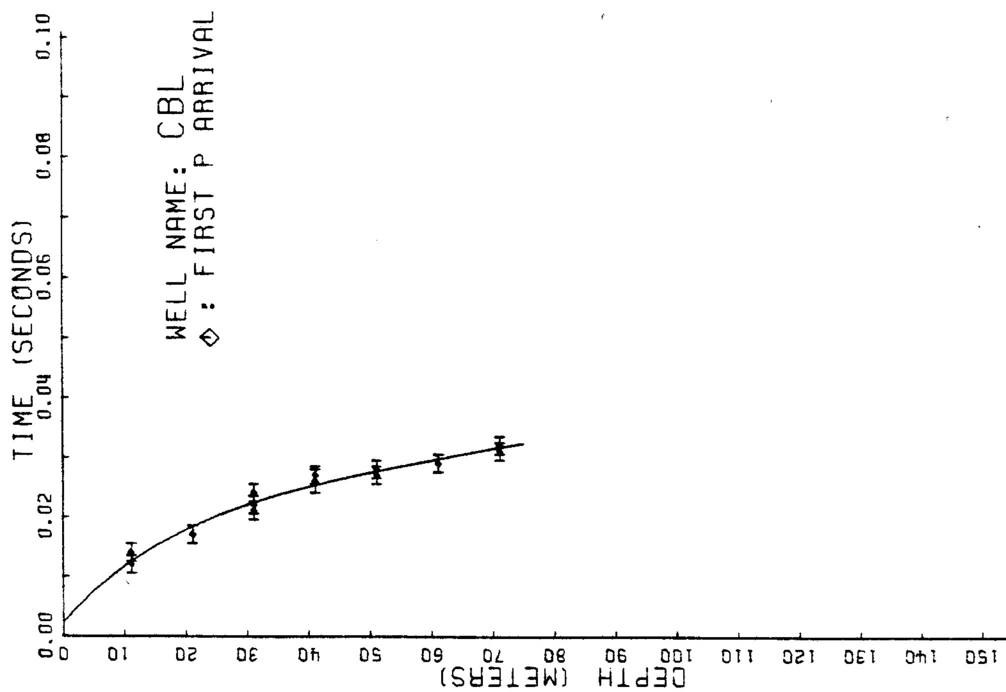

Figure A12d - Exponential, Subjective Coefficients

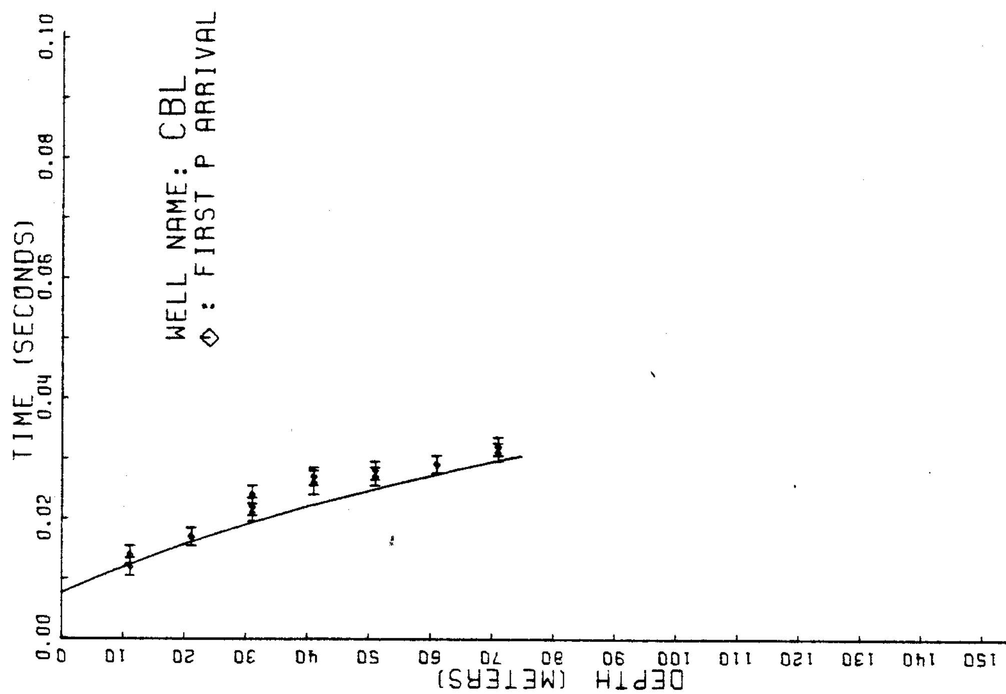

Figure A12e - Exponential, Empirical Coefficients

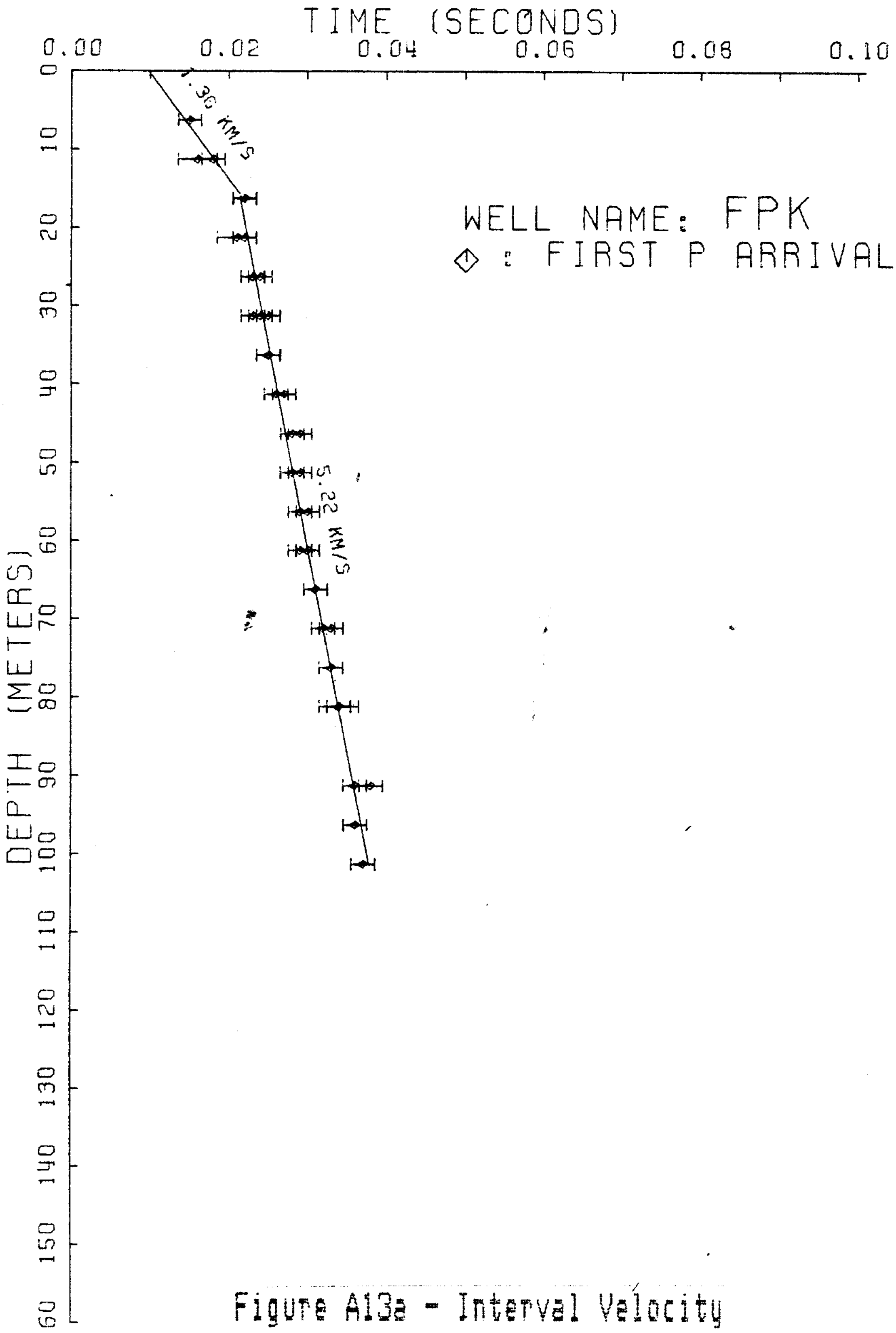

Figure A13a - Interval Velocity

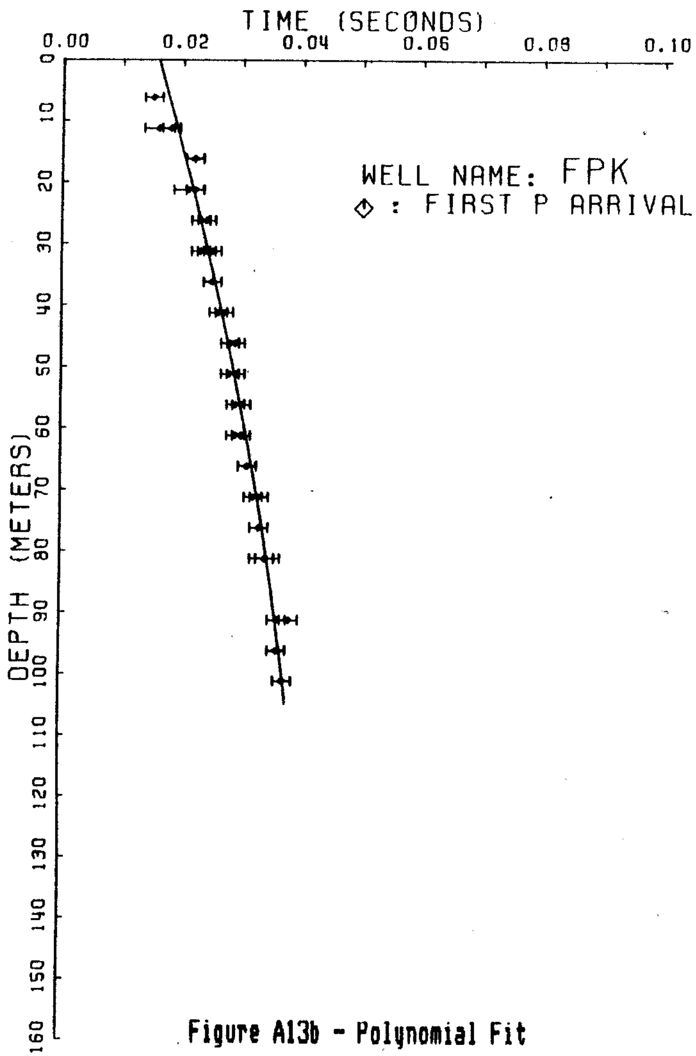

Figure A13b - Polynomial Fit

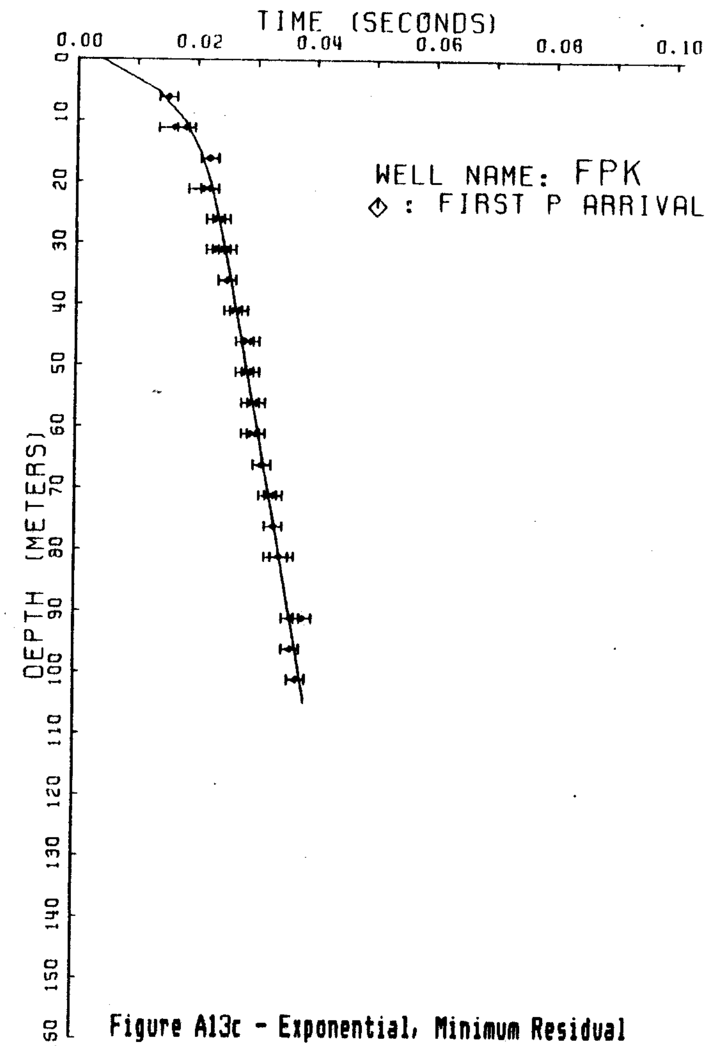

Figure A13c - Exponential, Minimum Residual

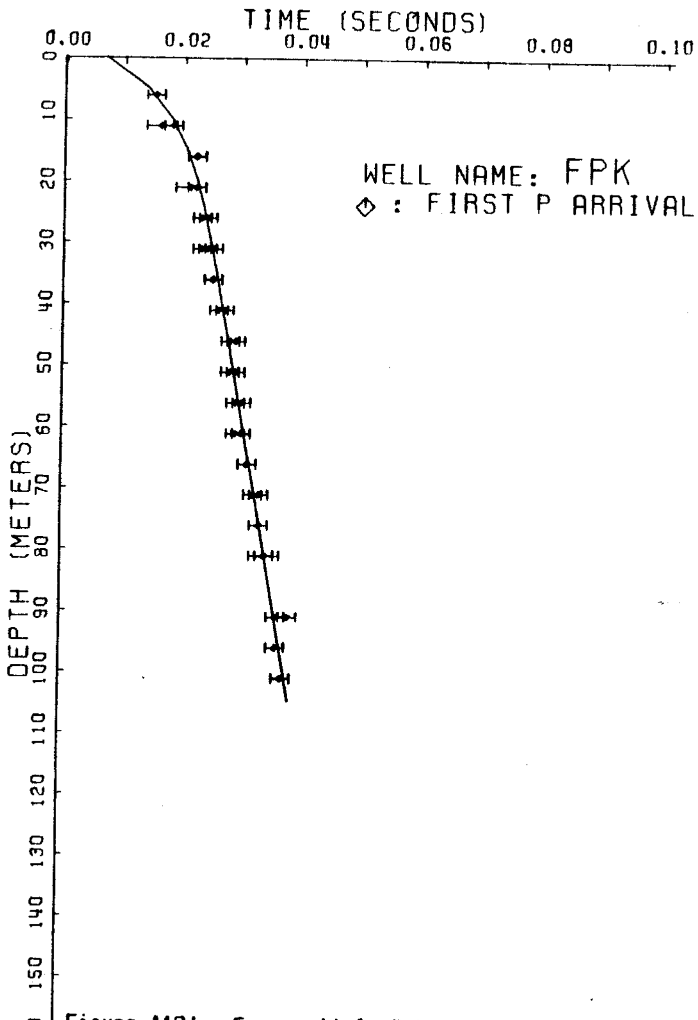

Figure A13d - Exponential, Subjective Coefficients

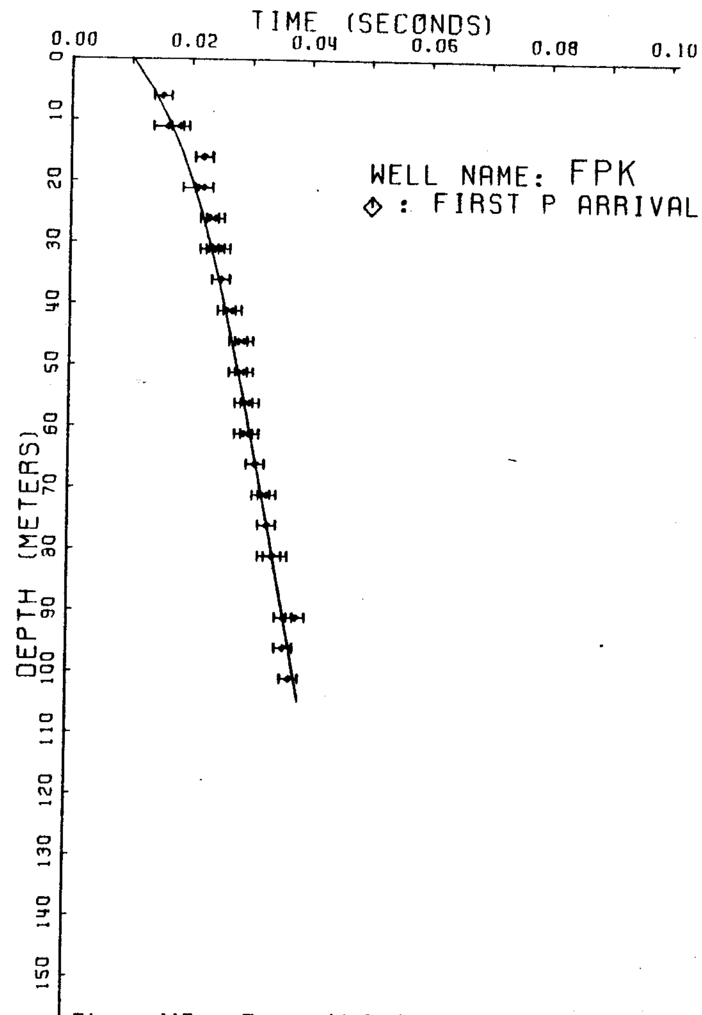

Figure A13e - Exponential, Empirical Coefficients

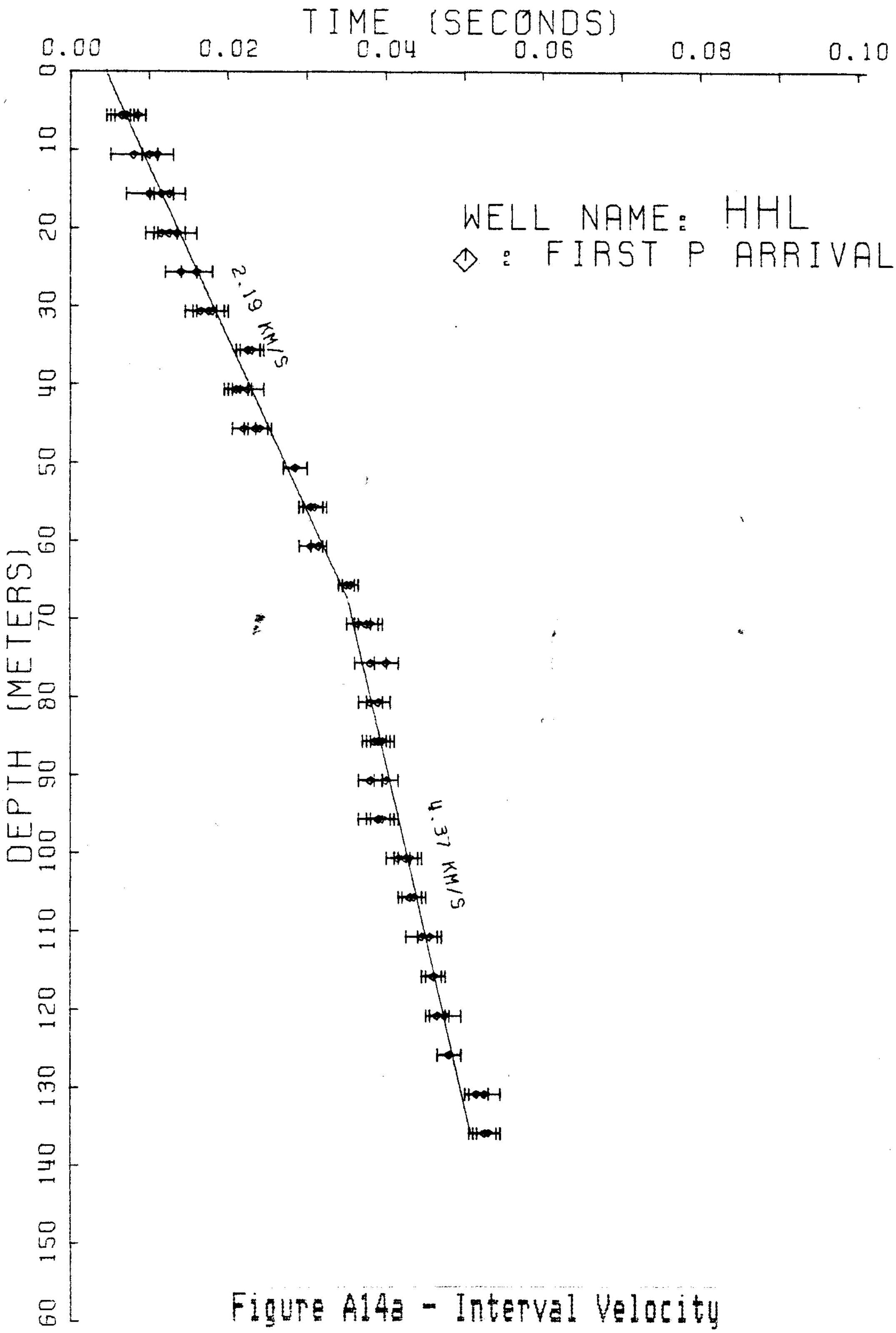

Figure A14a - Interval Velocity

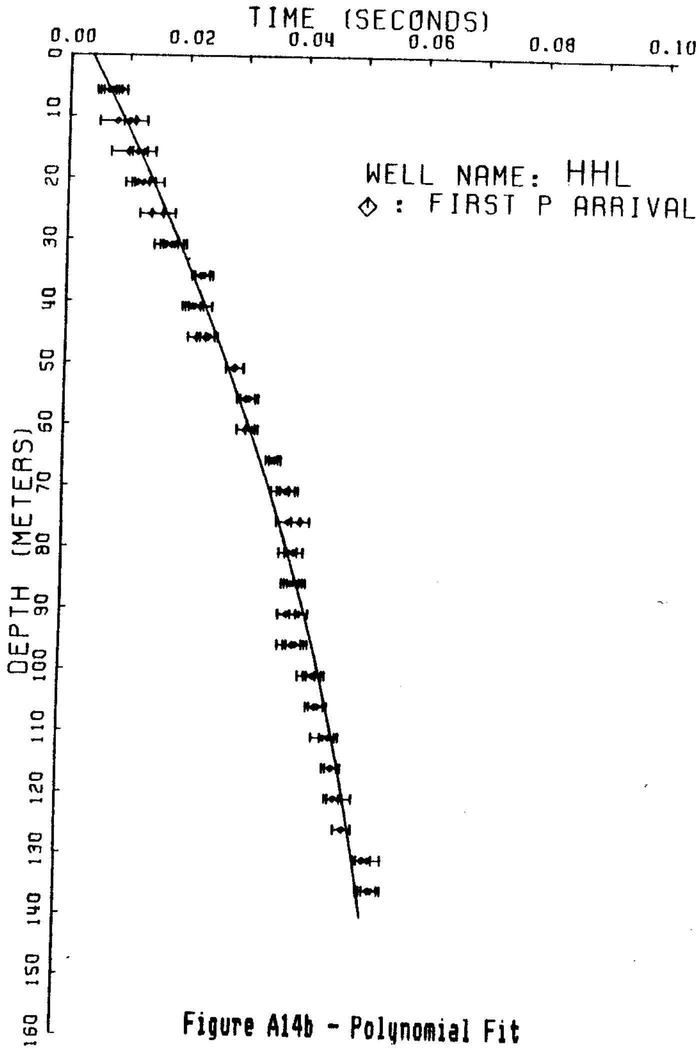

Figure A14b - Polynomial Fit

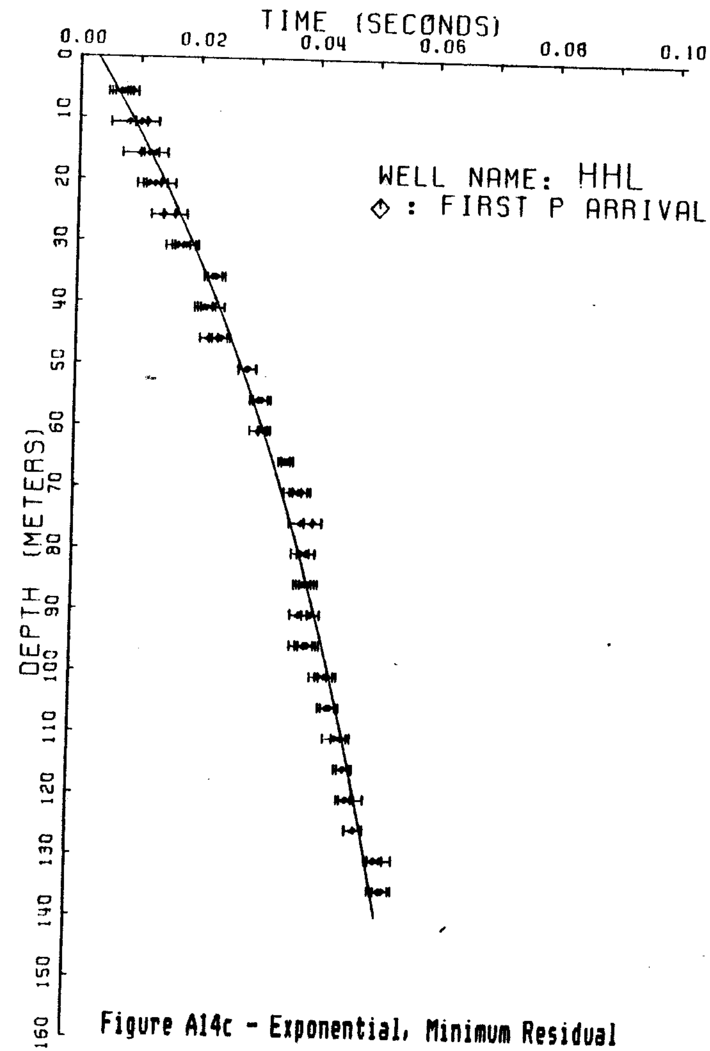

Figure A14c - Exponential, Minimum Residual

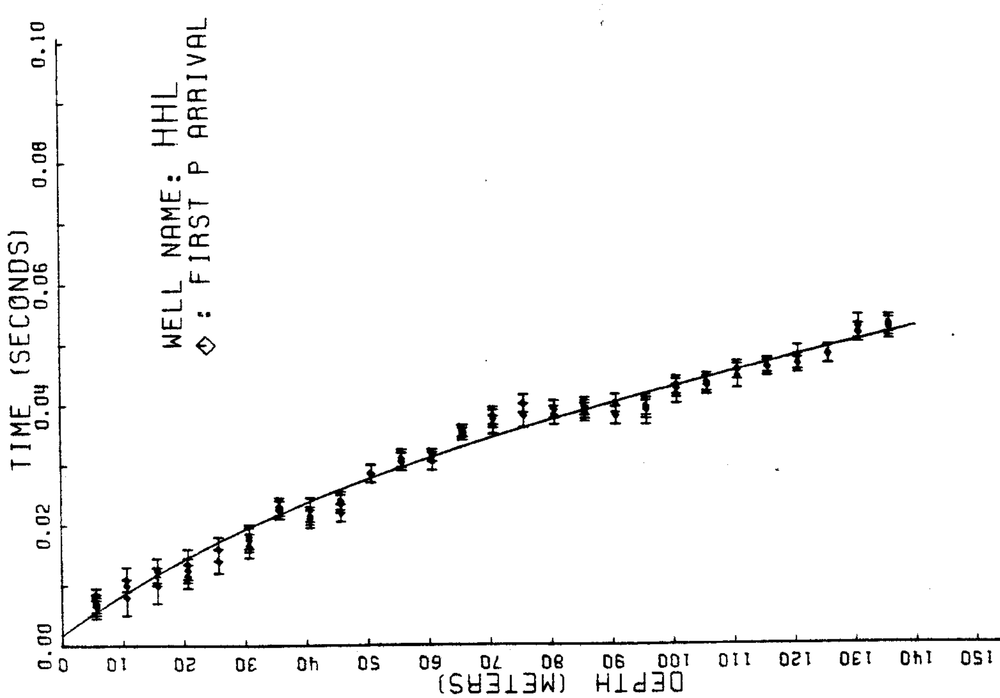

Figure A14d - Exponential, Subjective Coefficients

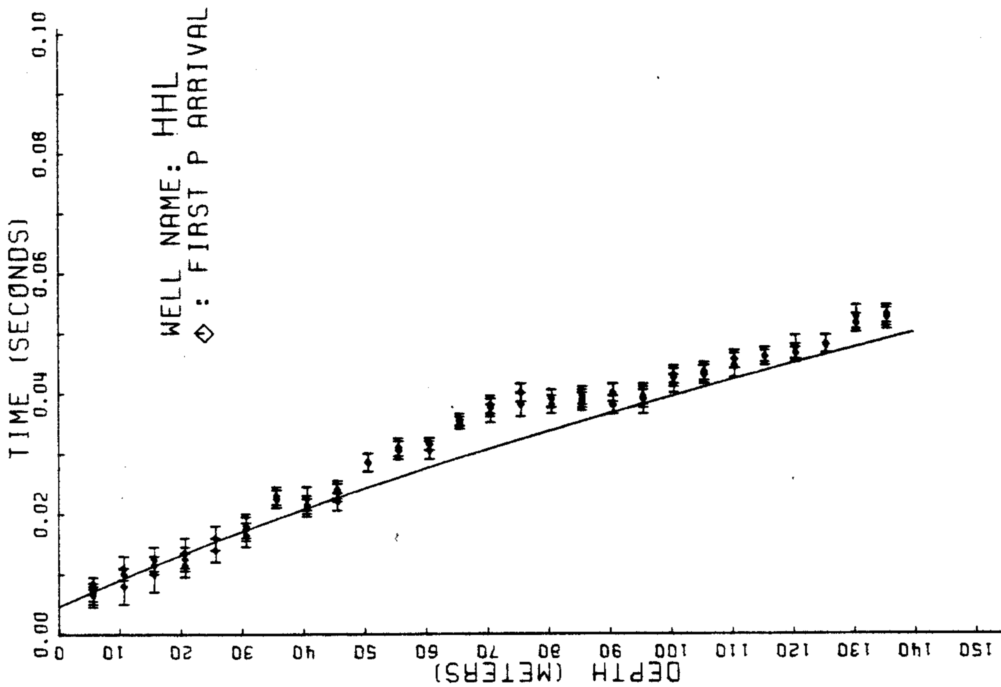

Figure A14e - Exponential, Empirical Coefficients

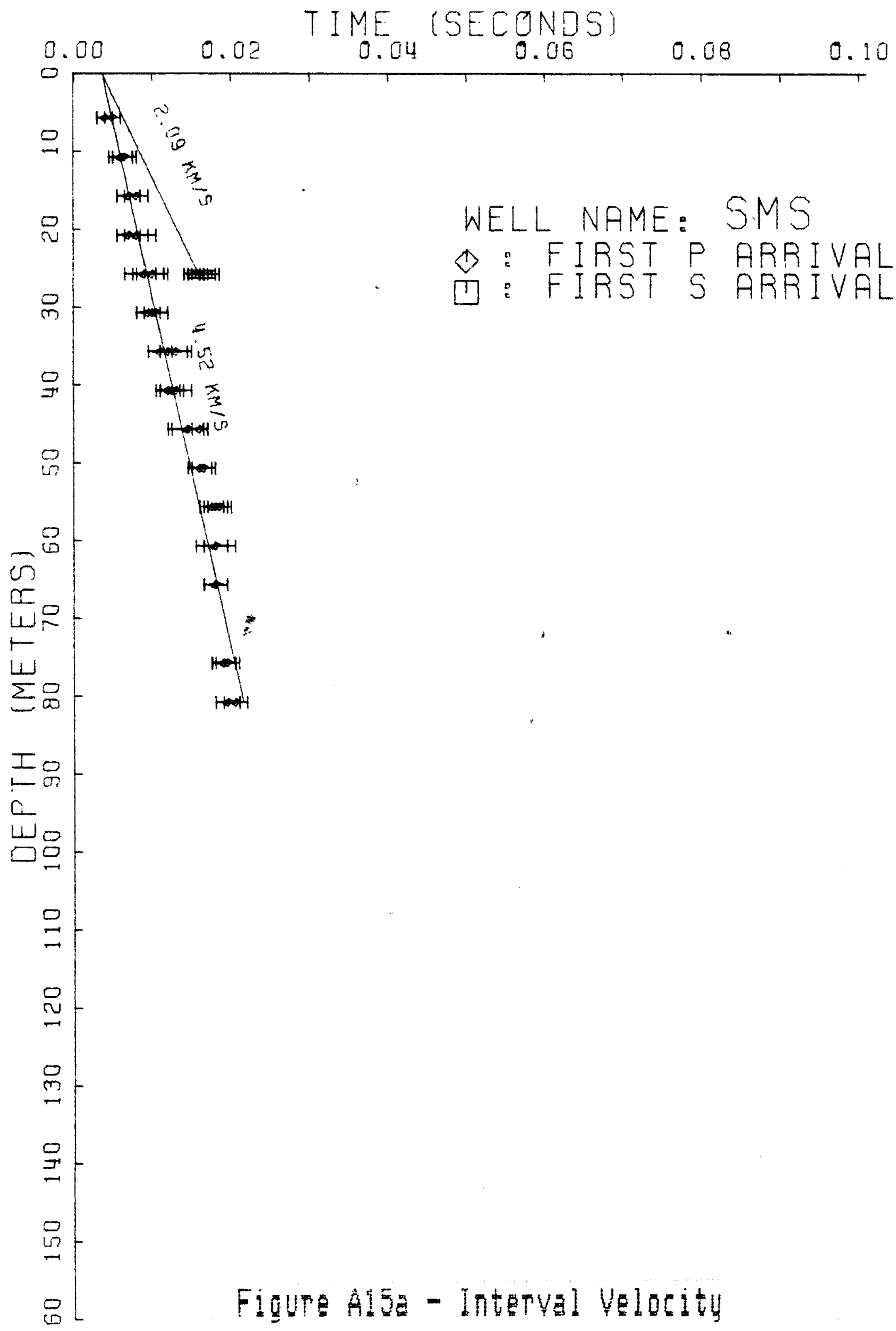

Figure A15a - Interval Velocity

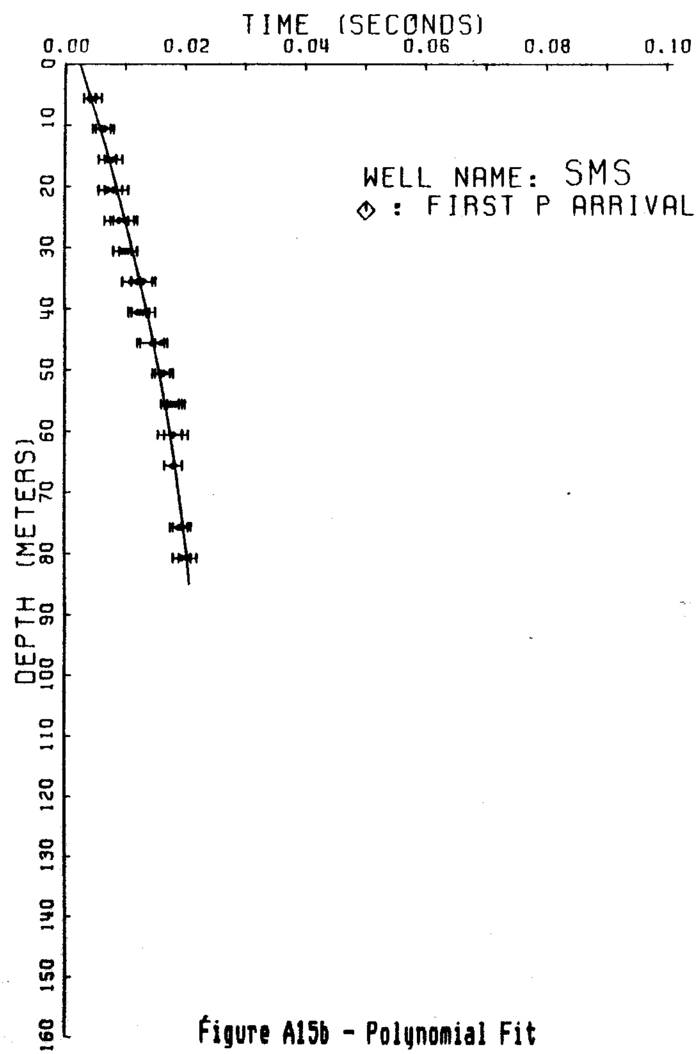

Figure A15b - Polynomial Fit

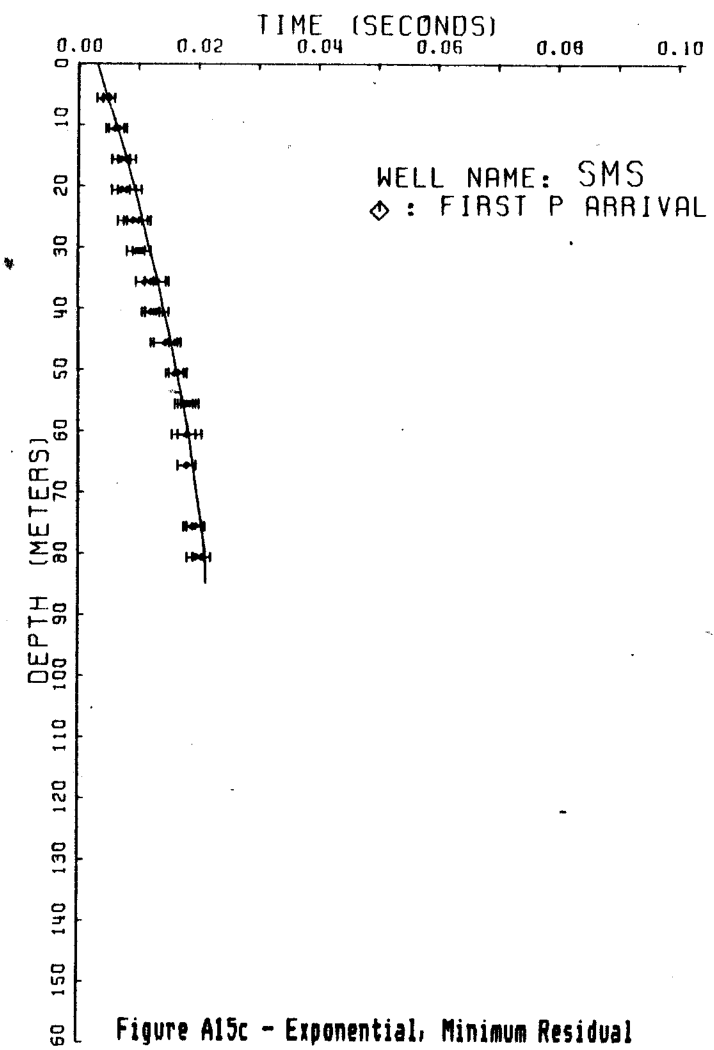

Figure A15c - Exponential, Minimum Residual

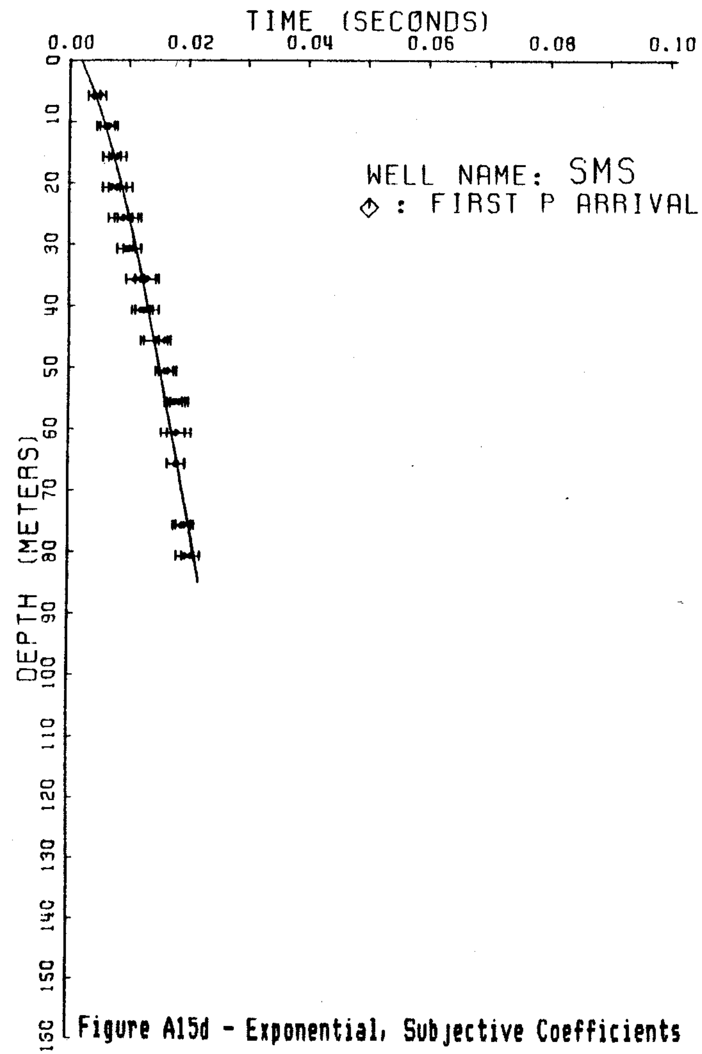

Figure A15d - Exponential, Subjective Coefficients

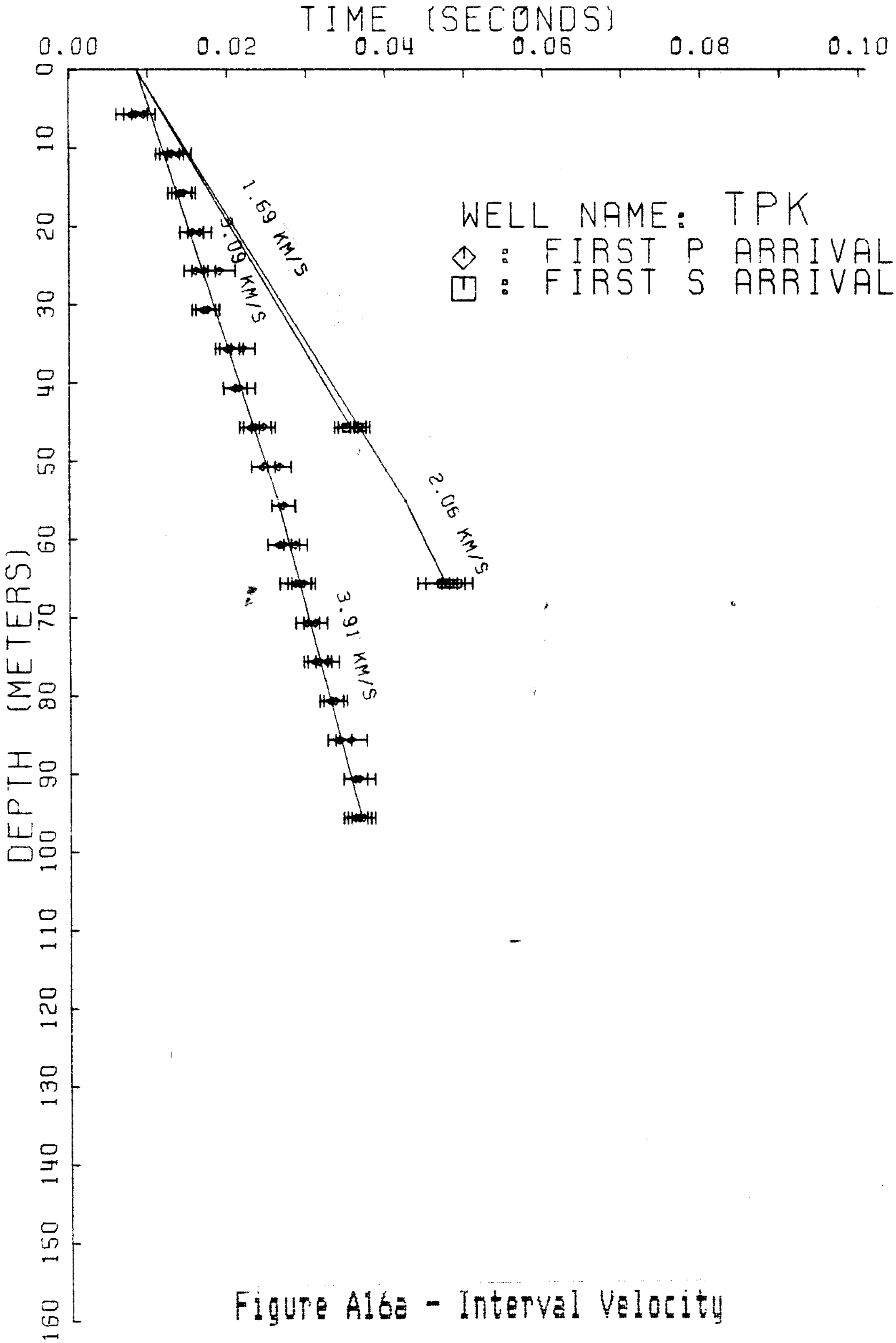

Figure A16a - Interval Velocity

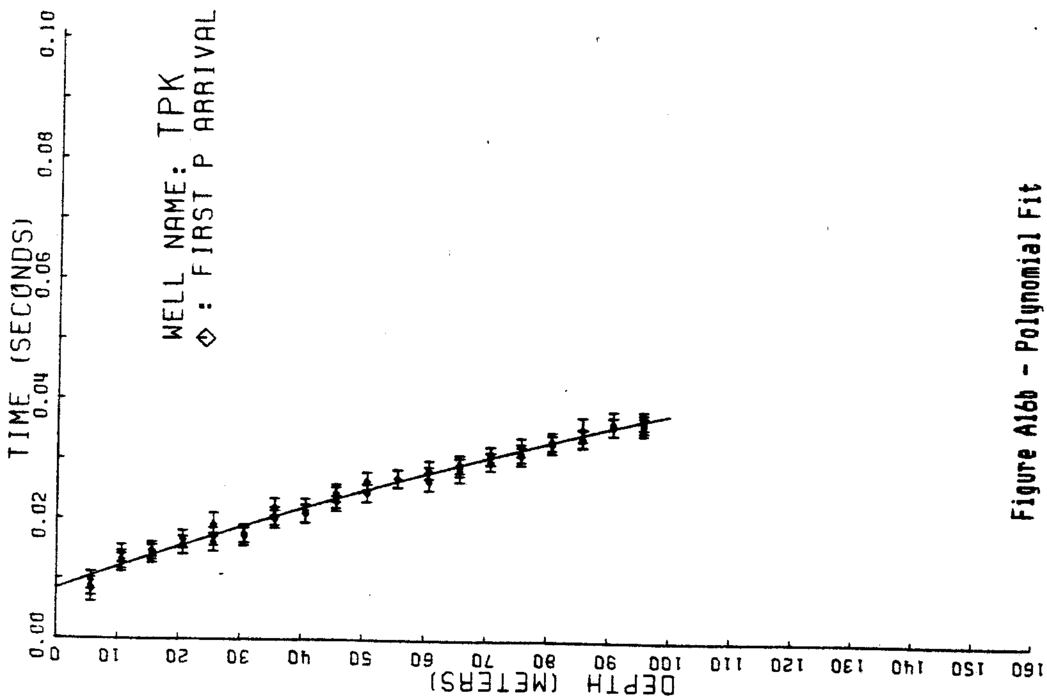

Figure A16b - Polynomial Fit

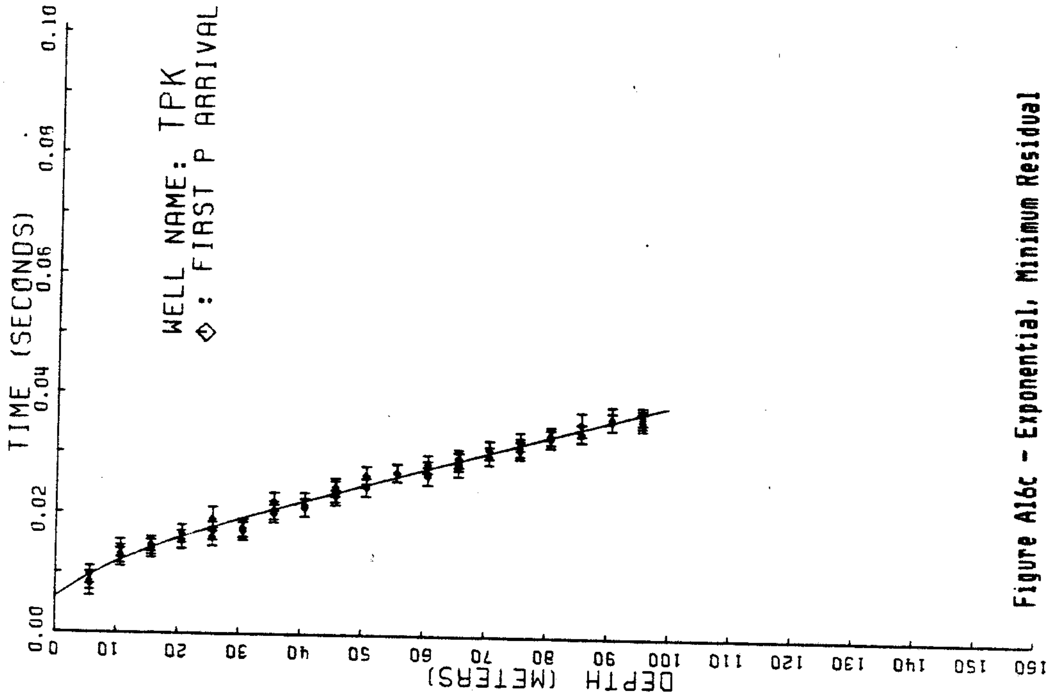

Figure A16c - Exponential, Minimum Residual

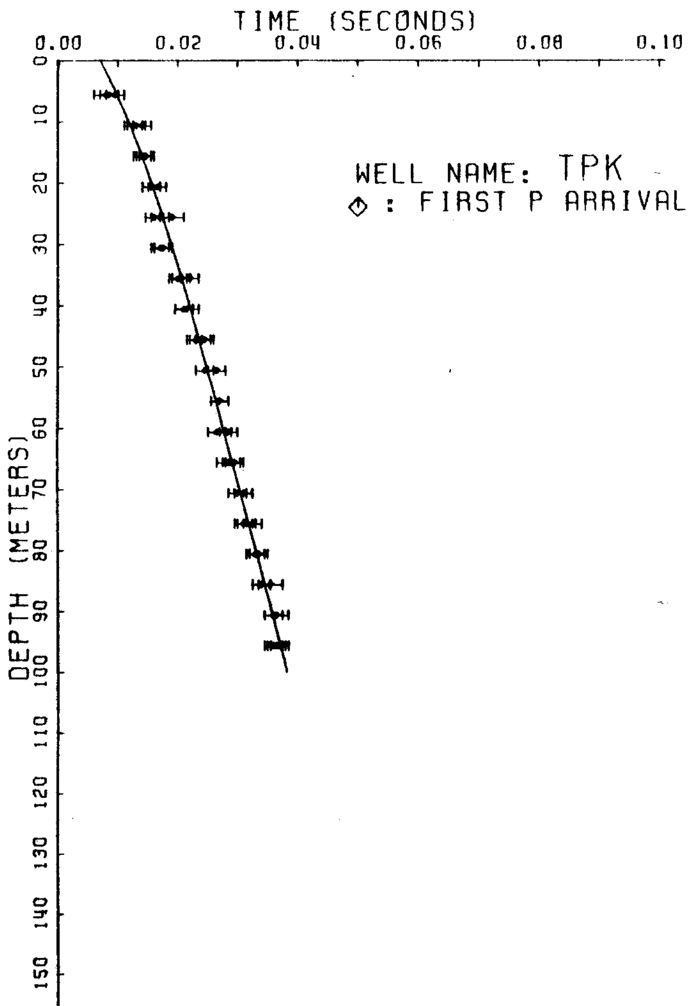

Figure A16d - Exponential, Subjective Coefficients

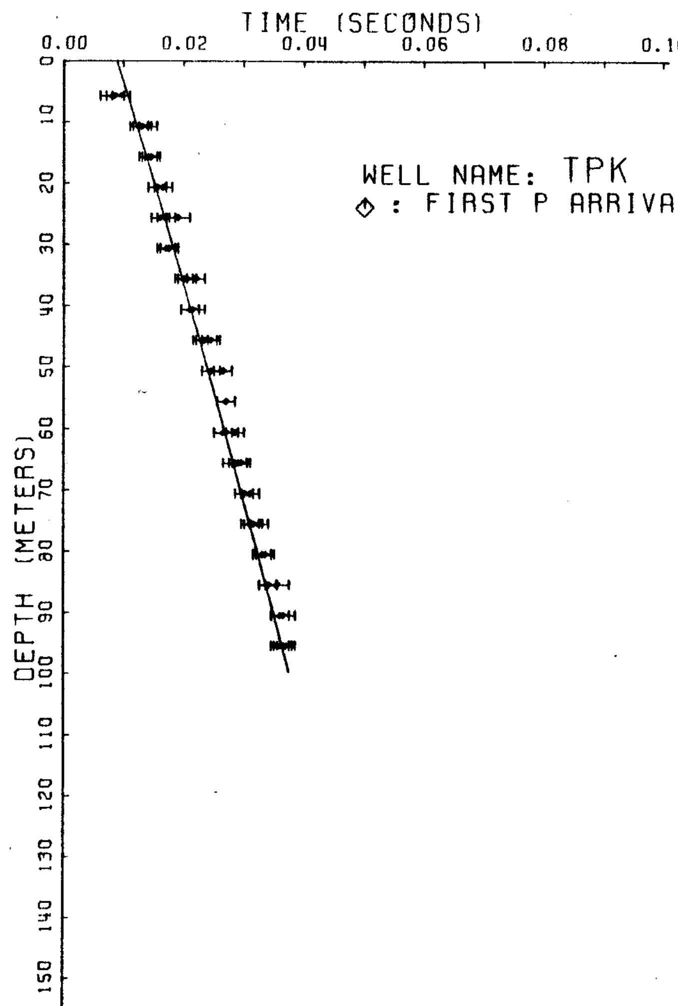

Figure A16e - Exponential, Empirical Coefficients

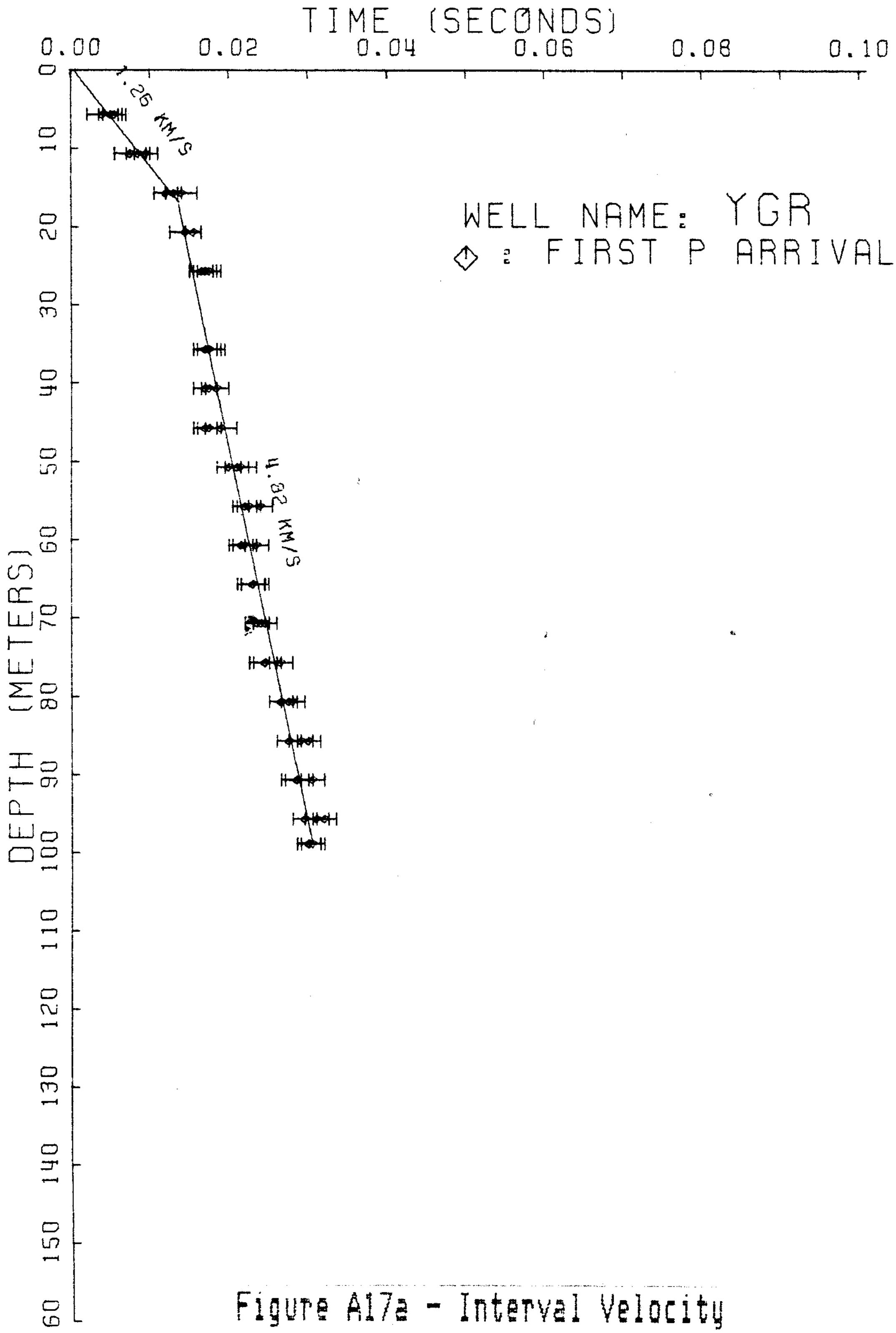

Figure A17a - Interval Velocity

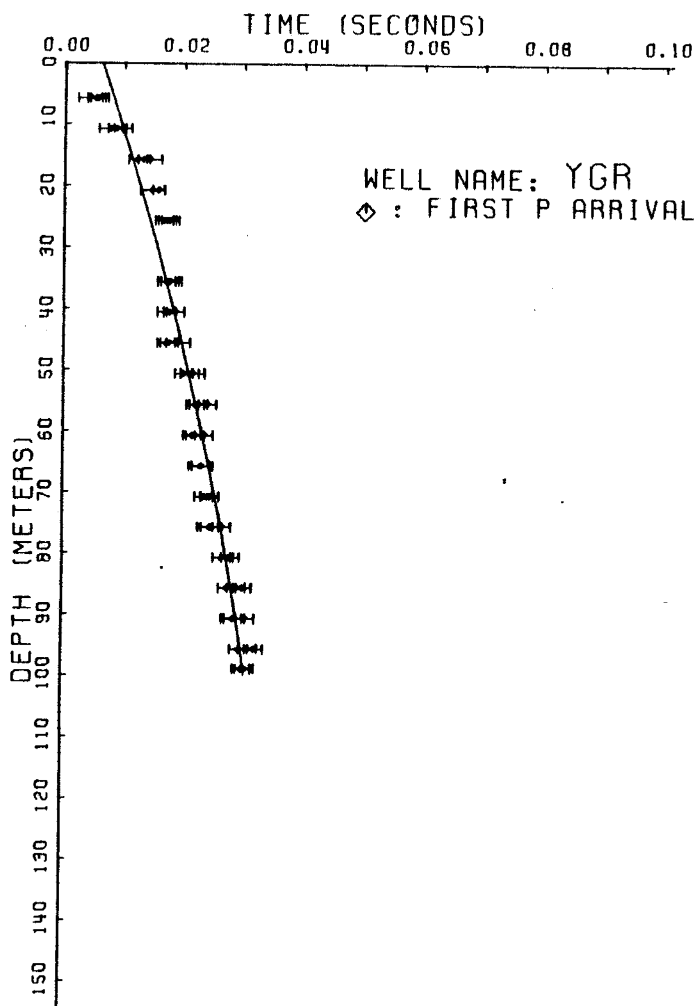

Figure A17b - Polynomial Fit

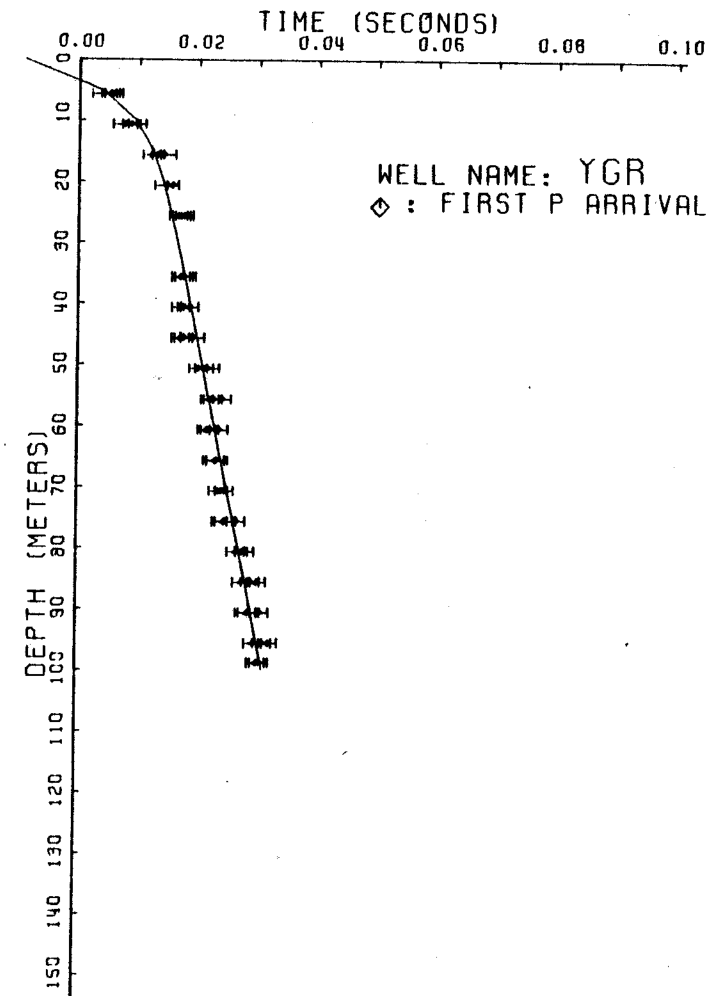

Figure A17c - Exponential, Minimum Residual

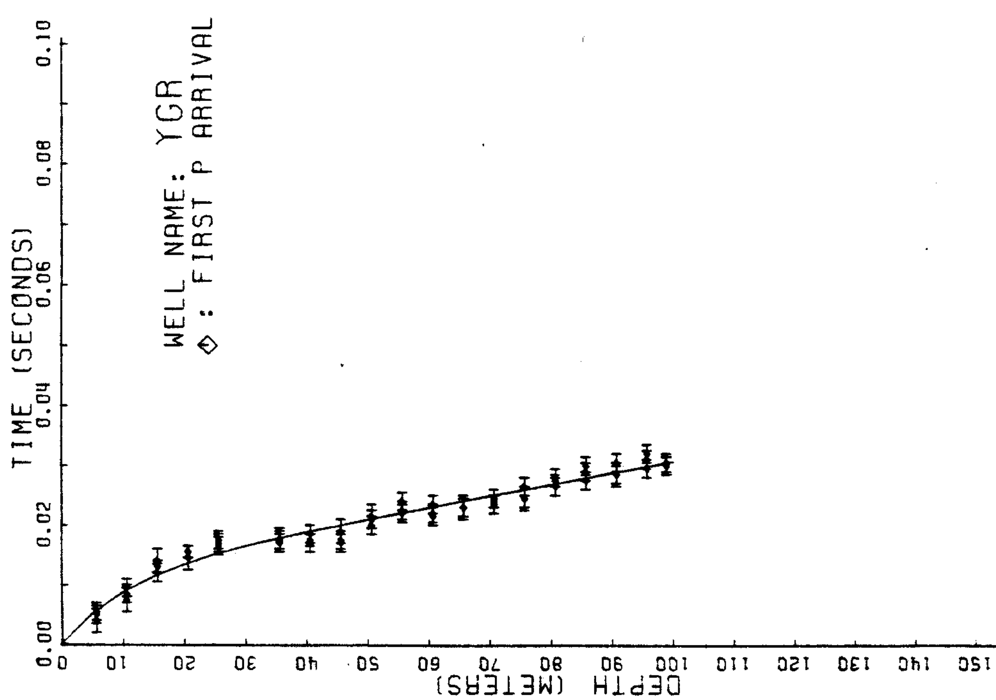

Figure A17d - Exponential, Subjective Coefficients

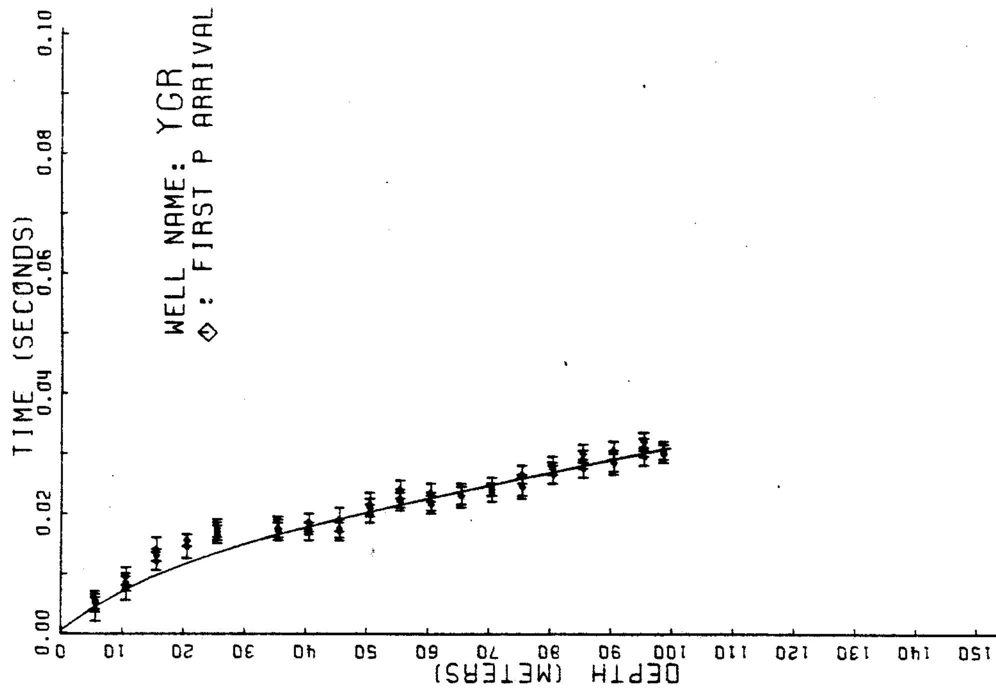

Figure A17e - Exponential, Empirical Coefficients